FLT3 specific antibody-drug-conjugate for the treatment of acute myeloid leukemia

DISSERTATION DER FAKULTÄT FÜR BIOLOGIE
DER LUDWIG-MAXIMILIANS-UNIVERSITÄT MÜNCHEN

MAIKE KATHARINA LUZIE ROAS
GEBOREN IN ERLANGEN

25. NOVEMBER 2021

Dissertation

FLT3 specific antibody-drug-conjugate for the treatment of acute myeloid leukemia

zur Erlangung des Doktorgrades der Naturwissenschaften

Doctor rerum naturalium (Dr.rer.nat.)

an der Fakultät für Biologie

der Ludwig-Maximilians-Universität München

vorgelegt von

Maike Katharina Luzie Roas

geboren in Erlangen

Diese Dissertation wurde angefertigt unter der Leitung von

Prof. Dr. Heinrich Leonhardt im Bereich für Human Biology & BioImaging.

an der Ludwig-Maximilians-Universität München

Erstgutachter: Prof. Dr. Heinrich Leonhardt

Zweitgutachter: Prof. Dr. Karsten Spiekermann

Tag der Abgabe: 25.11.2021

Tag der mündlichen Prüfung: 25.07.2022

Eidesstattliche Erklärung

Ich versichere hiermit an Eides statt, dass die vorgelegte Dissertation von mir selbstständig und ohne unerlaubte Hilfe angefertigt ist.

Hiermit erkläre ich, dass die Dissertation nicht ganz oder in wesentlichen Teilen einer anderen Prüfungskommission vorgelegt worden ist. Ich habe noch zu keinem früheren Zeitpunkt versucht, eine Dissertation einzureichen oder an einer Doktorprüfung teilzunehmen.

München, den 25.11.2021 Maike Roas

Table of content

Abstract

Acute myeloid leukemia (AML) is a malignant clonal myeloid malignancy. The 5-year survival rate of AML is still low and shows the high medical need to improve therapy. In the last years, tyrosine kinase inhibitors (TKI) targeting fms like tyrosine kinase 3 (FLT3) were approved for increasing the efficacy of the standard chemotherapy. FLT3 is a cell surface receptor expressed at high levels in 93 % of AML patients and constantly active FLT3-ITD mutations occur in approximately 23 % of AML patients. FLT3-ITD mutations are associated with an increased risk of relapse, decreased overall survival and can be targeted by TKIs. The wildtype FLT3 cannot be inhibited by TKIs but offers an excellent expression profile to be targeted by antibody-based FLT3-specific therapies, providing a therapy for many AML patients. One class of antibody-based therapies are antibody-drug-conjugates (ADCs), which unite the specificity of an antibody with the toxicity of a drug.

In this project, a novel FLT3 targeting ADC for AML treatment was developed. Firstly, FLT3 specific antibodies were generated, chimerized with human IgG1 and assessed for binding, affinity, internalization, epitope specificity and stability. By choosing the IgG1 backbone, the strategy of double targeting FLT3 and the Fc receptor CD64, which is also expressed on AML cells, was explored. The newly generated 20D9-mab was functionalized by coupling the tubulin inhibitor MMAF via the recently established P5- technology. 20D9-ADC showed strong and selective cytotoxicity in FLT3 positive cell lines *in vitro.* A clear advantage of FLT3 and CD64 targeting was detected *in vitro* by comparison of native 20D9-ADC with a deglycosylated 20D9-ADC, which is deficient in CD64 binding. *In vivo*, an effective response of aggressive AML cell lines and AML patient derived xenograft to 20D9-ADC independent from the tumor burden at start of treatment was found. Interestingly, *in vivo*, the deglycosylated 20D9-ADC achieved almost the same efficacy compared to the native 20D9-ADC, showing that double targeting of FLT3 and CD64 had no advantage in the mouse model. Further, it is already known that TKI treatment increased the surface expression of FLT3 on FLT3-ITD positive AML cells. Here, the combination of the FLT3 specific ADC with FLT3 TKIs was explored and an enhanced cytotoxic effect by synergistic mechanisms was shown. Further, hematotoxicity was evaluated in human CD43 positive cells, which were not affected by 20D9-ADC in concentrations in the range of IC_{50} values of AML cell lines, indicating a favourable toxicity profile.

In conclusion, these results show that FLT3 is a clinically promising target for ADC application which should be further evaluated in clinical studies in combination with FLT3 inhibitors.

Zusammenfassung

Die akute myeloische Leukämie (AML) ist eine maligne klonale myeloische Erkrankung mit einer geringen 5-Jahres-Überlebensrate, was den hohen Bedarf an neuen Therapieoptionen zeigt. In den letzten Jahren wurden fms like tyrosine kinase 3 (FLT3) spezifische Tyrosinkinase-Inhibitoren (TKI) zur Behandlung einer FLT3-ITD positiven AML zugelassen. FLT3 ist bei 93 % der AML-Patienten überexprimiert und bei etwa 23 % treten aktivierende FLT3-ITD-Mutationen auf, welche mit einem erhöhten Rückfallrisiko und einem verringerten Gesamtüberleben assoziiert sind und mit TKIs gehemmt werden können. Wildtyp FLT3 kann durch TKIs nicht gehemmt werden, bietet jedoch ein gutes Expressionsprofil und ist eine optimale Zielstruktur für eine antikörperbasierte Therapie, die für eine Vielzahl der AML Patienten anwendbar wäre. Eine vielversprechende antikörperbasierte Wirkstoffklasse sind Antikörper-Toxin-Konjugate (ADCs), welche die Spezifität eines Antikörpers mit der Toxizität eines Chemotherapeutikums vereinen.

In diesem Projekt wurde ein FLT3 spezifischer ADC für die Behandlung der AML entwickelt. Zunächst wurden FLT3-spezifische Antikörper erzeugt, mit humanem IgG1 chimärisiert und auf Bindung, Affinität, Internalisierung, Epitopspezifität und Stabilität untersucht. Durch die Wahl des IgG1-Rückgrats wurde zusätzlich zur FLT3 Bindung auch eine Spezifität zum Fc Rezeptor CD64, welcher auf AML Zellen exprimiert ist, generiert. Der so hergestellte 20D9-mab wurde mittels der neu etablierten P5-Technologie an den Tubulin-Inhibitor MMAF gekoppelt. In FLT3-positiven Zelllinien *in vitro* wies der 20D9-ADC eine starke Zytotoxizität auf und es konnte ein klarer Vorteil der doppelten Spezifität durch den Vergleich von 20D9-ADC mit einem deglykosylierten 20D9-ADC, welcher defizient für die CD64 Bindung ist, festgestellt werden. *In vivo* wurde ein Ansprechen von AML-Zelllinien und AML-Patienten-abgeleiteten Xenograft-Zellen auf den 20D9-ADC unabhängig von der Tumorlast zu Beginn der Behandlung gezeigt. Interessanterweise erreichte der deglykosylierte 20D9-ADC fast die gleiche Wirksamkeit wie der native 20D9-ADC. Dies zeigt, dass die zweifache Spezifität zu FLT3 und CD64 im Mausmodell keinen Vorteil hatte. Es ist bereits bekannt, dass die TKI-Behandlung die Oberflächenexpression von FLT3 auf FLT3-ITD-positiven AML-Zellen erhöht. Die Kombination des FLT3-spezifischen ADC mit FLT3-TKIs wurde untersucht und es konnte eine synergistische zytotoxische Wirkung beider Substanzen gezeigt werden. Außerdem wurde die Hämatoxizität des 20D9-ADC in humanen CD43-positiven Zellen untersucht. Konzentrationen des 20D9-ADC im Bereich der IC_{50}-Werte von AML-Zelllinien führten zu keiner Toxizität, was auf ein günstiges Toxizitätsprofil hinweist.

Zusammenfassend zeigen unsere Ergebnisse, dass FLT3 ein klinisch vielversprechendes Ziel für eine ADC-basierte Therapie in der AML ist und eine Kombination des 20D9-ADC mit FLT3-Inhibitoren in klinischen Studien weiter evaluiert werden sollte.

1 Introduction

About 400 BC, Hippocrates described outwardly visible, malignant solid tumors with surrounding dark veins to look like a crab stretching their arms on all sides. He named them *karkinos*, the greek word for crab, from which the modern word cancer was derived[1]. It took until the 19th century until the understanding of tumors as a mass of cells rather than an imbalance of body fluids emerged. After Theodor Boveri discovered the genetic basis of cancer 1902, the understanding of the cancer biology, mutations and clonal evolution was radically transformed[2]. Cancer occurs in almost all types of tissue and can be classified based on its cellular origin and morphological appearance. In total, over 100 types of cancer have been described until today and they all share common features like uncontrolled proliferation, insensitivity to growth repressors, resistance towards cell death, the ability to induce angiogenesis, formation of metastasis, the escape from the body's immune system and an adjusted energy metabolism[3,4].

In 2020, approximately 19.3 million new cases of cancer were diagnosed and 10 million deaths caused by cancer were documented worldwide[5]. According to the world health organisation (WHO) cancer is the second leading cause (20 %) of death after cardiovascular diseases. The most common diagnosed cancer in the United States (US) is breast cancer among women (30 %) and prostate cancer among men (26 %). Hematologic malignancies, comprising leukemia and lymphoma, account for 7-9 %[6]. Nowadays, in the western world, cancer can be cured if detected early. But more than 70 % of all cancer deaths occur in low- and middle-income countries, which have few or no resources for prevention, diagnosis and treatment of cancer [7].

1.1 Acute myeloid leukemia

1.1.1 Incidence and symptoms of AML

Acute myeloid leukemia (AML) is a malignant clonal myeloid malignancy characterized by uncontrolled growth of differentiation-arrested hematopoietic stem and progenitor cells. AML accounts for approximately 25 % of all leukemias and is therefore the most frequent form of leukemia in adults. In the US the incidence of AML is 4.3 per 100,000 inhabitants annually (SEER data 2016-2018), with 20,240 estimated new cases in 2021. The 5-year survival was 29.5 % (SEER data 2011-2017), resulting in 11,400 estimated deaths for 2021. AML is primarily a disease of later adulthood with a median age of onset of 68 years, but also young children and teens can be affected with an incidence of 0.8 per 100,000[8,9].

Symptoms of AML are fatigue, bleeding and susceptibility to infection and fever due to anemia, thrombyocytopenia and granulocytopenia. High numbers of leukemic blasts are found in the peripheral blood (leukocytosis) and if the number exceeds 100,000 cells/µl, there is a risk of

leukostasis resulting in hypoxia, dyspnoe, retinal hemorrhages and neurological symptoms like headache, somnolence and coma. Aleukemic cases with normal or even reduced white blood cell counts are less common but occur in secondary or therapy-associated AML. In the myelomonocytic/monoblastic AML subtype, extramedullary manifestations such as skin infiltrates, meningiosis leukaemica, gingival hyperplasia and infiltration of the spleen and liver are observed. Risk factors for AML are exposure to radioactive radiation, benzenes, petroleum products, paints, ethylene oxides, herbicides, pesticides and smoking. AML is often associated with myelodysplastic syndromes (MDS) und age-associated clonal hematopoiesis (ARCH/CHIP). Further, a preceding therapy of a tumor disease with cytostatics (e.g. alkylating agents, anthracyclines, anthraquinones, epipodophylotoxine) can promote AML development[10–13].

1.1.2 Pathophysiology of AML

In normal hematopoiesis, multipotent hematopoietic stem cells give rise to common myeloid progenitor cells which differentiate to megakaryocytes/platelets, erythrocytes, granulocytes and monocytes/macrophages and common lymphoid progenitor cells, which develop to B-cells, T-cells and natural killer cells. In leukemia, hematopoietic stem cells or progenitor cells acquire mutations and abnormal proliferative potential and develop to leukemic stem cells which give rise to a bulk of immature blood cells. According to the affected cell type, leukemia is classified as myeloid or lymphatic leukemia. Further, it is sub-classified into chronic leukemia which is slow growing and acute leukemia which is fast growing[14,15]. Acute myeloid leukemia originates from differentiation arrested myeloid precursor cells in bone marrow and blood, and can develop as *de novo* AML or as *secondary* AML (approximately 25 %) based on myelodysplasia-related changes or as therapy related AML after a cytotoxic agent or radiation[16,17].

The abnormal proliferation is driven by cytogenetic abnormalities, gene fusions and mutations that lead to abnormal protein function, altered expression and epigenetic changes. 40 % of AML patients have cytogenetic aberrations like chromosomal aneuploidies (e.g., -5/-5q. -7, and -17/-17p) or translocations t(8; 21), inv(16)/t(16; 16), t(9;11), t(6;9), inv(3)/t(3;3) or t(15,17) leading to RUNX1-RUNX1T1, CBFB-MYH11, KMT2A-MLL, DEK-NUP214, GATA2 MECOM or PML-RARA fusion genes. Often, more than 3 chromosomal aberrations are detected (complex karyotype)[16]. Multiple mutations in genes involved in signal transduction, transcription factors, chromatin modifiers, cohesin complex, RNA splicing, tumor suppressors and DNA methylation play an important role for stratification, prognosis and prediction of therapy response (Figure 1). The most frequent mutations are FLT3 (39 %), NPM1 (33 %) and DNMT3A (31 %), NRAS (22 %), RUNX1 (15 %), IDH2 (14 %), WT1(13 %), TP53 (9 %) and CEBPA (8 %). Also, KIT, ASXL1 and TET2 are often mutated. Compared to most solid-tumor malignancies, the AML genome has fewer

mutations in coding regions with an average of only 5. However, at least one driver mutation or fusion is identified in 96 % of patients with *de novo* AML, with 86 % harbouring ≥2 driver mutations[18–21]. Among others, RUNX1 or GATA2 mutations also occur as germline mutations in the hereditary myeloid malignancy syndromes[17].

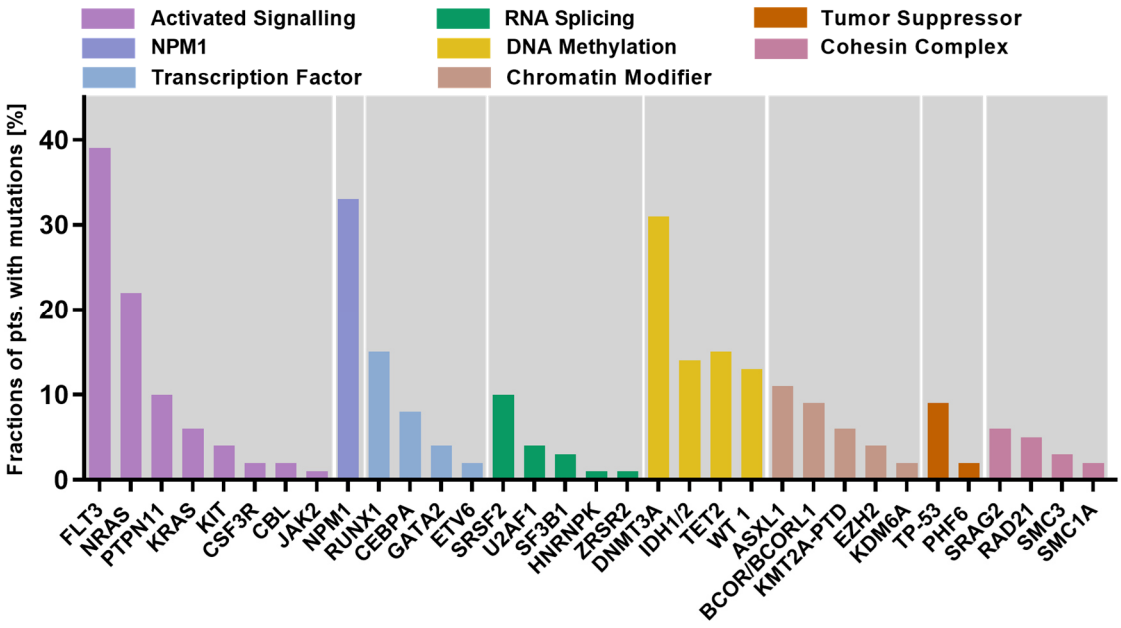

Figure 1 Driver mutations in AML summarized in specific functional groups. Histogram illustrating driver mutations detected in >1 % of patients in a cohort of 664 AML patients. Data obtained from Metzeler et al.[18]

1.1.3 Diagnosis and prognosis

Cytomorphology, immunophenotyping, cytogenetics and molecular genetics of blood and bone marrow samples are necessary to make the diagnosis and determine the subtype of leukemia. Since AML is very heterogenous, a precise subtyping is important for prognosis, disease monitoring and treatment decision. There are two different systems for diagnosis and subclassification, the old American-French-British (FAB) system and the newer World Health Organization system, which is currently used[22]. Briefly, a myeloblast count of ≥20 % of the peripheral blood and recurrent genetic abnormalities define the AML diagnosis[16]. The overall 5-year survival rate in the US is currently 29.5 % (SEER data, 2011-2017). The rate is strongly depending on age. Children with the age of 0-14 years have a 5-year survival of 67 % while patients older than 65 years have only 5 %, having poor tolerance of intensive chemotherapy and increased risk of treatment-related mortality [14]. The survival of de novo AML has changed since the 1970s significantly as reported from MD Anderson data from 1970 to 2017. Especially in patients <60 years, as they had a 5-year survival rate of 13 % in the 1970s and 55 % in the 2010s. In older patients, the improvement of survival was from 8 % (1970s) to 17 % (2010s). If untreated, AML leads to death within few weeks to months[23].

The mutations and chromosomal abnormalities not only play a role in diagnosis but also in prognosis. According to the ELN guidelines for risk stratification, there are favourable, intermediate and adverse risk groups[16]. The combination of different mutations is crucial for the prognosis. For example, mutated NPM1 without FLT3 mutations is favourable but mutated NPM1 with FLT3-ITD mutation has an intermediate risk profile[16]. Besides the risk stratification, that account for the current treatment options related to the mutational and cytological status, another decisive factor for prognosis is the age. Since AML occur mostly in older patients, several comorbidities and poor general conditions do not allow the application of available therapy options. Patients <60 years have an estimated 5-year overall survival (OS) of 64 % (favourable), 42 % (intermediate) and 20 % (adverse-risk)[24]. Patients aged ≥60 years, 5-year OS rates were 37 %, 16 %, and 6 %, respectively.[24] Acute promyelocytic leukemia (APL) holds a special position, the prognosis of which is the highest of all AML subentities with a long-term survival rate of over 80 %.

1.2 AML treatment

Only in the second half of the 20th century, scientific advances and profound insights into cell biology and genetics led to therapy options beyond radiation and surgical intervention[25]. In the mid-twentieth century, chemotherapy was applied successfully in pediatric acute lymphoid leukemia first and was then widely used for treatment of other cancer entities[25]. Chemotherapy works by inhibition of proliferation via different mechanisms. Fast proliferating tumor cells but also healthy hematopoietic stem cells, hair follicles cells, epithelial cells in the mouth and digestive tract and cells of the reproductive system are attacked, which leads to side effects[26].

1.2.1 Conventional therapy

In the 1970's, anthracyclines and cytarabine (ara-C) were effectively combined in a 7+3 treatment scheme in AML and are considered as the standard of care since then[27]. The treatment consists of 3 days anthracycline (daunorubicin or idarubicin or mitoxantrone), that inhibit RNA and DNA synthesis, combined with 7 days continuously infusion of cytarabine, which inhibits DNA polymerase. The aim of the highly intensive induction chemotherapy is clearing of leukemic cells from blood and bone marrow. Afterwards, the healthy hematopoietic stem cells should at least partly recover the blood cells leading the patient in complete remission (CR) or complete remission with incomplete hematologic recovery (CRi) or partial remission (PR)[16]. Age and fitness are the most important factor to decide if the 7+3 treatment scheme is applicable. In the worst

case, patients can only receive supportive care, including growth factors and/or blood transfusions.

In remission, a consolidation therapy should prevent relapse. The conventional post remission therapy consists of high dose cytarabine for patients with favourable risk. Patients with adverse and intermediate-risk features should be considered for allogeneic stem cell transplantation. Patients considered not as candidates for intensive therapy receive demethylating agents like azacytidine or decitabine that can be combined with venetoclax[16,23]. Demethylating agents are thought to reactivate silenced tumor suppressor genes through DNA hypomethylation and induce DNA damage and apoptosis[28]. One exception from this standard treatment scheme represents the AML subtype APL. It is treated (and mostly cured) with all-trans retinoic acid and arsenic trioxide, which degrade the oncogenic fusion PML-RARa.

1.2.2 Newly approved therapy options

Since 2017, new therapies were approved by the FDA in the US. Already known established therapies are available in different formulations providing better bioavailability like liposomal cytarabine and daunorubicin (CPX-351, 2017) and oral hypomethylating agents like oral azacytidine (CC-486, 2020) and oral decitabine-cedazuridine (2020)[28].

Unravelling the heterogeneity of AML at the cytogenetic and molecular level allowed a precise subtyping of the disease and the association with outcome and treatment efficacy, which improved the risk stratification and treatment decision. Further, the knowledge of expression patterns and functional disease mechanisms allow the development of targeted therapy for specific AML subsets. Inhibitors against FLT3, Bcl-2, IDH1/2 and the hedgehog pathway were recently approved by the FDA (Table 1)[29,30]. Further, Gemtuzumab ozogamycin (Mylotarg), a CD33-specific antibody-drug-conjugate (ADC), delivering the toxic agent calicheamicin to CD33 expressing AML cells, was reapproved 2017. It is used in adults with newly diagnosed CD33-positive AML and refractory-relapsed CD33-positive AML in patients ≥2 years of age [23].

Name	Target	Therapy	Approval
Midostaurin	FLT3	With 7+3 in newly diagnosed FLT3 AML	2017
Gilteritinib	FLT3 ITD/TKD	R/R AML with FLT3 mutations	2018
Venetoclax	Bcl-2	With azacytidine in de novo AML, unfit for 7+3	2018
Enasidenib	IDH 1	R/R AML with IDH2 mutation	2017
Ivosidenib	IDH2	R/R AML with IDH1 mutation	2018
Glasdegib	SMO receptor	With low dose chemotherapy in newly diagnosed AML	2018

Table 1 Approved inhibitors for AML therapy. Adapted from Stanchina et al.[31]

1.2.3 Next generation targeted therapies

In the last years, the field of therapy regimes is growing rapidly, and some new approaches are evaluated in preclinical and clinical studies. There are new inhibitors in development that target mutated FLT3, quizartinib and crenolanib. The tyrosine kinase inhibitor sorafenib is approved in other indications but is currently investigated in consolidation therapy of ITD-positive AML after stem cell transplantation. In AML, alterations of the MAPK signalling pathway are common, therefore the MEK1/MEK2 inhibitors selumetinib and trametinib are tested in relapsed or refractory RAS-mutated AML. In the setting of TP53 mutated AML, the TP53 modulator APR246 might improve prognosis [20,32]. As targeting the apoptotic pathway with venetoclax was successful, the inhibition of the frequently over expressed anti-apoptotic protein MCL1 is evaluated[20]. Apoptosis can also be dysregulated through functional inactivation of the p53 protein via MDM2 binding. Several MDM2 inhibitors (e.g. idasanutlin, milademetan) are evaluated in patients with AML[20,32].

AML specific expression of antigens can be used for targeting therapy using monoclonal antibodies or antibody-conjugates. Antibodies enhancing the T-cell immune responses to AML, like bispecific T-cell engagers targeting CD33xCD3 (BiTE® AMG 330) or CD123xCD3 (XmAb14045) deliver promising results. Besides the approved Mylotarg, other CD33-ADCs are in development and ADCs against new targets like CD123[33,34], FLT3[35] and CLL-1[36]. Antibodies can be also coupled to radioisotopes, for example anti-CD33 antibody–radioisotope conjugate 225Ac-lintuzumab and CD45-targeted radioisotope antibodies (e.g. Iomab-B or 90Y-BC8-DOTA)[20,32].

AML cells often have increased expression of inhibitory coreceptors modulating the T-cell checkpoints, sending a “don’t eat me” signal to the cells of the immune system. Blockade of these inhibitory checkpoints by anti-CTLA4 (ipilimumab), anti-PD-1 (nivolumab) and anti -TIM3 (INCAGN02390) demonstrated promising immune-mediated antileukemic effect. Targeting “macrophage checkpoints” with anti-CD47 antibody (magrolimab) blocks the CD47- SIRPα interaction and enhances macrophage-mediated phagocytosis[23].

The development of chimeric antigen receptor (CAR) T-cells for AML is also ongoing. This therapy is based on patient-specific T-cell receptor-target engineered T cells, that are retransfused in the patient and enhance the immune response against the specific target. Targets including CD33, CD123, CLEC12A are under investigation but none have shown clear efficacy and safety in AML treatment. Since AML harbours no exclusively specific antigen, the development of CAR-T cells is facing several issues [20,32].

1.2.4 Therapy resistance and relapse

One of the major challenges in the treatment of AML are therapy resistance and relapse. Since AML is a heterogenic disease, it comprises several populations that may harbour mutations leading to therapy resistance. Applying the 7+3 regimen, CR is achieved in 60 % to 80 % of younger adults and in 40- 60 % of older adults (60 years or above)[16,37,38]. Salvage chemotherapy regimens in younger patients not responding to initial induction chemotherapy are reported with CR rates ranging from 40- 65 %, for older patients ~30 %[39]. After successful initial therapy response and remission, relapse is one of the major challenges in AML treatment. It results from the survival of leukemic stem cells despite intensive chemotherapy or even stem cell transplantation. It can be caused by several mechanisms of clonal evolution: (1) a resistant subclone with leukemic-initiation capacity was already present in diagnosis, persisted undetected during treatment and grows out; (2) a leukemic cell, that harbours early and late leukemogeneic driver mutations acquires new mutations during therapy, persists and grows out; (3) all leukemic main and subclones were similarly sensitive towards therapy, but clearing the niche altered the dynamic evolutionary landscape allowing a faster rise of a fitter sub clone[40]. Relapse occurs in 40-50 % of younger and the great majority of elderly patients. In higher risk AML patients, the relapse rate is over 60 %[39]. The prognosis in relapsed AML patients is generally poor but depends largely on the timing of relapse (early versus late) and the possibility of (second) allogeneic hematopoietic stem cell transplantation[41]. Patients with relapsed and/or refractory disease have cure rates of less than 10 %[42].

The detection of minimal or measurable residual disease (MRD) in peripheral blood or bone marrow by flow cytometry or qPCR in remission allows the identification of persistent AML cells far below the morphology-based 5 % blast threshold[43,44]. The identification of the MRD status can refine clinical decision-making, for example early stem cell transplantation for MRD positive patients or treatment reduction for MRD negative patients.

1.3 Fms-like tyrosine kinase 3

1.3.1 Expression and function

The human fibroblast-macrophage stimulating factor like tyrosine kinase receptor 3 (FLT3) gene is located on chromosome 13q12, consists of 24 exons and encodes the FLT3 protein comprising 993 amino acids. FLT3 protein is N-linked glycosylated which increases the molecular weight from 110 kDa to 155 kDa[45]. FLT3 is a member of the class III protein receptor tyrosine kinases (RTK) that are characterized by five immunoglobulin-like domains, a juxtamembrane (JM) and two protein tyrosine kinase domains (TKD) separated by an interkinase domain. The first three

of the five IgG-like modules are responsible for binding the FLT3 ligand, while the other two mediate receptor dimerization. The receptor is monomeric in the inactive state and has structural similarities to KIT, CSF1R, PDGFRα and PDGFRβ. After translation, RTKs are transported via the Golgi apparatus to the plasma membrane where they undergo constitutive internalization (endocytosis). Since constitutive internalization is much slower than the transport, the receptors accumulate at the cell surface. The extracellular domain is glycosylated and has a high affinity for the FLT3 ligand (FL). The FLT3 Ligand is expressed from a wide range of tissues as membrane-bound precursors that can be proteolytically cleaved to release the soluble ligand or the soluble ligand is produced by alternative splicing. The ligand dimerizes, binds the FLT3 receptor, which oligomerizes and subsequent structural changes in the intracellular domain of FLT3 activate the receptor´s catalytic function. The autoinhibitory juxtamembrane domain is released from the kinase domain, making it accessible to ATP and initiate autophosphorylation on several tyrosine residues, which is considered as the hallmark of activation. This leads to activation of further effector pathways (PI3K, RAS and subsequently AKT, STAT, ERK) and subsequent internalization and degradation of the FL-pFLT3 complex[46,47]. Thus, the activation of FLT3 downregulates the recepotor cell surface expression mainly by clathrin-dependent endocytosis which is mediated through ubiquitinylation[48,49].

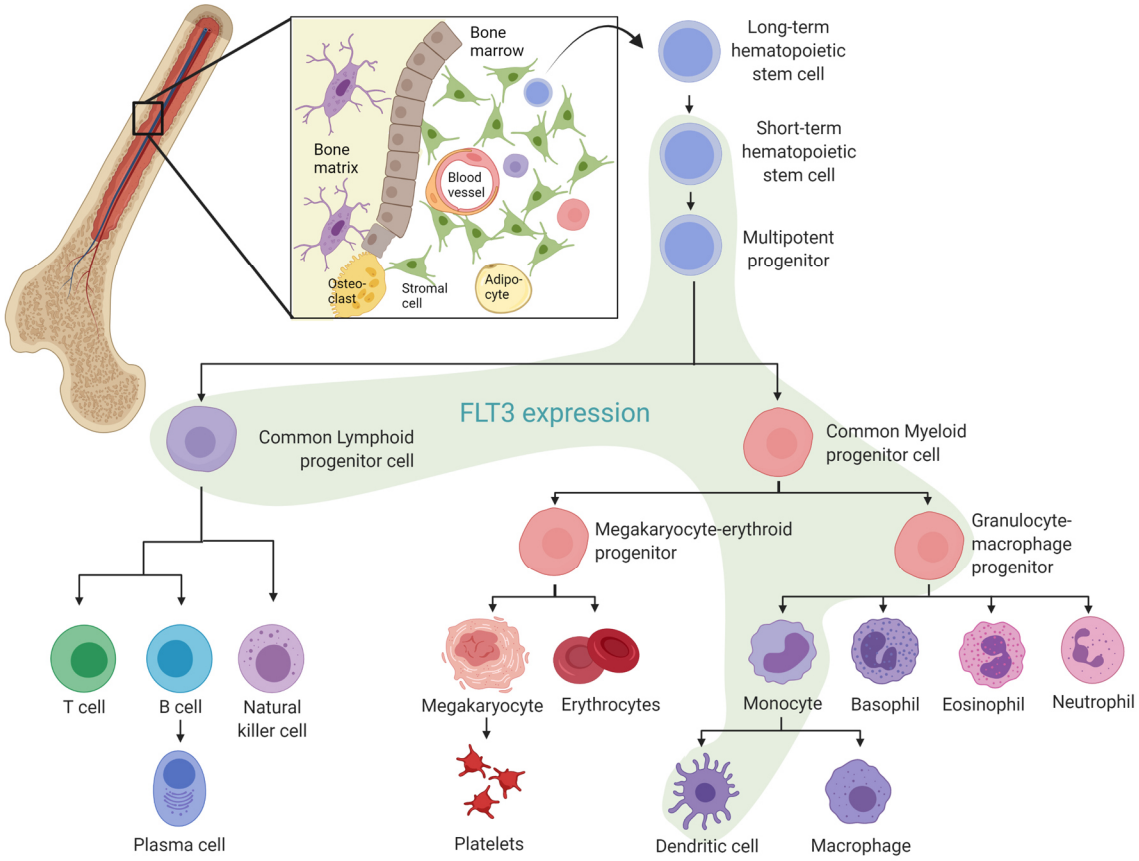

Figure 2 Expression of FLT3 in hematopoiesis. Adapted from Levis et al.[50]. Created with Biorender.

FLT3 is expressed in healthy bone marrow by a subset of CD34 positive hematopoietic stem cells, granulocyte/macrophage progenitors, B-lymphatic progenitors, while erythrocyte progenitor cells do not show FLT3 expression. Further, it is expressed on a subpopulation of differentiated monocytes, dendritic cells and NK cells. FLT3 is also expressed in non hemaotopoietic tissue like spleen, thymus, lymph nodes, brain and pancreas. For cerebellum and pancreas, the expression is reported as intracellular or at low levels[46,51–53]. FLT3 plays a role in hematopoiesis in survival and proliferation signalling. But FLT3 appears to be non-essential. In mice, knock out of FL or FLT3 is non-lethal, but it does reduce the capacity to repopulate an aplastic marrow and results in the marked absence of NK and dendritic cells [52,54].

1.3.2 The role of FLT3 in AML pathology

It was reported that the wildtype FLT3 receptor is expressed at high levels in 93 % of AML patients, almost 100 % of B-cell acute lymphoblastic leukemia and 87 % of T-cell acute lymphoblastic leukemia and plays a role in survival and proliferation of leukemic cells[46,55]. In a recent study of Brauchle et. al, they identified 78 % of AML samples to be positive for FLT3 expression. Due to the subclonal character of AML, interpatient heterogeneity of FLT3 expression was observed. Cell surface expression of FLT3 was also observed for leukemic stem cells (CD43+/CD83-) in 79 % of patients samples. Remarkably, the levels of AML bulk and leukemic stem cells were higher in comparison to normal hematopoietic cells and stem cells[56]. In another study, FLT3 was found to be particularly high expressed in M5 classified AMLs[57].

30 % of AML patients have activating FLT3 mutations, which can be divided into two categories: Internal tandem duplications (characterized by repetitive amino acid sequences) in the region that codes for the juxtamembranous domain (FLT3-ITD) and point mutations that involve amino acid substitution in the tyrosine kinase domain (FLT3-TKD)[47]. FLT3 mutations are found in all subtypes of AML while ITD are more prominent in the M5 Fab subgroup[58]. FLT3-ITDs occur in approximately 23 % of AML patients and originate from duplicated fragments of the coding region of the juxtamembranous domain (exons 14 and 15), which are inserted in a direct 5‘-3‘ orientation. The length of these ITDs can vary between 3 and 400 nucleotides and the mutation is most found in the heterozygous state. The FLT3-ITD mutation weakens the autoinhibitory function of the JM domain and ligand-independent oligomerization occurs, followed by phosphorylation. The constitutively activated receptors lead to uncontrolled proliferation. In contrast to the WT receptor and TKD mutants, ITD mutants strongly activate STAT5[59]. Because STAT5 activation alone is sufficient for cellular transformation, this pathway is probably the main signalling difference between wildtype and the ITD receptor and is important for cell growth. The anti-apoptotic effect of STAT5 is mediated by transcriptional regulation of cyclin D1, BCL-XL, PIM,

p21 and c-MYC[46,47,60–62]. FLT3-TKD mutations occur in approximately 8-12 % of AML patients, but there is no significant association with white blood cell counts or the cytogenetic profile. FLT3-TKD mutations cause an amino acid substitution in the TK domain. The substituted amino acids are part of the activation loop that prevents ATP and substrate from accessing the kinase domain when the receptor is inactive. FLT3-TKD mutations constitutively activate the receptor and growth factor-independent proliferation via RAS/MAPK, PI3K/AKT and STAT5 signalling occur[46,63].

Apart from AML, FLT3-ITD mutations are also reported in ALL and several fusion proteins involving FLT3 are reported in myeloproliferative disease[45].

1.3.3 Relevance of FLT3 for AML prognosis and treatment

FLT3 mutated AML shows similar response rates to induction chemotherapy but the remission is shorter. Especially FLT3-ITD are associated with an increased risk of relapse and decreased disease-free and overall survival[60,64]. They have impact on prognosis of AML patients and are part of the ELN risk stratification in combination with NPM1 mutations. FLT3-ITD with a high or low allelic ratio in combination with mutated or wildtype NPM1 mutation, respectively, has an intermediate risk status. Wildtype NPM1 and FLT3-ITD with high allelic ratio has an adverse prognosis[16]. The FLT3 allelic ratio is calculated by the ratio of the area under the curve of mutant to wildtype alleles (FLT3-ITD/FLT3-WT). Higher allelic burden of the FLT3-ITD mutation has been associated with worse outcomes[60]. Furthermore, FLT3-ITDs are associated with higher leukocyte count and higher degree of bone marrow infiltration (advanced leukemia)[47]. In relapse, it has been reported, that most of FLT3-ITD mutations in diagnosis are maintained and gain a higher allelic ratio in the relapse. Clonal evolution can also lead to gain of new FLT3 mutations (8 % FLT3-ITD and 2 % TKD) or to a loss of FLT3 mutated subclones[60]. Besides from mutations, a high level of FLT3 receptor expression was reported as risk factor[65]. Further, detecting mutated FLT3 in MRD has demonstrated prognostic relevance but is still controversially discussed[54].

In first line therapy, a mono therapy of FLT3 inhibitory agents is mostly not useful because only a proportion of blasts harbour mutated FLT3. In FLT3-mutated AML patients, the combination of 7+3 chemotherapy with midostaurin has resulted in an overall survival benefit (CR rate 59 % versus 54 %, median survival 74.7 vs 25.6 month, estimated 5-year survival 50 % vs 42 %)[66]. FLT3 targeting was also evaluated in the relapse setting. Gilteritinib was more effective than standard salvage chemotherapy in FLT3 mutated patients (CR 34 % versus 15.3 % and OS 9.3 months versus 5.3 months). Importantly, patients included in this study received no FLT3 targeting first

line therapy. If FLT3 inhibitors are more frequently utilized in first line therapy, its relevance in relapsed/refractory AML could change[54].

1.3.4 FLT3 specific therapy

The oncogenic signalling of FLT3 in AML cells represents the rational for development of targeted therapies against FLT3 and several small molecule tyrosine kinase inhibitors are already approved or in development[60]. FLT3 inhibitors can be stratified in first- and second-generation inhibitors. Midostaurin (PKC412), lestaurtinib (CEP-701), sunitinib (SU11248), and sorafenib (BAY43-9006) belong to the first generation and inhibit multiple kinases. The antitumor efficacy may not exclusively depend on FLT3 inhibition and the multi targeting can enhance side effects. For example, midostaurin targets FLT3, PKC, SYK, FLK-1, AKT, PKA, KIT, FGR, SRC, PDGFRα/β, VEGFR1/2. Next generation TKIs for example, gilteritinib, crenolanib, and quizartinib, have a greater FT3-specificity and already showed higher potency also when applied as single agent. Additionally, the TKIs differ in the inhibitory mechansims and are therefore divided in type I and II inhibitors. Midostaurin, gilteritinib, lestaurtinib, and crenolanib (type I inhibitors) both inhibit FLT3-ITD and FLT3-TKD, since they bind the FLT3 receptor in the active conformation. Quizartinib and sorafenib (type II inhibitors) mostly target FLT3-ITD because they bind at the ATP binding site in the inactive conformation and TKD mutations lead to active kinase conformation[67]. Resistance mechanisms are an emerging problem in the field of TKIs, for example accumulation of TKD point mutations using quizartinib or F691I/L gatekeeper mutation and mutations in the RAS pathway downstream of FLT3 signalling using gilteritinib. FF-10101 is a novel FLT3 inhibitor, which is currently in clinical trials. It binds covalently and irreversible to FLT3 and is mostly unaffected by common resistance mutations[54,67]. Interestingly, the TKIs not only inhibit the mutant FLT3 proliferative signalling, but also enhance the FLT3 expression level on the cell surface through upregulation of FLT3 and glycosylation of FLT3-ITD. Thus, TKI treatment can enhance the efficacy of FLT3-directed immunotherapy[68].

The overexpression of FLT3 in AML can be exploited by targeted therapies using antibodies, antibody-conjugates or CAR-T cells providing FLT3 specific therapies to patients independent of FLT3 mutations. There are several anti FLT3 antibodies, which rely primarily on antibody dependent cell-mediated cytotoxicity (ADCC) via natural killer (NK) cells. An anti-FLT3 Fc optimized mab (4G8 SDIEM) showed ADCC against FLT3-expressing cells in preclinical studies[69]. Another anti-FLT3 antibody (LY3012218, IMC-EB10) additionally prevents binding of the FLT3-ligand and downstream signalling, but the clinical study NCT00887926 was terminated due to lack of efficacy[70]. The new anti-FLT3 chimeric IgG1- antibody FLYSYN will be evaluated in a clinical study (NCT02789254, not yet recruiting)[71]. The use of naked monoclonal antibodies in

AML disease is challenging, because of qualitative defects of NK cells in AML patients, that may reduce the efficacy[20,72]. It might be more promising to specifically deliver a toxin via antibody-drug-conjugates to FLT3 positive AML cells or enhance the T-cell immune reaction by dual targeting of FLT3 and a T cell antigen. The anti-FLT3-CD3 immunoglobulin G (IgG)-based bispecific antibody (7370, Pfizer) and FLT3 x CD3 bispecific T cell engager (BiTE® AMG 427, NCT03541369) were reported to mediate T-cell dependent cellular cytotoxicity (TDCC); the latter is already in a clinical trial[56,73]. The development of a FLT3 specific ADC (AGS62P1) from Astellas Pharma was terminated due to lack of efficacy (NCT02864290)[35,74]. Chimeric antigen receptor (CAR) T-cell therapies are successful in other hematologic malignancies (ALL, diffuse large B-cell lymphoma, and multiple myeloma) but AML do not possess an exclusively AML-specific surface antigen, which may cause safety issues. Here, FLT3 might be a promising target, which is investigated for example by Jetani et al. with engineered T-cells expressing a FLT3-specific CAR with a targeting domain derived from 4G8 mab[75]. Further, the FLT3-specific CAR T-cell therapy using AMG 553 is already in clinical trials (NCT03904069)[76].

1.4 Antibody-drug-conjugates

ADCs consist of a monoclonal tumor antigen-specific antibody conjugated via a linker to a cytotoxic agent, named payload. After binding of the antibody to the antigen, the complex is internalized, and the payload is directly delivered to the cancer cell which might result in greater efficacy and less side effects (improved therapeutic index) compared to a normal chemotherapy. This therapeutic class is rapidly expanding and bridges conventional chemotherapy with targeted innovative immunotherapy.

1.4.1 Approved ADCs

Until now, ten ADCs have been approved by the FDA and all are in oncological indications: Adcetris®, Besponsa®, Mylotarg®, Polivy®, Blenrep®, and Zynlonta™ in hematological malignancys, Kadcyla®, Padcev®, Enhertu® and Trodelvy® in solid tumors (Table 2). More than 80 ADCs are currently under clinical development. Around 20% of them are in hematological indications[77]. The first-generation ADCs (Mylotarg) were developed in the early 2000s and faced several toxicity problems. Some improvements were made in the second-generation ADCs (Kadcyla, Adcetris), especially concerning higher levels of cytotoxic drug conjugation, lower levels of naked antibodies and more-stable linkers between the drug and the antibody. In the third generation ADCs, more stable conjugation chemistry and engineering of antibodies for site-specific drug conjugation solved deconjugation problems and enhanced homogeneity.[77,78]

ADC	name	target	antibody	linker	payload	indication	Manufacturer, Approval year	DAR
Hemaotologic malignancies								
Adcetris	Brentuximab vedotin	CD30	Chimeric IgG1	Val-Cit	MMAE	Previously untreated stage III or stage IV classical Hodgkins Lymphoma (cHL); relapsed or refractory cHL; cHL after failure of auto-HSCT or failure of at least two prior multi-agent chemotherapy regimens; systemic anaplastic large cell lymphoma, primary cutaneous anaplastic large cell lymphoma other CD30-expressing peripheral T-cell lymphoma	Seattle Genetics, 2011	4
Besponsa	Inotuzumab ozogamicin	CD22	Humanized IgG4	ActBut	Calicheamycin	Monotherapy in adults with relapsed or refractory B-cell precursor acute lymphoblastic leukemia (ALL)	Pfizer, 2017	6
Mylotarg	Gemtuzumab ozogamicin	CD33	Humanized IgG4	ActBut	Calicheamycin	Single-agent and combinational therapy in newly diagnosed CD33-positive acute myeloid leukemia (AML) in adults and relapsed or refractory CD33- positive AML in adults and pediatric patients (≥2 years)	Pfizer, 2000; 2017	2-3
Polivy	Polatuzumab vedotin	CD79b	Humanized IgG1	Val-Cit	MMAE	Combinational use with bendamustine and a rituximab product in adult patients with relapsed or refractory diffuse B-cell lymphoma	Genentech, 2019	3.8
Blenrep	Belantamab mafdotin	BCMA	Humanized IgG1	Maleimido-capryl	MMAF	Adult patients with relapsed or refractory multiple myeloma who have received at least 4 prior treatments	GSK, 2020	4
Zynlonta	Loncastuximab tesirine	CD19	Humanized IgG1	Valin-alanin	SG3249 PBD dimer	adult patients with relapsed or refractory large B-cell lymphoma after two or more lines of systemic therapy, including DLBCL not otherwise specified, DLBCL arising from low grade lymphoma, and high- grade B-cell lymphoma	ADC Therapeutics, 2021	2.3
Solid tumors								
Kadcyla	Trastuzumab emantisine	HER2	Humanized IgG1	SMCC	DM1	HER2-positive, metastatic breast cancer	Genentech 2013	3.5
Padcev	Enfortumab vedotin	Nectin-4	Human IgG1	Val-Cit	MMAE	Adult patients with locally advanced or metastatic urothelial cancer	Astellas Pharma, 2019	3.8
Enhertu	Trasuzumab deruxtecan	Her2	Humanized IgG1	Tetrapeptid	Exatecan-derivate topoisome	Adults with unresectable or metastatic HER2-positive breast cancer	Daiichi Sankyo 2019	8
Trodelvy	Sacituzumab govitecan	Trop-2	Humanized IgG1	Hydrol-ysable L2A	SN-38 Topo I inhibitor	Adult patients with metastatic triple-negative breast cancer who have received at least two prior therapies for metastatic disease	Immunomedics 2020	7.6

Table 2 Approved antibody-drug-conjugates. 4-(4′-acetylphenoxy) butanoic acid (AcBut); 7-ethyl-10-hydroxycamptothecin (SN-38); GlaxoSmithKline (GSK); Emtansine (DM1); Monomethyl auristatin E (MMAE); Monomethyl auristatin F (MMAF); Pyrrolobenzodiazepine (PBD); Succinimidyl 4-(N-maleimidomethyl) cyclohexane-1-carboxylate (SMCC); Trophoblast-cell surface antigen 2 (Trop2). Adapted from Dean et al[77].

1.4.2 Structure of ADCs and considerations for development

The critical characteristics of an ADC are 1) target antigen depending on indication, 2) type of antibody, 3) type of payload, 4) type of linker and spacer and 5) conjugation platform.

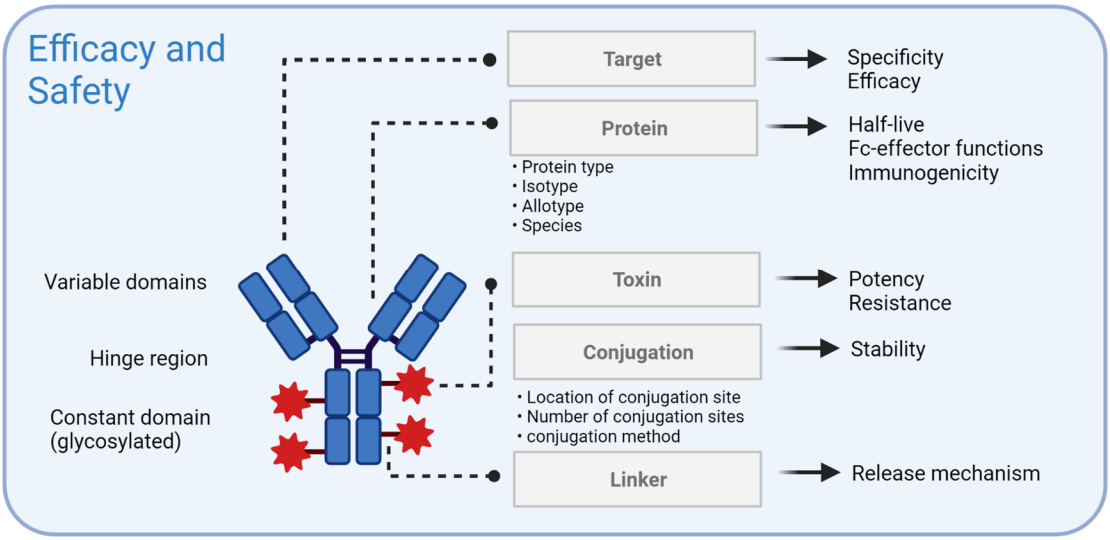

Figure 3 ADC structure and consequences for ADC performance. Adapted from Goulet et al.[79] and Dean et al[77]. Created with Biorender.

1.4.2.1 The target

The target molecule is specific for the disease and must be accessible by the circulating ADC. Mostly in oncological indications, target molecules are chosen on the surface of tumor or tumor stem cells but also targeting specifically the tumor microenvironment or tumor vasculature is an option. In any case, some critical parameters for choosing the optimal target should be considered. The receptor should not be shed into the circulation, this limits the amount of available ADC targeting the tumor. Ideally, target antigens should have a high expression level in tumors and little or no expression in normal tissues, or at least expression limited to a tissue type to reduce off-target toxicity[78,79]. The antigen density plays an important role, but there is no specific required density since various ADCs have shown efficacy over a wide range of antigen expression levels. Gemtuzumab ozogamicin has demonstrated efficacy at a relatively low expression of CD33 (5,000 to 10,000 receptors per cell)[80]. For most targets, a high internalization capability of the target receptor is important, but there are also ADCs which only exhibit their cytotoxic potential via the bystander effect and do not require internalization. Further, the mode of internalization

and therefore the trafficking route must be regarded, especially for ADCs requiring proteolytic activation of the toxin in the lysosomal compartment. Further, dual targeting of tumor antigens might be an advantage obtaining higher tumor specificity and reduced off-target effects and prevent resistance. ADCs targeting one antigen may be prone to tumor resistance mechanisms such as downregulation of the antigen receptor. Bridging a rapidly internalizing protein with a tumor specific marker is also another recent method to construct bispecific antibodies[77,81].

1.4.2.2 The antibody molecule

Antibodies are proteins of about 150 kDa weight and 10 nm in size, roughly forming a Y shape. All approved ADCs are full-length antibodies; there are also many constructs in development that are based on smaller antibody fragments, such as Fab-drug conjugates, scFv-drug conjugates, or nano bodies. The benefit of a fully human antibody is a longer half-live and slower clearance in comparison to the smaller formats. The monomeric isotype immunoglobulin G is often utilized for therapeutic ADCs. IgG has four subgroups defined by the heavy chains (HC), IgG1-IgG4. Except for IgG3, all of them are used to generate antibody-based drugs and differ in Fc effector function. The kappa light chain (LC) is usually preferred over lambda. A native antibody is composed of two identical HC and two identical LC which are assembled into three functional domains. Two domains are responsible for antigen binding (antigen-binding fragments (Fab)). The N-terminal region of the Fab-region contains the variable sequences both from heavy and light chain, which each form three loops, called the complementarity-determining regions (CDR), responsible for the antigen binding. The Fc domain binds to Fc receptors to elicit effector functions on immune cells. Finally, antibodies are modified with glycan molecules that fine-tune FcR interactions[79]. In IgG1, two pairs of interchain disulfide bonds in the flexible hinge region link the heavy chains to each other and one pair links each heavy chain to its light chain.

Antibodies are typically derived in mouse or rat through immunization with the desired antigen and should be therefore chimerized or fully humanized to avoid human anti-mouse/rat response. Since some allotypes have proven to be immunogenic, they may be relevant to consider when developing therapeutic antibodies. The main allelic forms for IgG1 are G1m (z,a), G1m (f), and G1m (f,a). For example, the G1m (f) allele is only found in caucasians, whereas the G1m (f,a) allele is common in orientals[82].

<u>Antigen interaction</u>

The antibody should have a high target specificity, which is defined by low or none cross-reactivity with other human tissue antigens to minimize side effects and toxicity[79]. Cross-reactivity to animal orthologues may be desirable to simplify toxicity studies. It is discussed and not clear, whether

there is a required maximum affinity for effective ADCs, but binding affinity around Kd = 10 nM is common for effective internalization. A rapid internalization can raise both efficacy but also safety simultaneously since it reduces the opportunity for off-target release. Ideally, affinity and internalization upon binding is efficient in target-overexpressing tumor cells but inefficient in healthy tissue with low level of target expression. Also the internalization efficacy is not only depending on the target but on the antibody itself and has to be considered when choose the lead antibody candidate[81].

Fc interactions

In the development of ADCs, the IgG subtypes IgG1, IgG2 or IgG4, which differ for example in effector functions, half-life and number of disulfide bonds, are used. The IgG3 subtype shows proteolytic and pharmacokinetic instability and is therefore not suitable. A major distinction can be made between IgG2/IgG4, which show reduced affinity to a number of FcγR and IgG1/IgG3 that interact efficiently with most FcγR and enhances effector functions[82]. In humans, there are 6 FcγRs: FcγRI (CD64), FcγRIIa (CD32a), FcγRIIb (CD32b), FcγRIIc (CD32c), FcγRIIIa (CD16a) and FcγRIIIb(CD16b) that differ based on the affinity of IgG binding and the downstream response of binding. The FcγRIIb is an inhibitory receptor, all others are activating receptors. In general, most FcγRs have a low affinity for IgG and thus bind only to oligomeric immune complexes. FcγRI binds with high affinity to physiological concentrations of monomeric IgG1, IgG3, and IgG4. Myeloid cells such as macrophages, monocytes, and dendritic cells express FcγRI and FcγRIIa. These receptors are involved in antibody-dependent cellular phagocytosis (ADCP). FcγRIIIa is highly expressed on NK cells and is responsible for ADCC[79]. Interestingly, many AML cells, especially monocytic AMLs also express Fc receptors[83,84]. Further, the IgG1 Fc fragment also regulates the half-life of the antibody in circulation through its interaction with neonatal Fc receptor.

1.4.2.3 The drug

The payload (also termed warhead) is one key component of ADC exerting cytotoxic effects and should meet the following requirements: (1) highly cytotoxic, usually with the IC_{50} value at low nanomolar or picomolar level, too toxic for a stand-alone treatment, (2) well defined target and action mechanism, (3) potential chemical attachment site for conjugation to the antibody, (4) relative hydrophilicity, (5) a lack of susceptibility to multidrug resistance transporter 1 (MDR1) which is a common resistance mechanism[78,85].

The first methotrexate-, doxorubicin- and vinca alkaloid-based ADC were not potent enough and failed in the clinical studies. Now, many ADCs incorporate the microtubule inhibitors like maytansine derivatives (DM1/DM4), auristatins (MMAE/MMAF) and tubulysins. Tubulin

inhibitors typically induce apoptosis in cells undergoing mitosis by causing cell cycle arrest at G2/M. Therefore, they selectively eradicate rapidly proliferating cells but may not be effective toward cells that are not highly proliferative. Another group of ADC toxins are DNA damaging drugs e.g. calicheamicin, pyrrolobenzodiazepines and indolinobenzodiazepine, duocarmycins and camptothecin, targeting the minor groove of DNA and can address also quiescent cells. Payloads such as topoisomerase inhibitors (e.g. quinoline alkaloids SN- 38), are gaining interest as cytotoxic agents that may be less toxic, allowing for ADCs with a higher DAR. Some new innovative drugs for ADC generation are e.g. Bcl-xL inhibitors (apoptosis inducers), thailanstatin (targeting the spliceosome) and amatoxins (transcription inhibitors)[77,85].

It was reported that some side effects and toxicity in clinical studies of ADCs are related to the toxin. For example, neutropenia and peripheral neuropathy were consistently reported for MMAE, thrombocytopenia and hepatic toxicity for DM1, and ocular toxicity for MMAF. Many ADCs are discontinued in clinical studies due to lack of efficacy or high toxicity. Both can be influenced by choosing a suitable toxin for the indication and desired mechanisms of the ADC[86,87].

1.4.2.4 The linker

The chemical linker covalently joins the antibody and the cytotoxic payload and plays a critical role in stability and drug release. The linker should (1) not induce aggregation and ensure solubility, (2) limit premature release of the drug and (3) efficiently release the toxin at the targeted site[85]. Since (part of) the linker remains attached to the toxin, it is important that the function of the toxin is not altered. Additionally, drugs are mostly hydrophobic, which leads to difficulties in conjugation but more importantly, makes them more sensitive to multidrug transporters. It was reported that the incorporation of a hydrophilic PEG(4) to the linker leads to a more hydrophilic drug complex, that is less sensitive to MDR1 transport, thus avoiding MDR1-mediated resistance[88].

There are two classes of linkers, cleavable and non- cleavable. Non-cleavable linkers have better plasma stability and the antibody must be degraded in the lysosome to release the toxin-linker construct. The toxin-linker construct is active intracellular but usually cannot exert bystander effects due to the higher hydrophobicity. One example for a non-cleavable linker is SMCC (N-succinimidyl-4-(maleimidomethyl) cyclohexane-1-carboxylate) in trastuzamab-emantisine[89]. Cleavable acid-sensitive likers have acid-sensitive hydrazone groups which remains stable in systemic circulation (pH 7.5) and gets hydrolyzed in lysosomal (pH 4.8) and endosomal (pH 5–6) acidic environment. This linker type is for example found in Mylotarg. Protease-cleavable peptide linkers, for example the cathepsin B- sensitive valine-citrulline linker, is used in Adcetris.

Proteases are inactive in high pH (serum) and active in low pH lysosomes, where the dipeptide linker gets cleaved. Further, other linker types are available, for example glutathione-sensitive disulfide linkers and β-Glucuronidase-sensitive linkers[85].

1.4.2.5 The conjugation

The conjugation strategy and chemistry influence the (1) number of toxins per antibody (Drug to Antibody Ratio, DAR), (2) homogeneity of the product, (3) proportion of unconjugated antibodies and the (4) stability of the covalent binding, which in turn impact the efficacy and toxicity profile.

Lysine residues already present within the polypeptide structure can be used as a point of conjugation. The average IgG1 molecule possesses approximately 90 lysine residues and 30 of these are exposed to the surface. The lysine- amine coupling results in a DAR of 0-8 and heterogeneity with about one million different ADC species. This strategy was applied for generation of the first ADCs e.g. Mylotarg, facing several stability and aggregation issues. Additionally, this stochastic conjugation methods left half of the antibody unconjugated. Another reactive group in the antibody molecule are the cysteine residues, which are covalently linked in 4 disulfide bridges. The most prominent example for this conjugation method is Adcetris[78,90]. A DAR of 8 and homogeneous product can be obtained with a full conjugation and all lower DARs implicate a higher product heterogenicity. Further, the type of chemical reaction is important for the serum stability of the ADC and strongly depends on the chemical characteristics of the conjugation. Maleimide conjugation to lysin and cysteine residues, as applied for example in Adcetris, is susceptible towards retro-Michael-additions. This leads to premature drug cleavage during circulation and reattachment to reactive thiol groups of albumin, free cysteine or gluthation (maleimide exchange). Thereby, they show a higher off target cytotoxicity[78,90].

The maleimide technology is an easy click chemistry widely used for bioconjugation. Recently, an improved click chemistry was developed from Kasper et al using ethynylphosphonamidates (P5-technology) as new reagents for the generation of ADCs from native non-engineered monoclonal antibodies. Further, ethynylphosphonamidates can be easily substituted with hydrophilic residues for optimizing the solubility[90,91].

To obtain a defined DAR, a variety of novel approaches for the site-specific drug conjugation has been developed over the last years. Site- specific technologies range from chemical methods, to genetic engineering and chemoenzymatic manufacturing and have the potential to broaden the range of possible chemical reactions[92,93]. For example, an approach to reduce heterogeneity of cysteine-based conjugated ADCs is the engineering of additional cysteine residues to the antibody leaving the interchain disulfides untouched, this was first done by Junutula et al, called

THIOMAB[94]. Another option is incorporation of unnatural amino acids containing a bioorthogonal handle that enables the site-specific attachment of a payload in the presence of all naturally occurring functional groups. One example is here the enzymatical method Tub tag labelling. A recombinantly fused motif on the antibody is recognized by the enzyme tubulin-tyrosine-ligase, which attaches an unnatural tyrosine derivate that carries uniquely reactive groups for chemo selective conjugation such as strain-promoted alkyne azide cycloadditions[92,95,96].

1.4.3 Mechanisms of action of ADCs

ADCs are very complex biochemical molecules and the mechanism of action is just beginning to be understood. ADCs require in many cases processing and metabolization by the target cells before they exert their function.

ADCs have poor oral bioavailability and are administered intravenously to prevent degradation by digestive enzymes. Due to incomplete conjugation or linker lability, ADCs circulate as three components: naked antibody, free payload and intact conjugate. The percentages of each component vary between ADCs, depending on their stability characteristics and change over time after administration. For example, the ADC trastuzumab-emantisine has a half-life of 4 days in human plasma. ADCs are large molecules and the delivery into tumor tissue via passive diffusion can be inefficient and it is reported that only a small fraction of the administered ADC dose reaches tumor cells. After binding the target, the ADC seem to retain the functionality of their naked mab counterparts and can excert for example inhibitory signals or prevent ligand binding. After binding, the ADC is internalized via clathrin- or caveolae-mediated endocytosis and shuttled to early endosomes, which mature into late endosomes before fusing with lysosomes. An antigen-independent process of pinocytosis is also described. After internalization, ADCs with cleavable linkers release their toxin in early endosome (acid labile linkers) or late endosome/lysosome (enzymatical cleavage and proteolysis). ADCs with non-cleavable linker undergo complex proteolytic cleavage in lysosomes. Following, the toxin is released from lysosomes to the cytoplasm and either targets DNA and induces single- or double-stranded DNA breaks or disrupts microtubules, resulting in apoptosis or other means of cell death. The time from antigen engagement to terminal processing and payload release can be >24 hours[80,93].

Some ADCs kill not only antigen-positive cells but also other cells in the vicinity irrespective of the expression of the target antigen. This bystander effect can occur via different mechanisms. It was reported that extracellular payload release in tumor tissue can occur with most linker types, owing to the redox environment, low pH and extracellular proteases found in the tumor microenvironment. Moreover, an intracellularly released toxin with lipophilic properties can

diffuse in the microenvironment of the targeted cell. For ADCs that incorporate MMAE, such as brentuximab vedotin, cleavage of the ADC releases MMAE, which is neutral of charge and able to cross biomembranes. In contrast, MMAF such as denintuzumab mafodotin, cleavage results in a metabolite with a charged carboxy- terminal phenylalanine residue. The bystander effect may overcome the challenge of heterogenous cell populations within a tumor since it extends the ADC's space of action. In turn, the off-target, off-tumor effects may lead to a enhanced side- toxicity[78].

The contribution of IgG– FcγR interactions to toxicity and efficacy are not clear yet. ADCs with an intact IgG1 or IgG2 backbone might activate the immune system via antibody dependent cellular toxicity (ADCC), complement-dependent cytotoxicity (CDC) or antibody dependent cellular phagocytosis (ADCP)[80]. For example, trastuzumab-emantisine was described to exert Fc receptor mediated engagement of immune cells, which may result in ADCC. Brentuximab has been described to induce ADCP *in vivo*, which is believed to contribute to the observed potent anti-tumor efficacy[97–99]. On the other hand, up- take and processing of ADCs by Fc-receptor bearing cells has been proposed as a potential mechanism of toxicity. T-DM1 affected FcR positive megakaryocytes and might result in thrombocytopenia, which was observed as side effect of Trastuzumab-emtansine[100]. In contrast, another group could not confirm these observations and described ADC induced micropinocytosis in megakaryocytes that leads to thrombocytopenia[101].

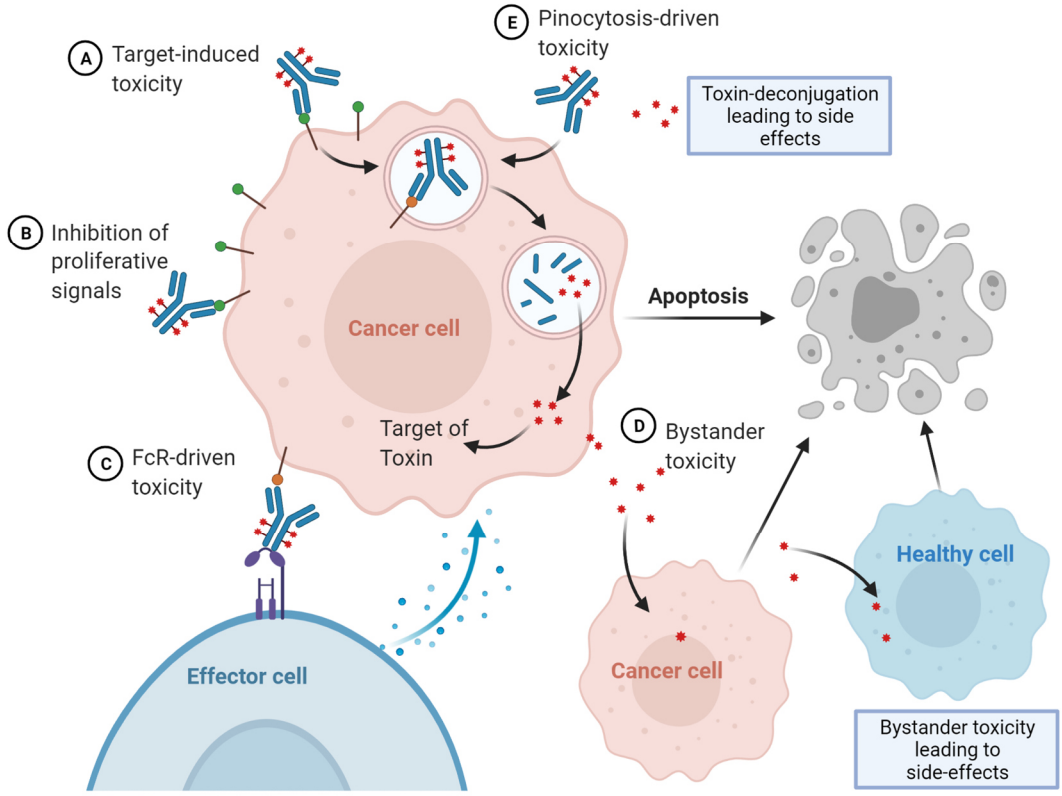

Figure 4 Mechanisms of action of antibody-drug-conjugates. Adapted from Drago et al[93] and de Goeij et al.[102] Created with Biorender.

1.5 Aim of the project

Although in the last years, several new targeting therapeutic agents for AML treatment were approved, the prognosis of patients is still poor, and improvement of therapy is required. Fms like tyrosine kinase 3 is a suitable receptor for targeted therapy due to its overexpression and the occurrence of activating mutations on AML cells. Mutated FLT3 has already been proven as a safe and efficient target for inhibitors in AML treatment. Importantly, wildtype FLT3 also presents an excellent target in AML therapy. Compared to other possible targets like CD33, CD123 and CLL1, FLT3 provides the largest therapeutic index, which is predicted by an AML specific overexpression, restricted and low expression in a subset of healthy hematopoietic cells and low abundance in non-hematopoietic tissue. Thus, agents targeting FLT3 in AML are expected to have little to no healthy tissue toxicity beyond potential hematologic toxicities[73].

The aim of this project was the development of a novel FLT3 targeting ADC for AML treatment using the recently established P5- technology to couple the tubulin inhibitor MMAF to a human IgG1-based FLT3-targeting antibody. The ADC was characterized for binding, affinity, internalization, stability and *in vitro* efficacy using several transgenic Ba/F3-cell line models, AML cell lines and ex vivo patient derived xenograft cells. *In vivo*, MOLM-13 cell line and PDX mouse models were treated with the FLT3 specific ADC to determine the *in vivo* efficacy. Experiments using CD34 positive bone marrow cells were performed to estimate the hematotoxicity of FLT3 targeting ADC. Furthermore, a combination of the FLT3 specific ADC with FLT3 TKIs was explored to enhance the cytotoxic effect by synergistic mechanisms.

2 Material and Methods

2.1 Material

2.1.1 Laboratory equipment and consumables

Laboratory equipment

Equipment	Provider
ÄKTA FPLC system	GE Healthcare (United States)
Analytical balance ABJ 220-4NM	Kern & Sohn (Balingen-Frommern, Germany)
Bench-top incubation shaker Celltron	Infors AG (Bottmingen, Switzerland)
BioPhotometer	Eppendorf (Hamburg, Germany)
Bio-Rad Mini Protean Tetra blotting system	Biorad (Hercules, CA, USA)
Centrifuge 5415D, 5424R	Eppendorf (Hamburg, Germany)
CO_2 incubator C 170	BINDER (Tuttlingen, Germany)
Confocal scanning microscope	Leica Microsystems GmbH (Wetzlar, Germany)
E-BOX VX2	Vilber Lourmat (Eberhardzell, Germany)
Flow Cytometer Canto II	BD Bioscience (Franklin Lakes, USA)
Fluorescent microscope DMi8	Leica Microsystems (Wetzlar, Germany)
Freezer -20 °C	Liebherr (Bulle FR, Switzerland)
Freezer -80 °C, TLE	Thermo Fisher Scientific (Waltham, MA, USA)
Freezing container Mr. Frosty	Thermo Fisher Scientific (Waltham, MA, USA)
Fusion SL4 imaging system	Vilber Lourmat (Eberhardzell, Germany)
Heating block Thermomixer compact	Eppendorf (Hamburg, Germany)
High precision scale PCB 2500-2	Kern & Sohn (Balingen-Frommern, Germany)
Ice machine FM-170AKE	Hoshizaki (Amsterdam, NL)
Incubator 9040-0013	Binder (Tuttlingen, Germany)
Liquid nitrogen tank	Cryoson (Schöllkrippen, Germany)
Magnetic stirrer MR3001	Heidolph (Schwabach, Germany)
Microplate reader GloMax® Discover	Promega (Madison, WI, USA)
Microscope ID03	Carl Zeiss (Oberkochen, Germany)
Multichannel pipettes Research Pro	Eppendorf (Hamburg, Germany)
Nanodrop spectrophotometer 1000	Thermo Fisher Scientific (Waltham, MA, USA)
PCR cycler PeqSTAR 2x Gradient	Peqlab (Wilmington, DE, USA)
pH meter inoLab® pH 7110	WTW (Weilheim, Germany)
Pipettes (0.25-2.00 µl, 2.0-20.0 µl)	Gilson (Limburg, Germany)
Pipettes (20-200 µl, 200-1000 µl)	Gilson (Limburg, Germany)
Pipetus accu-jet pro	Brand (Wertheim, Germany)
Protein purification system Äkta	GE Healthcare GmbH (Freiburg, Germany)
Real-time PCR instrument LightCycler® 480 Instrument II	Roche Diagnostics GmbH (Mannheim, Germany)
RS-TR 5 Tube-roller	Phoenix instrument (Garbsen, Germany)
Ultrapure water system Milli-Q System	Merck Millipore (Darmstadt, Germany)
VARIOKLAV Type 500	HP-Medizintechnik (Oberschleißheim, Germany)
Vertical Autoclave VX-150	Systec (Linden, Germany)
Vi-CELLTM Cell Viability Analyzer XR	Beckman Coulter (Krefeld, Germany)
Vortexer	Cenco (Breda, NL)
Water Bath Type 1003	GFL (Burgwedel, Germany)
X1R Centrifuge Hareaus	Thermo Fisher Scientific (Waltham, MA, USA)

Table 3 List of used laboratory equipment.

Consumables

Consumable	Provider
Amersham Protran Nitrocellulose membrane, 0.45 µM	GE Healthcare (Little Chalfont, UK)
Amicon® Ultra Centrifugal Filters (15 ml, 0.5 ml)	Merck Chemical GmbH (Darmstadt, Germany)
Combitips advanced (0.5 ml, 1 ml, 5 ml)	Eppendorf (Hamburg, Germany)
Cryo Tube Vial	Thermo Fisher Scientific (Waltham, MA, USA)
Diamond Tower Pack (D10, D200, D1000)	Gilson (Middleton, WI, USA)
Disposable bags	Brand (Wertheim, Germany)
DURAN Erlenmeyer flasks (50 ml, 250 ml, 500 ml, 1000 ml)	DURAN Group (Mainz, Germany)
DURAN GL 45 Lab Bottles (100 ml, 250 ml, 500 ml, 1000 ml)	DURAN Group (Mainz, Germany)
Gel-loading pipet tips	Sigma-Aldrich (St. Louis, MO, USA)
HiTrap MabSelect	GE Healthcare Europe GmbH (Freiburg, Germany)
Erlenmeyer flasks with lid (100, 250, 500, 1000 ml)	Schott AG (Mainz, Germany)
Maxisorp plate, black, 96 well	Thermo Fisher Scientific (Waltham, MA, USA)
Micro tube 1.5 ml SafeSeal (1.5 ml, 2 ml)	Sarstedt (Nümbrecht, Germany)
Microscope coverslips (18x18 mm)	Carl Roth(Karlsruhe, Germany)
Microscope slides SuperFrost®	Carl Roth(Karlsruhe, Germany)
Neubauer Zählkammer	Paul Marienfeld GmbH & Co. KG (Lauda Königshofen, Germany)
Novex Empty Gel Cassette,1.0 mm	Thermo Fisher Scientific (Waltham, MA,USA)
PARAFILM	Sigma-Aldrich (St. Louis, MO, USA)
PCR plate, 96-well	Brand (Wertheim, Germany)
PCR tubes 0.2 m.	Biozym Scientific (Oldendorf, Germany)
Petri dish 10 cm/30 cm	Sarstedt (Nümbrecht, Germany)
Round Bottom Polystyrene Tube 5 ml	Thermo Fisher Scientific (Waltham, MA, USA)
Round bottom tube	Eppendorf (Hamburg, Germany)
serological Pipets 25 ml	Greiner Bio One (Frickenhausen, Germany)
Sorenson low binding standard tips	Sigma-Aldrich (St. Louis, MO, USA)
Stripette serological Pipets (10, 5, 2, 1 ml)	Corning (Corning, NY, USA)
Superdex 200 10/300 GL	GE Healthcare Europe GmbH (Freiburg, Germany)
TC Flask T25, T75, T175, standard	Sarstedt (Nümbrecht, Germany)
TC Flask T25, T75, T175, suspension	Sarstedt (Nümbrecht, Germany)
TC Plate 6-well - 96-well, standard	Sarstedt (Nümbrecht, Germany)
TC Plate 6-well - 96-well, suspension	Sarstedt (Nümbrecht, Germany)
Tube 15 ml, 120x17 mm	Sarstedt (Nümbrecht, Germany)
Tube 50 ml, 114x28 mm	Sarstedt (Nümbrecht, Germany)
Vasco Nitrile Blue Gloves	B. Braun (Melsungen, Germany)
V-bottom plate, 96-well	Greiner Bio One (Frickenhausen, Germany)
Vivaspin centrifugal concentrators	Sartorius (Germany)
Zeba™ Spin Desalting Columns (7K, 40K)	Thermo Fisher Scientific (Waltham, MA, USA)

Table 4 List of used consumables.

2.1.2 Chemicals, reagents and cytotoxic agents

Chemicals and reagents

Reagent	Provider
1 kb ladder	Promega (Madison, WI, USA)
2-propanol	AppliChem (Darmstadt, Germany)
Agarose	Carl Roth (Karlsruhe, Germany)
Albumin (IgG free)	Carl Roth(Karlsruhe, Germany)
Albumin fraction V (pH 7.0) (BSA)	AppliChem (Darmstadt, Germany)
Ampicillin sodium salt	Sigma-Aldrich (St. Louis, MO, USA)
Annexin V- FITC	BD Bioscience (Franklin Lakes, USA)
Annexin-V- APC	BD Bioscience (Franklin Lakes, USA)
Aprotinin	Sigma-Aldrich (St. Louis, MO, USA)
APS (Ammonium persulfate)	Carl Roth (Karlsruhe, Germany)
Attophos Fluorescent substrate system	Promega (Madison, WI, USA)
Biocoll Separating Solution	Sigma-Aldrich (St. Louis, MO, USA)
Bradford Protein Assay Dye	Bio-Rad (Hercules, CA, USA)
Bradford Reagent	Thermo Fisher Scientific (Waltham, MA, USA)
Bromophenol blue	Sigma-Aldrich (St. Louis, MO, USA)
Calcium chloride 2-hydrate	AppliChem (Darmstadt, Germany)
Coulter Clenz Cleaning Agent	Beckman Coulter (Krefeld, Germany)
Coulter Isoton II Diluent	Beckman Coulter (Krefeld, Germany)
CutSmart Buffer	New England Biolabs (Frankfurt, Germany)
DAPI	Sigma-Aldrich (St. Louis, MO,USA)
DEPC-treated water	Thermo Fisher Scientific (Waltham, MA, USA)
DH5α competent bacteria	Thermo Fisher Scientific (Waltham, MA, USA)
Dimethyl sulfoxide (DMSO)	Sigma-Aldrich (St. Louis, MO,USA)
Disodium hydrogen phosphate (Na_2HPO_4)	Carl Roth (Karlsruhe, Germany)
DMEM high glucose, Gibco	Thermo Fisher Scientific (Waltham, MA, USA)
DNase I	Roche (Basel, CH)
EcoRI	New England Biolabs (Frankfurt, Germany)
Endo S	New England Biolabs (Frankfurt, Germany)
Ethanol	Merck Millipore (Darmstadt, Germany)
Ethanol, absolute	Sigma-Aldrich (St. Louis, MO, USA)
Ethanol, technical	Carl Roth (Karlsruhe, Germany)
Fetal bovine serum (FBS)	PAN-Biotech (Aidenbach, Germany)
FLT3-human Fc tag protein Asn27-541	R&D Systems (Minneapolis, USA)
Formaldehyde (30 %)	Carl Roth (Karlsruhe, Germany)
FreeStyle™ 293 Medium Gibco™	Thermo Fisher Scientific (Waltham, USA)
FreeStyle™ MAX Reagent Gibco™	Thermo Fisher Scientific (Waltham, USA)
Gel loading dye purple 6x	New England Biolabs (Frankfurt, Germany)
HBS 2x	Sigma-Aldrich (St. Louis, MO, USA)
HEPES	AppliChem (Darmstadt, Germany)
Human FLT3 extracellular domain HIS-tag	Sino Biological (Hong Kong, China)
Hydrochloric acid (HCl)	Carl Roth (Karlsruhe, Germany)
Hygromycin	Invitrogen (Carlsbad, USA)
Kanamycin Sulfate	Sigma-Aldrich (St. Louis, MO, USA)
Korsolex	Bode Chemie GmbH (Hamburg, Germany)
LB-agar	Carl Roth (Karlsruhe, Germany)
LB-medium	Carl Roth (Karlsruhe, Germany)
L-glutamine	Thermo Scientific, Schwerte, Germany
Lipofectamine 3000	Thermo Fisher Scientific (Waltham, MA, USA)
Methanol	Carl Roth (Karlsruhe, Germany)

Milk powder (for blotting)	Carl Roth (Karlsruhe, Germany)
Murine FLT3 extracellular domain HIS-tag	Sino Biological (Hong Kong, China)
MyTaq polymerase	Bioline (London, UK)
Opti-MEM I Reduced Serum Medium, Gibco	Thermo Fisher Scientific (Waltham, MA, USA)
OptiPRO™ SFM Gibco™	Thermo Scientific, Schwerte, Germany
PageRuler Prestained Protein Ladder	Thermo Fisher Scientific (Waltham, MA, USA)
PBS Dulbecco w/o Mg^{2+}, Ca^{2+}	PAN-Biotech (Aidenbach, Germany)
Penicillin-Streptomycin, Gibco	Thermo Fisher Scientific (Waltham, MA, USA)
Phenylmethylsulfonyl fluoride (PMSF)	Sigma-Aldrich (St. Louis, MO, USA)
Pierce ECL Plus Western Blotting Substrate	Thermo Fisher Scientific (Waltham, MA, USA)
Polybrene	Sigma-Aldrich (St. Louis, MO, USA)
Poly-L-lysine hydrobromide	Sigma-Aldrich (St. Louis, MO, USA)
Potassium chloride (KCl)	Carl Roth (Karlsruhe, Germany)
Potassium dihydrogen phosphate (KH_2PO_4)	Merck Chemicals GmbH (Darmstadt, Germany)
Pre-diluted BGG Protein Assay Standard	Thermo Fisher Scientific (Waltham, MA, USA)
Propidium iodide solution	Sigma-Aldrich (St. Louis, MO, USA)
Proteinase K	New England Biolabs (Frankfurt, Germany)
Quick-Load Purple 50 bp DNA ladder	New England Biolabs (Frankfurt, Germany)
Recombinant human thrombopoietin	R&D Systems (Minneapolis, MN, USA)
Recombinant human FLT3 ligand	R&D Systems (Minneapolis, MN, USA)
Recombinant human IL-3 protein	R&D Systems (Minneapolis, MN, USA)
Recombinant human SCF protein	R&D Systems (Minneapolis, MN, USA)
Resazurin	Thermo Fisher Scientific (Waltham, MA, USA)
RNase AWAY	Carl Roth (Karlsruhe, Germany)
Rotiphorese gel 30	Carl Roth (Karlsruhe, Germany)
Rotiphorese® Gel 30 (37, 5:1)	Carl Roth (Karlsruhe, Germany)
RPMI 1640 + Glutamax, Gibco	Invitrogen (Darmstadt, Germany)
S.O.C. Medium	Invitrogen (Darmstadt, Germany)
Sodium chloride (NaCl)	Carl Roth (Karlsruhe, Germany)
Sodium dihydrogen phosphate (NaH_2PO_4)	Carl Roth (Karlsruhe, Germany)
Sodium dodecyl sulfate (SDS)	Sigma-Aldrich (St. Louis, MO, USA)
Sodium fluoride NaF	Sigma-Aldrich (St. Louis, MO, USA)
Sodium hydroxide (NaOH)	Carl Roth (Karlsruhe, Germany)
Sodium orthovanadate	Sigma-Aldrich (St. Louis, MO, USA)
Sodium pyruvate 100mM	Biochrom (Berlin, Germany)
ß-Mercaptoethanol	Sigma-Aldrich (St. Louis, MO, USA)
StemPro-34 SFM Media	Thermo Fisher Scientific (Waltham, MA, USA)
SYBR Safe DNA gel stain	Invitrogen (Darmstadt, Germany)
SYPRO® Orange Protein Gel Stain	Sigma-Aldrich (St. Louis, MO, USA)
TAE Buffer 10x	Apotheke LMU Klinikum (Munich, Germany)
TBS Buffer 10x	Apotheke LMU Klinikum (Munich, Germany)
TCEP	Merck KGaA (Germany)
Tetramethylethylenediamine (TEMED)	Sigma-Aldrich (St. Louis, MO, USA)
TRIS	Carl Roth (Karlsruhe, Germany)
Tris-(hydroxymethyl)- aminomethane (TRIS)	Carl Roth (Karlsruhe, Germany)
Triton X-100	Sigma-Aldrich (St. Louis, MO, USA)
Trypan Blue	Sigma-Aldrich (St. Louis, MO, USA)
Trypsin-EDTA (0.05 %), phenol red	Thermo Fisher Scientific (Waltham, MA, USA)
Tween20	Sigma-Aldrich (St. Louis, MO, USA)
Vectashield® Mounting Medium	Vector Laboratories (Burlingame, USA)
Vybrant™ DiO Cell-labeling Solution	Invitrogen (Darmstadt, Germany)
XhoI	New England Biolabs (Frankfurt, Germany)

Table 5 List of used chemicals and reagents.

Chemotherapeutic substances and inhibitors

Substance	Provider
20D9-ADC	This work
Cytarabin	SelleckChem (Houston, USA)
Dasatinib	MedChemExpress (Monmouth Junction, USA)
Daunorubicin	SelleckChem (Houston, USA)
Giletritinib	MedChemExpress (Monmouth Junction, USA)
IgG1-ADC	This work
Midostaurin	MedChemExpress (Monmouth Junction, USA)
MMAE	cfm Oskar Tropitzsch GmbH (Marktredwitz, Germany)
MMAF	cfm Oskar Tropitzsch GmbH (Marktredwitz, Germany)
Quizartinib	SelleckChem (Houston, USA)
Sorafenib	MedChemExpress (Monmouth Junction, USA)

Table 6 List of used chemotherapeutics and inhibitors.

2.1.3 Kits

Kit	Application	Provider
Endofree Plasmid Maxi Kit	Maxi preparation of plasmid DNA	Qiagen (Hilden, Germany)
InFusion HD Plus Cloning	Vector cloning	Takara Bio (Saint-Germain-en-Laye, France)
Mouse Cell Depletion Kit	Purification of human cells from PDX material	Miltenyi Biotec (Bergisch Gladbach, Germany)
MycoAlert Mycoplasma Detection Kit	Detection of mycoplasma contamination in cell culture	Lonza (Basel, CH)
QIAamp DNA Blood Mini Kit	Isolation of gDNA from cells and tissues	Qiagen (Hilden, Germany)
QIAprep Spin Miniprep Kit	Mini preparation of plasmid DNA	Qiagen (Hilden, Germany)
QIAquick Gel Extraction Kit	DNA extraction from agarose gels	Qiagen (Hilden, Germany)
QIAquick PCR Purification Kit	Amplicon purification	Qiagen (Hilden, Germany)
QuikChange II Site directed mutagenesis Kit	Gene mutagenesis	Agilent Technologies (Santa Clara, USA)
Rapid Gold BCA Protein Assay	Determination of Protein concentration	Thermo Fisher Scientific (Waltham, MA, USA)
RNAse-Free DNase Kit	DNase digest for RNA isolation pre-treatment	Qiagen (Hilden, Germany)
RNeasy Mini Kit	RNA isolation	Qiagen (Hilden, Germany)
StemMACS HSC-CFU Media	CD34 Progenitor Cell Isolation	Miltenyi Biotec (Bergisch-Gladbach, Germany)

Table 7 List of used kits.

2.1.4 Buffers and solutions

Buffer	Composition
Agarose gels (1 % - 1.5 %)	1-1.5 % agarose in 1x TAE buffer with SYBR Safe (1:10,000)
Blocking buffer (ELISA)	PBS, 0.5 % BSA IgG-free
Blocking solution (IF)	2 % BSA in PBS-T
Blocking solution (WB)	5 % non-fat milk in TBS-T or 5 % BSA in TBS-T

Coomassie stain	1 g Coomassie Brilliant Blue in 1 l of: 50 % methanol, 10 % glacial acetic acid, 40 % H_2O
FACS buffer	PBS + 1 % FCS, 1 mg/l propidium iodide Storage: Light protected, at 4 °C
Fixation Solution	3.7 % formaldehyde in PBS
Freezing buffer	10 % DMSO in FBS. Stored at 4 °C
Gel electrophoresis buffer 10x	151.4 mg Tris, 720.7 g glycin, 50 g sodium dodecyl sulfate. Add up to 5 l d_2H_20
KCM 5x	5 ml 3 M KCl, 4.5 ml 1 M $CaCl_2$, 7.5 ml 1 M $MgCl_2$
Laemmli buffer 4x	50 mM Tris-HCl pH 6.8, 0.8 g sodium dodecyl sulfate, 10 % glycerol, 1 % ß-mercaptoethanol, 12.5 mM EDTA, 8 mg bromophenol blue
LB agar plates	35 g LB-agar, add up to 1 l d_2H_20
LB medium	20 g LB-medium, add up to 1 l d_2H_20
$LB_{ampicillin}$ plates	LB-agar 20 ml, 100 µg/ml ampicillin
Lysis buffer for whole cell lysis	25 ml 1 M HEPES, pH 7.5, 15 ml 5 M NaCl, 2.5 ml 200 mM EGTA, 100 ml 50% glycerol, 5 ml Triton X-100, 2.1 g NaF, 2.2 g $Na_4P_2O_7x10H_2O$, add ddH_20. Freshly added before each lysis: 5 mM PMSF, 25 µg/ml aprotinin, 50 µg/ml sodium orthovanadate.
Permeabilization buffer	0.5 % Triton X-100 in PBS
Protein A Binding buffer	20 mM sodiumphosphate, 150 mM NaCl, adjust to pH 7.2
Protein A Elution buffer	100 mM sodiumcitrate, adjust to pH 3.0
TAE buffer 1x	100 ml TAE buffer 10x, 900 ml d_2H_20
TBS 10x	60.57 g Tris, 483.3 g sodium chloride
TBS-T	100 ml TBS buffer 10x, 900 ml ddH_20, 1 % Tween-20
Tris pH 6.8	5 l: 908.55 g Tris (pH 6.8), add H_20 dest.
Tris pH 8.8	5 l: 908.55 g Tris (pH 8.8), add H_20 dest.
Washing buffer ELISA	PBS, 0.05 % Tween20
Western blot buffer 10x	15 g Tris, 71 g glycin, 790 g methanol, add up to 5 l ddH_20

Table 8 List and recipe of used solutions.

2.1.5 Antibodies

Technical antibodies

Antibody	Application	Provider/Number
Alkaline phosphatase- rabbit anti-human IgG	ELISA	Jackson Immunoresearch (2339661)
Anti-human IgG-647	FACS	BD Bioscience (2015-31)
Anti-CD123-BV510	FACS	BioLegend (clone 6H6)
Anti-CD34-FITC	FACS	BD Bioscience (clone 581)
Anti-CD45-PE-CY5.5	FACS	BioLegend (clone HI30)
Anti-CD45RA- PE-Cy7	FACS	BD Bioscience (clone HI100)
Anti-CD64-APC	FACS	eBioscience
Anti-CD90-PE	FACS	BD Bioscience (clone 5E10)
Anti-CD38-APC	FACS	BD Bioscience (clone HB7)
Goat anti-human Ig-PE	FACS	Southern Biotech (2012-09)
Goat anti-mouse IgG(H+L)-PE	FACS	Southern Biotech (1032-09)
Goat anti-rat IgG(H+L)-PE	FACS	Southern Biotech (3052-09)
Human IgG1	FACS	Abcam (ab206198)
Isotype mouse IgG1-PE	FACS	BD Bioscience (555749)
Mouse anti human CD135 -PE	FACS	BD Bioscience (558996)
Mouse IgG1 kappa Isotype - PE	FACS	BD Bioscience (555749)
Mouse anti-human-CD16 PE	FACS	BD Bioscience (555407)
Mouse anti-human-CD32 -PE	FACS	BD Bioscience (552884)
Mouse anti-human-CD64 .PE	FACS	BD Bioscience (558592
Rat IgG1	FACS	R&D Systems (MAB005)
Donkey anti-rabbit IgG (H+L) -Alexa Fluor 594	IF	Thermo Scientific (R37119)
Donkey anti-rat IgG (H+L)-Alexa Fluor 594	IF	Thermo Scientific (A21209)
Goat anti-human IgG (H+L)-Alexa Fluor 594	IF	Thermo Scientific (A-11014)
Rabbit anti-EEA1	IF	Cell Signalling Technologies (C45B10)
Rabbit anti-RAB7	IF	Cell Signalling Technologies (D95F2)
Rat anti-LAMP1	IF	Santa Cruz Biotechnology (1D4B)
Goat anti-mouse m-IgGkappa HRP	WB	Santa Cruz Biotechnology (sc-516102)
Goat anti rat IgG-HRP	WB	Santa Cruz Biotechnology (sc-2006)
Goat anti-rabbit IgG1-HRP	WB	Sigma-Aldrich (sc-2004)
Mouse anti-Flag	WB	Sigma-Aldrich (clone M2, F3165).
Mouse anti-β-actin	WB	Sigma Aldrich (A5441)
Mouse anti-GAPDH clone 6C5	WB	Santa Cruz Biotechnology (sc-32233)
Rabbit anti-human FLT3	WB	Santa Cruz Biotechnology (SC-480-S-18)

Table 9 List of used technical antibodies.

Experimental antibodies

Antibody	Provider
Rat IgG2a anti-human FLT3 (20D9)	Own production
Rat IgG2a anti-human FLT3 (4B12)	Own production
Rat IgG2a anti-human FLT3 (19H5)	Own production
Rat IgG2a anti-human FLT3 (2F12)	Own production
Mouse IgG2b anti-human FLT3 (30B12)	Own production
Mouse IgG2a anti-human FLT3 (29H1)	Own production

Mouse IgG2a anti-human FLT3 (27E7)	Own production
Chimerized human IgG1 anti-human FLT3 (20D9)	Own production
Chimerized human IgG1 anti-human FLT3 (4B12)	Own production
Chimerized human IgG1 anti-human FLT3 (19H5)	Own production
Chimerized human IgG1 anti-human FLT3 (2F12)	Own production
Chimerized human IgG1 anti-human FLT3 (30B12)	Own production
Chimerized human IgG1 anti-human FLT3 (29H1)	Own production
Chimerized human IgG1 anti-human FLT3 (27E7)	Own production
Synagis (Palivizumab IgG1 anti RSV)	AbbVie (404770)

Table 10 List of used experimental antibodies.

2.1.6 Plasmids and oligonucleotides

Oligonucleotides

Name	5‘ → 3‘ sequence	Application
Cd16_SeqFOR1	tggagagtacaggtgccaga	Sequencing
Cd16_SeqFOR2	tccttttgcagtggacaca	Sequencing
Cd16_SeqREV1	agcaacagccagccgata	Sequencing
Cd32_SeqFOR1	ctttccgaatggctggtg	Sequencing
Cd32_SeqFOR2	ctgtgaaggctgcccaat	Sequencing
Cd32_SeqREV1	agaggcttgtccttccagc	Sequencing
Cd64_SeqFOR1	ctctggccttgaggtgtcat	Sequencing
Cd64_SeqFOR2	gactctgggttatactggtgcg	Sequencing
Cd64_SeqREV1	gaaaaacttaaaggctttgcca	Sequencing
FragCynoFLt3.FOR	ctaggcgccggaattcatgccggcgttggc	Cloning pMIY
FragCynoFLT3.REV	tcgagtttttctcgagtcatgaatcttcgacctgagcctttggag	Cloning pMIY
FragCynoFLt3Flag.REV	tcgagtttttctcgagctacttatcgtcgtcatccttgtaatctcc	Cloning pMIY
mFLT3_SequePrimer 1	cactgtggagtgggtgctc	Sequencing
mFLT3_SequePrimer 2	ctggaggatgggtacagcata	Sequencing
mFLT3_SequePrimer 3	taagtgggagttcccgagag	Sequencing
MIY mFLT3_1804.FOR	ctaggcgccggaattcgttaagcttggtaccgagctcggat	Cloning pMIY
MIY mFLT3_1804.REV	tcgagtttttctcgagctgatcagcgggtttatcact	Cloning pMIY
MR S001 pVITRO for	cactccggccgcactat	Sequencing
MR S002 alt. pVITRO for	gagtttggagcgaggctaat	Sequencing
MR S002 pVITRO for	ccgctaattcaaagcatccgga	Sequencing
MR S003 pVITRO for	tacgcctaggagcagg	Sequencing
MR S004 pVITRO for	agggtcaattcttgtgctgatgg	Sequencing
MR S005 pVITRO for	ggactgatggatgtgttgaagt	Sequencing
MR S006 pVITRO for	ggaatgtgtgtcagttaggg	Sequencing
MR S007 pVITRO for	ccctgctgccttcga	Sequencing
MR S008 pVITRO for	caccgctaattcaaagcaac	Sequencing
MR S009 pVITRO rev	tcatgtctggccagctagct	Sequencing
MR S010 pVITRO for	agctagctggccagacatga	Sequencing
MR S011 pVITRO for	gcgtgagctatgagaaag	Sequencing
MR S012 pVITRO for	atcgctattaccatgatgatgc	Sequencing
MutPrimer 1 P54R Motiv1	gggattctgataccatgcgatatgatgatgacttccc	Mutant hFLT3
MutPrimer 2 P54R Motiv1	gggaagtcatcatcatatcgcatggtatcagaatccc	Mutant hFLT3
MutPrimer 3 S50P Motiv1	ccatgcgatatgatgatggcttccccactgatgaatc	Mutant hFLT3
MutPrimer 4 S50P Motiv1	gattcatcagtggggaagccatcatcatatcgcatgg	Mutant hFLT3

pMIY-CD16-INFUSI.FOR	ctaggcgccggaattcatgggtggaggggctggg	Cloning pMIY
pMIY-CD16-INFUSI.REV	tcgagtttttctcgagttaaaccttatcgtcgtcatccttgtaatccag	Cloning pMIY
pMIY-CD32-INFUSI.FOR	ctaggcgccggaattcatgactatggagacccaaatgtctcagaat	Cloning pMIY
pMIY-CD32-INFUSI.REV	tcgagtttttctcgagttaaaccttatcgtcgtcatccttgtaatccag	Cloning pMIY
pMIY-CD64-INFUSI.FOR	ctaggcgccggaattcatgtggttcttgacaactctgctcct	Cloning pMIY
pMIY-CD64-INFUSI.REV	tcgagtttttctcgagttaaaccttatcgtcgtcatccttgtaatccag	Cloning pMIY

Table 11 List of used oligonucleotides.

Plasmids

Vector	**Application**	**Origin/Number**
enhanced firefly luciferase and mCherry	Lentiviral expression vector	Addgene (104833)
pCDH-EF1a-eGFP	Lentiviral expression vector	AG Jeremias, Helmholtz Zentrum, Munich
pcDNA3.1-C-(k)DYK-Murine FLT3	Cloning vector	Genescript (OMu21985D)
pcDNA6/HisA	Expression-vector	Invitrogen (V102520)
pCMV6-CD16a	Cloning vector	Origene (RC206429)
pCMV6-CD32a	Cloning vector	Origene (RC205786)
pCMV6-CD64a	Cloning vector	Origene (RC207487)
pMIY-CD16a	Retroviral expression vector	This work
pMIY-CD32a	Retroviral expression vector	This work
pMIY-CD64a	Retroviral expression vector	This work
pMIY-cyno FLT3	Retroviral expression vector	This work
pMIY-FLT3 (NM_004119)	Retroviral expression vector	Ag Spiekermann, LMU Klinikum
pMIY-FLT3 ITD w51	Retroviral expression vector	Ag Spiekermann, LMU Klinikum
pMIY-FLT3 K466R	Retroviral expression vector	Ag Spiekermann, LMU Klinikum
pMIY-human FLT3 S50P/P54R	Retroviral expression vector	This work
pMSCV-IRES-GFP pMIG	Retroviral expression vector	R.K. Humphries (Vancouver, CAN)
pMSCV-IRES-YFP pMIY	Retroviral expression vector	R.K. Humphries (Vancouver, CAN)
pVITRO_chFLT3_19H5	Expression vector	AG Leonhardt, LMU, Munich
pVITRO_chFLT3_20D9	Expression vector	AG Leonhardt, LMU, Munich
pVITRO_chFLT3_27E7	Expression vector	AG Leonhardt, LMU, Munich
pVITRO_chFLT3_29H1	Expression vector	AG Leonhardt, LMU, Munich
pVITRO_chFLT3_2F12	Expression vector	AG Leonhardt, LMU, Munich
pVITRO_chFLT3_30B12	Expression vector	AG Leonhardt, LMU, Munich
pVITRO_chFLT3_4B12	Expression vector	AG Leonhardt, LMU, Munich
pVITRO-EF1a-MCS	Expression vector	AG Leonhardt, LMU, Munich

Table 12 List of used plasmids.

Gene synthesis

Name	**Template**	**Manufacturer**
Cynomolgus monkey FLT3 gene	XM_015439107.1	Eurofins

Table 13 List of synthesized genes.

2.1.7 Biological material

Cell lines

Name	Cultivation	Cell culture medium	Tissue/tumor	Gender
Ba/F3	suspension	RPMI, 10 % FCS, 1 % P/S, 10 ng/ml mIL-3	Lymphatic origin	
HEK-293 Freestyle	suspension	TF Medium + 8 mM Glutamin	Embryonic kidney	female
HEK 293T	adherent	DMEM, 10 % FCS, 1 % P/S	Embryonic kidney	female
HL-60	suspension	RPMI, 20 % FCS, 1 % P/S	AML	female
K-562	suspension	RPMI, 20 % FCS, 1 % P/S	CML	female
Karpas 422	suspension	RPMI, 20 % FCS, 1 % P/S	B-Cell NHL	female
Kasumi-1	suspension	RPMI, 20 % FCS, 1 % P/S	AML	male
KG-1a	suspension	RPMI, 20 % FCS, 1 % P/S	AML	male
L-428	suspension	RPMI, 10 % FCS, 1 % P/S	HL	female
MM-1	suspension	RPMI, 20 % FCS, 1 % P/S + NaPyruvat + non-essential AS	Acute monocytic leukemia	male
MM-6	suspension	RPMI, 20 % FCS, 1 % P/S + NaPyruvat + non-essential AS + Insulin 10 µg/ml	Acute monocytic leukemia	male
MOLM-13	suspension	RPMI, 20 % FCS, 1 %P/S	AML	male
MV4-11	suspension	RPMI, 20 % FCS, 1 %P/S	Acute monocytic leukemia	male
NOMO-1	suspension	RPMI, 20 % FCS, 1 %P/S	AML	female
OCI-AML3	suspension	aMEM+20 % FCS + 10 ng/ml GM-CSF	AML	male
OCI-AML5	suspension	aMEM+20 % FCS	AML	male
Phenix Eco	adherent	DMEM, 10 % FCS, 1 %P/S	Embryonic kidney	female
PL-21	suspension	RPMI, 20 % FCS, 1 %P/S	AML	male
THP-1	suspension	RPMI, 20 % FCS, 1 %P/S	Acute monocytic leukemia	male
U-937	suspension	RPMI, 20 % FCS, 1 %P/S	Histiocytic lymphoma	male

Table 14 List of used cell lines. AML=acute myeloid leukemia; CML=chronic myeloid leukemia; NHL=non-Hodgkin lymphoma; HL=Hodgkin lymphoma. All cell lines are human, except for the murine Ba/F3 cell line. All cell line except MV4-11 were purchased from DSMZ (Braunschweig, Germany). MV4-11 was purchased from ATCC.

Patient derived xenograft samples

Sample	Disease stage	Age [years]	Sex	Cytogenetics	Mutations (panel seq) [18]	FLT3-ITD (VAF)
AML-415	R2	69	f	normal	DNMT3AV527I, DNMT3AS714C, NPM1L287fs, FLT3-ITD, IDH1R132H	E598delinsDDFREYE (1.0)
AML-573	R1	64	f	t(5;11) (p1?;q?13)	DNMT3A^{S663L}, DNMT3A^{A644S}, FLT3-ITD, WT1$^{c.1075fs}$, WT1$^{c.1054fs}$, IDH2^{R140Q}	E604delinsDPSDNEYFY VDFREYEYDLKWE (0.35)
AML-579	R	51	m	normal	DNMT3A^{R882C}, DNMT3A^{F868L}, NPM1^{L287fs}, FLT3-ITD, IDH1^{R132H}	E598delinsDYVDFREYE (1.0)

AML-640	ID	79	m	t(11;15) (p1?1;q?22)	DNMT3A$^{c.2173fs}$, NPM1^{L287fs}, FLT3-ITD, IDH1^{R132H}	F612delinsVDFREYEYD LKWEFPRENLEF (0.5); L610delinsFGSSDNEYFY VDFREYEYDLKWEFPRE NL (0.2)

Table 15 List and characteristics of used patient derived cell lines. NOD scid gamma mice were purchased from The Jackson Laboratory, Bar Harbour, ME, USA.

2.1.8 Software

Software	Application	Provider
Biorender	Illustration and design of biological figures	Biorender AG (Münchwilen TG, CH)
CompuSyn	Synergy calculation	ComboSyn Incorporated
E-Capt 15.06	Agarose gel recording and documentation	Vilber Lourmat (Eberhardzell, Germany)
FusionCapt Advance 16.11	Western blot recording and analysis	Vilber Lourmat (Eberhardzell, Germany)
GraphPad Prism 6.07	Data visualization, statistical analysis	GraphPad Software (La Jolla, CA, USA)
ImageJ version 1.50d	Western blot quantification	ImageJ developers, online
Microsoft Office 2010	Data analysis (such as sequencing), text editing	Microsoft (Redmond, WA, USA)
SnapGene 3.3.4	Primer design, sequencing analysis, creation of vector maps	GSL Biotech LLC (Chicago, IL, USA)
Synergy Finder	Synergy calculation	Network Pharmacology for Precision Medicine, University of Helsinki

Table 16 List of used software.

2.2 Methods

2.2.1 Cell biological methods

2.2.1.1 Cell cultivation and handling

Human cell lines

Human and mouse cell lines were purchased and cultured under conventional cell culture conditions at 37 °C and 5 % CO_2 according to the supplier's recommendation. Cell viability was measured with the Vi-Cell Cell Viability Analyzer. Cells were only used for further experiments when viability was more than 90 %. Prewarmed media was used for culturing and experiments.

Adherent cells were grown in DMEM, supplemented with 10 % (v/v) FBS, 0.5 % (v/v) penicillin/streptomycin. To sub-culture the cells, they were gently washed with PBS followed by incubation with trypsin-EDTA at 37 °C for 2-3 min to ensure detachment. Prewarmed DMEM was added to stop the activity of trypsin and cells were harvested or passaged. HEK293T cells that

were grown to 80-90 % confluence were sub cultured in a ratio of 1:10 every 2-3 days. Cell lines were cultured in the media indicated in Table 14. Leukemic cell lines were subcultured 2-3 times a week and density was kept between 0.4–1.2 x 10^6 cells/ml as recommended specifically for the cell lines by DSMZ.

Primary AML patient samples

Primary AML patient derived xenograft samples (PDX-AML samples) were isolated from patients' blood (EDTA blood) or bone marrow sample by Ficoll separation, enriched with the mouse cell depletion kit, engrafted and passaged in mice and re-isolated for *in vitro* cultivation in the laboratory of AG Jeremias as it has been previously described[103]. Patient material for PDX-AML sample generation was derived from AML patients from trials AMLCG-99 (NCT00266136) and AMLCG-2008 (NCT01382147), and the Department of Medicine III, University Hospital, LMU, Großhadern. Written informed consent for usage of sample material for research was obtained from all participants in agreement with the Declaration of Helsinki.

PDX cells were cultured up to 7 days according to Martin Wermke (Dresden, Blood 2015) with StemPro-34 medium, supplemented with 0.5 % penicillin/streptomycin, 2 % FBS and appropriate nutrient supplement, 0.5 % L-Glutamine, 0.02 % SCF (stock 50 µg/ml), 0.02% TPO (stock 50 µg/ml), 0.02 % IL-3 (stock 50 µg/ml) and 0.01 % FLT3-L (stock 100 µg/ml PBS + 0.1 % BSA). Nutrient supplement was slowly thawed at 4 °C. Medium was always prepared freshly before PDX cell cultivation.

Primary healthy bone marrow samples

Healthy bone marrow samples were obtained (approval number TUM 538/16) and isolated as described before in the laboratories of AG Götze[104]. Healthy BM samples were collected from femoral heads of patients undergoing hip replacement surgery without known hematologic disease. After disintegrating and mincing the femoral head, BM fragments were transferred into tubes with PBS, and BM cells were harvested by shaking the BM suspension and filtered through a 70 µm cell strainer. Mononuclear cells were isolated from the BM cell suspension by density gradient centrifugation and enriched by magnetic activated cell sorting for CD34 expression.

Cell isolation by density gradient centrifugation

To isolate human mononuclear cells from peripheral blood, 15 ml Biocoll Separating Solution were placed in a Falcon. The blood sample tube was filled up to 30 ml with PBS. The mixture was carefully and slowly layered onto the 15 ml Biocoll Separating Solution and centrifuged at 2270 rpm for 30 min at 20 °C without brake. After centrifugation, the mononuclear cell ring was collected, placed in a new tube and washed with 50 ml with PBS. After centrifugation, the supernatant was discarded, and the pellet was resuspended in 1 ml PBS.

Freezing and thawing

For cell freezing, 2-6 x 10^6 viable cells were centrifuged (1100 rpm, 5 min, RT). The cell pellet was resuspended in 1 ml FBS supplemented with 10 % (v/v) DMSO and aliquoted in 1.5 ml cryotubes (NuncTM Cryo Tube). The tubes were first places in an isopropanol freezing container (Mr. FrostyTM Freezing Container) in the -80 °C freezer to gently cool down with a freezing rate of 1 °C/minute. For long term storage, the samples were transferred to liquid nitrogen at -196 °C.

For cell thawing, the vial was quickly thawed at 37 °C in a waterbath and transferred in a 15 ml tube already containing 5 ml prewarmed medium to reduce the harming potential of DMSO. After centrifugation for 5 min at 300 g RT, the cell pellet was resuspended in 3-5 ml fresh medium and transferred into a T25 cell culture flask for suspension or adherent cells, respectively.

PDX AML cell were thawed according to the protocol of Dominique Bonnet to ensure high viability. Briefly, cells were quickly thawn at 37 °C followed by drop wise adding of 100 µl of DNase I (1 mg/ml). Cell suspension was gently mixed, incubated for 1 min and transferred into a 50 ml centrifuge tube. 1 ml FBS was added drop wise and cell suspension was gently mixed. After 1 min, 10 ml PBS with (v/v) 2 % FBS were slowly added followed by incubation for 1 min. Then, volume was carefully filled up to 30 ml with PBS containing 2 % (v/v) FBS. Cells were centrifuged (1100 rpm, 5 min, 4 °C) and resuspended in DD medium.

Mycoplasma test

Mycoplasma contamination was assessed during cell culture continuously by using the MycoAlert Mycoplasma detection kit according to supplier's recommendations. The method is based luciferase activity, which requires free ATP, a characteristic of mycoplasma contamination. Briefly, after centrifugation of 1 ml of cell culture (300 g, 5 min), 25 µl of supernatant were transferred to a white bottom 96 well plate and mixed with 25 µl of MycoAlertTM Reagent. The plate was incubated for 5 min at RT and the background luminescence was measured with a microplate reader (read A). Then, 25 µl of substrate solution was added, incubated 10 min in the dark and luminescence was measured a second time (read B). The ratio (B/A) indicates whether cells were contaminated (>1.1.) or not (<0.9).

2.2.1.2 Protein overexpression in cells

Transient transfection

This transfection method is based on calcium-phosphate precipitation. 7 x 10^6 HEK293T cells were seeded in a 10 cm dish. The next day at a confluency of 80-90 %, medium was changed. After 4-5 h, 13 µg endotoxin-free plasmid DNA diluted in 450 µl sterile H_2O was mixed with 50 µl of 2 M CaCl2. After 4-5 h, the mixture was slowly added to 500 µl HBS buffer and incubated for 3-4 min.

The solution was added drop wise to the cell suspension. The cells were incubated at 37 °C and medium was changed after 13-15 h. For further analysis and dependent on purpose, cells were lysed 48-72 h after transfection or the supernatant was collected for generation of viral conditioned medium.

Stable transduction of Ba/F3 cells

For stable recombinant protein expression, Ba/F3 cells were retroviral transduced as described before[105]. Briefly, transient transfection is used for production of virus-containing medium, which can then be applied for the transduction of Ba/F3 cells. The adherent Phoenix Eco cells produced the desired retroviral supernatant via calcium-phosphate transfection of the pMSCV-IRES-EGFP/EYFP vector. The viral conditioned medium was removed 2-3 days after transfection and filtered. 1.5 x 10^6 Ba/F3 cells were resuspended in 3 ml medium and polybrene (8 µg/ml) and the same amount of virus containing medium was added. The suspension was mixed and divided to two wells of a 6-well plate. The plate was centrifuged for 90 min at 2500 rpm and 32 °C. After 2.5 h incubation, the medium was changed. The cells were expanded and sorted after 4-5 days for GFP or YFP positivity. A second sorting is applied after one week to obtain a >95 % positive population.

2.2.1.3 Analysis of cell surface protein expression

To analyze the cell surface expression on cell lines, flow cytometry was used. 0.5 × 10^6 cells were centrifuged at 200 g for 3 min, washed with ice cold PBS and incubated for 30 min in the dark on ice with specific antibody as well as its isotype control using the supplier's recommended concentrations diluted in FACS-buffer (PBS + 1 % FCS). The cells were washed twice with cold FACS buffer, resuspended in 300 µl of FACS buffer. The samples were kept on ice in the dark until analysis. Data was evaluated with FlowJo Software and geometric mean was calculated.

2.2.1.4 Apoptosis assay

The cells were double stained with annexin V (detects cells in the early apoptotic stage) and DAPI (late apoptotic stage) according to the manufacturer's protocol in 1X annexin binding buffer and analyzed by flow cytometry. AML cell lines were cultured with or without 300 ng/ml 20D9-ADC and 0.5 x 10^6 cells were harvested every day for 4 days. The cells were washed twice with cold PBS and resuspended in 100 µl 1x annexin binding buffer and stained with 4 µl annexin V-APC for 10 min at RT in the dark. The cells were analyzed in the FACS Canto flow cytometer. Immediately before analyzing, 2 µl DAPI (stock 1µg/µl) were added.

Healthy CD34+ BM cells were cultured for 4 days without or with 40, 200 or 1000 ng/ml 20D9-ADC or 1000 ng/ml IgG1-ADC. Annexin V- FITC and Propidium iodide solution were used for staining apoptotic cells. Statistical analysis was performed using Kruskal-Wallis-Test.

2.2.1.5 Proliferation assay

Proliferation assay with trypan blue exclusion

The method is based on the ability of viable cells to exclude actively the trypan dye. Dead cells were stained blue. Viable cell count was determined automatically with the Vi-Cell Cell Viability Analyzer. For proliferation assays of Ba/F3 cells with antibody-drug-conjugates, 0.9 ml of cell suspension with a density of 11,111.1 cells/ml were seeded in wells of a 48 well plate, obtaining 10,000 cells per well. The treatment in increasing concentrations specifically for the drug was prepared in 10-fold concentration and 0.1 ml were added to 0.9 ml cell suspension. All conditions were set up in duplicates. The suspension was gently mixed and incubated. To count viable cells after 72 h, cells were resuspended, and 0.6 ml was transferred to a counting vial. The vial was placed in the Vi-CELL Cell Viability Analyzer XR and the number of viable cells was counted. Cell number of untreated cells was considered as 100 % viable cells and all other conditions were normalized to the untreated condition.

Proliferation assay with resazurin

The method is based on determination of the metabolic activity of cells which is proportional to the viability of cells. Only metabolic active cells can convert the redox-dye resazurin into fluorescent end product resorufin that is measured using a plate reader.

For proliferation assays of AML cell lines and pdx AML samples applying one drug, 90 µl of cell suspension with a density of 111,111.1 cells/ml were seeded into wells of a 96 well plate to obtain 10,000 cells per well. Wells containing only media were included for background control of the fluorescence. The treatment was prepared in 10-fold concentrations in a two or three-fold serial dilution in cell culture media. For antibody-drug-conjugates, there was no additional solvent control necessary as they were diluted in PBS. For pure MMAF, a DMSO control in the highest concentration was included. 10 µl of drug mixture were added to the 90 µl cell suspension. All conditions were set up in triplicates. The suspension was gently mixed and incubated for 96 h.

For a cytotoxicity assay analyzing a combination of two drugs, 80 µl of a cell suspension with a density of 125,000 cells/ml were seeded into wells of a 96 well plate to obtain 10,000 cells per well. Wells containing only media were included for background control of the fluorescence. The ADC treatment was prepared in 10-fold concentrations in a two-fold serial dilution in cell culture media. The tyrosine kinase treatments were prepared in 100-fold concentrations in a two-fold

serial dilution in DMSO. Then, the dilution row was again diluted 1:10 in media. A DMSO control for the TKI treatment was included. Two times 10 µl were added to the 80 µl cell suspension obtaining all possible combinations of the different concentrations of both drugs and the controls. All conditions were set up in duplicates. The suspension was gently mixed and incubated for 96 h.

To analyze the cell viability, Resazurin was dissolved in PBS, sterile filtered and frozen as stock aliquots at -20 °C. For each measurement, a working solution was prepared in PBS. At 92 h, 10 µl of Resazurin working solution was added to each well containing cells or media reaching a final concentration of 50 µM. After gently mixing, the plates were incubated the last 4 hours at 37 °C. The fluorescence was measured in a plate reader with 530–570 nm for excitation and 580–620 nm for fluorescence emission.

2.2.1.6 CFU-C assay

CD34+ HSPCs were cultured in suspension without or with 40, 200 or 1000 ng/ml 20D9-ADC or 1000 ng/ml IgG1-ADC for 4 days. HSPCs were harvested and directly plated in growth factor–supplemented methylcellulose (StemMACS HSC-CFU Media, Miltenyi Biotec) in 35 mm petri dish in duplicates to assess colony-forming units (CFUs)[104]. Colonies were scored after 14 days at 37 °C, 5 % CO_2 in a humidified atmosphere. This assay was carried out in the laboratory of Katharina Götze, TU Munich.

2.2.1.7 *In vivo* analysis

Patient-derived xenograft (PDX) cells or MOLM-13 cells expressing enhanced firefly luciferase and mCherry (Addgene, Plasmid #104833) were established as described previously[103] in the laboratory of Irmela Jeremias, Helmholtz Zentrum Munich. For *in vivo* therapy trials, MOLM-13 cells or PDX cells were injected intravenously (i.v.) into 8–12-week-old male NSG mice (NOD scid gamma, The Jackson Laboratory, Bar Harbour, ME, USA), and tumor growth was regularly monitored by bioluminescence imaging (BLI) as described previously[103]. After successful engraftment, mice were treated with deglycosylated or native 20D9-ADC (1 or 3 mg/kg, i.v., 1 dose per week), IgG1-ADC (3 mg/kg), or midostaurin (SelleckChem, 50 mg/kg, oral gavage, 5 doses per week; in 5 % DMSO+45 % PEG300+50 % ddH_2O). Experimental end points were BLI values above $1x10^{10}$ Photons/sec or below detection limit ($4x10^6$ Photons/sec) for 90-150 days post injection. Mice showing clinical signs of illness or weight loss above 15 % under therapy were sacrificed.

All animal trials were performed in accordance with the current ethical standards (Regierung von Oberbayern, number ROB-55.2Vet-2532.Vet_02-16-7).

2.2.1.8 Statistical analysis and calculations

Synergy calculation

To calculate the synergy of a treatment combination, different concentration combinations of TKI and ADC were applied in a cross scheme to MOLM-13 cells in a cytotoxicity assay. The viability was assessed using resazurin as described above. The effect of the combination treatment was compared to a calculated value reflecting the expected combination efficacy based on the single agent treatment. This calculation was performed using two different software (freeware).

CompuSyn: Combination indices (CIs) with standard deviation were determined using CompuSyn software based on Chou-Talalay principles[106,107]. CI < 1 indicates synergy; CI = 1 additivity; CI > 1 antagonism.

Synergy Finder: Further, the synergy score δ was calculated by 'Synergy Finder' using zero interaction potency (ZIP) modelling comparing the change in the potency of the dose-response curves between individual drugs and their combinations[108,109]. For each concentration combination, the delta score value was calculated, quantifying the deviation from the expectation of zero interaction.

Statistical analysis

Statistical analysis of all proliferation and biochemical assays was performed using GraphPad Prism 9 (GraphPad Software (La Jolla, CA, USA)) software. All presented results were shown as mean ± SD of a minimum of three biological replicates, except indicated otherwise.

2.2.2 Antibody-drug-conjugate generation

2.2.2.1 Generation of monoclonal antibody against human FLT3

50 µg of the recombinant purified FLT3-human Fc tag protein (368-ST-050/CF, R&D Systems, Asn27-541, Accession#AAA18947) were injected intraperitoneally (i.p.) and subcutaneously (s.c.) into LOU/C rats or C57BL/6 mice, using incomplete Freund's adjuvant supplemented with 5 nmol CpG 2006 (for rats) or CpG 1668 (for mice, TIB MOLBIOL, Berlin, Germany). After a six-week interval a final boost with 50µg FLT3 and CpG was given i.p. and s.c. three days before fusion. Fusions of the myeloma cell line P3X63-Ag8.653 with the rat or mouse immune spleen cells were performed according to standard procedures. Hybridoma supernatants were tested in a solid-phase immunoassay with FLT3, or an irrelevant Fc fusion protein coated to ELISA plates. Bound antibodies from tissue culture supernatant were detected with HRP conjugated antibodies against mouse or rat IgG. HRP was visualized with ready to use TMB (1-StepTM Ultra TMB-ELISA, Thermo). The mabs 2F12, 4B12, 20D9 (all rat IgG2a) and 27E7, 29H1 (both mouse IgG2a),

recognizing the protein in flow cytometry-based cell binding assays, were stabilized by limiting dilution. Antibodies were generated before this doctoral project by Elizabeth Kremmer, Helmholtz Zentrum Munich.

2.2.2.2 Cloning of the chimeric antibody sequence

Total mRNA was isolated from hybridoma-clone cell pellets using the NucleoSpin Triprep Kit (Machery-Nagel) according to the manufacturer's instructions. Total mRNA was reverse transcribed to cDNA using RT-Kit either with random hexamer or oligo-dT primer. PCR amplification of VL and VH Domains and assembly of scFv genes was adapted from Schaefer et al.[110]. In short a set of forward primers covering the most abundant 5'-sequences of VL and VH genes and reverse primer matching the antibody subtype specific hinge (VH) or CL (VL) region were applied to amplify the VH-CH1 and VL-CL gene-fragments. The fragments were sequenced and reverse primer specific for the clone's VL and VH 3' end were designed and used for amplification. ScFv-fragments were assembled by overlap-extension PCR (OE-PCR) and subcloned into a bacterial expression vector by restriction digest and ligation. Assembled expression plasmids were used for transformation of chemically competent E. coli JM109. DNA of several clones was isolated, and the scFv-gene sequenced. A clone representing the most abundant sequence was processed further.

For chimeric antibody assembly by subcloning of VL and VH domains into eukaryotic human IgG1 expression vector pVitro-IgG1/κ, VL and VH sequences were amplified from the bacterial expression vector. Both fragments were inserted sequentially by restriction digest of the vector backbone and insertion of the respective fragment[111] by Gibson-Assembly using the NEBuilder® HiFi DNA Assembly Cloning Kit (NEB). Assembled Plasmids were amplified via transformation of E. coli JM109, purified using the PureYield™ Plasmid Midiprep System (Promega) and sequenced to ensure integrity. Antibodies were cloned and chimerized before this doctoral project by Andreas Stengl, AG Leonhardt, LMU Munich.

2.2.2.3 Recombinant antibody production

Transient transfection and antibody production

HEK FreeStyle™ 293-F cells were transiently transfected with FreeStyle™ MAX Reagent was used according to manufacturer's protocol. Briefly, 293F cells were prepared in a shake flask with a density of 1 x 10^6 cells/ml at a volume of 50 ml in serum free TF Medium. The plasmid DNA diluted in OptiProSFM medium was mixed with the FreeStyle MAX reagent diluted in OptiPro SFM to a final volume of 1.2 ml. After gently mixing, the solution was incubated for 10 min at RT. The transfection mix was added dropwise to the cell suspension and was incubated for at 37 °C and

5 % CO_2 while shaking at 135 rpm. After one day, add selection antibiotic hygromycin 1:1000. Supernatant was harvested after 7-10 days by centrifugation at 200 g for 20 min. The supernatant was collected and centrifuged a second time at 5,000 g for 10 min at 4 °C and sterile filtered using 0.2 µm syringe filters.

Selection of HEK cell line stable expressing mabs

The transfected HEK293 F cells were plated to a p150 cell culture dish for adherent culture in DMEM with 10 % FCS and 1:1000 selection antibiotic hygromycin. The cells were incubated several days at 37 °C and 5 % CO_2, until attachment to the dish surface can be observed. After washing, fresh selection medium (DMEM) was added. When the cells formed colonies, the cells were detached using trypsin and replated in DMEM supplemented with 1:1000 hygromycin. When the cultured reached 100 % confluency, the cells were incubated with FreeStyle medium + 1:1000 hygromycin. After several days, the cells detached and were cultured again in suspension shake flasks at 135 rpm at 37 °C with TF medium + 1:1000 hygromycin.

Antibody production using stable cell lines

HEK F cell line stably expressing monoclonal antibodies at a viability of >95 % were seeded in a density of 0.5 x 10^6 cells/ml in a desired volume in a shake flask in serum free TF medium. Usually, 50 ml expression culture was cultured in 200 ml shake flask, 200 ml culture in 1000 ml flask. Cells were incubated at 37 °C and 5 % CO_2 on an adhesive shaking plate in a cell culture incubator at 135 rpm. When cells reached a density of 4 x 10^6 cells approximately after 5 days, some media was added. Supernatant was harvested after 7-10 days by centrifugation at 200 g for 20 min. The supernatant was collected and centrifuged a second time at 5,000 g for 10 min at 4 °C and sterile filtered using 0.2 µm syringe filters.

Preparative Protein A purification

For antibody purification via protein A chromatography, the ÄKTA FPLC system equipped with a P-920 pump system, a UPC-900 detector, a FRAC-950 fraction collector and HiTrapMabSelect 1 ml column was used according to the manufacturer's protocol. All buffers were sterile filtered and degassed. Briefly, the tubing system was first equilibrated with sterile water and then with the respective buffer. Supernatant containing the antibodies was loaded by a sample pump. After washing with binding buffer, the antibody was eluated with 100 % elution buffer and UV chromatograms were recorded at 220 and 280 nm. The peak was fractionated in 1.5 ml Eppendorf tubes in the fraction collector. The maximum flow rate was 1 ml/min, the maximum applied system pressure was 0.5 MPa and the maximum delta column pressure 0.3 MPa. The fractions were pooled according to the FPLC-chromatogramm. The pump system and the column were equilibrated to water followed by equilibration with 20 % ethanol in sterile water. The volume of

the purified antibodies was constricted, and the buffer was exchanged to PBS (pH 7) by using Amicon® Ultra Centrifugal filters with a cutoff of 30 MW according to manufacturer's protocol (4 °C, 4000 g).

Preparative SEC purification

To further purify the antibodies or ADCs, a preparative size exclusion chromatography was applied using the Superdex 30/100 according to manufacturer's protocol. The ÄKTA FPLC system equipped with a P-920 pump system, a UPC-900 detector and a FRAC-950 fraction collector. The sample was applied by a capillary loop (500 µl) and the purification was performed with Phosphate buffer saline. The flow rate was 0.75 ml/min for PBS and water, for 20 % ethanol the flow rate must not exceed 0.5 MPa. The maximum system pressure was 4 MPa, the maximum delta column pressure 2 MPa. After the purification, the fractions were pooled according to the FPLC-chromatogram. The purified sample was concentrated to an ideal concentration of 1 mg/ml using Amicon® Ultra Centrifugal filters. The pump system and the column were equilibrated to water followed by equilibration with 20 % ethanol in sterile water. This method was performed in cooperation with Tubulis GmbH.

2.2.2.4 ADC conjugation and preparative size-exclusion chromatography

Native antibodies were labelled with ethynylphosphonamidates (P5-labelling) and conjugated to monomethyl auristatin F in cooperation with AG Hackenberger and Tubulis GmbH. The previously described ethynylphosphonamidate modified, cathepsin B cleavable MMAF construct has been synthesized as previously reported[90,91]. The 20D9 clone and IgG1 antibody (Palivizumab) has been modified with 8 toxin molecules per antibody, by applying a protocol, similar as previously reported[91]. The antibody has been concentrated to 10.0 mg/ml in a buffer, containing 50 mM Tris*HCl, 100 mM NaCl, 1 mM EDTA, pH 8.3 at room temperature, by using Vivaspin centrifugal concentrators with a MWCO of 30 kDa. 700 µl of this solution have been mixed with 37.3 µl of a 10 mM solution of TCEP in the same buffer. TCEP has been purchased as 0.5 mol/l neutral solution. Directly after TCEP addition, 23.3 µl of a solution containing 40 mM of the toxin molecule in DMSO have been added and the clear solution has been gently shaken for 16 h at 25 °C.

The ADC were purified by size-exclusion chromatography and quality was controlled by analytical hydrophobicity chromatography, size exclusion chromatography and mass spectrometry. Conjugation and quality assurance was performed in cooperation with AG Hackenberger, FMP Berlin.

2.2.2.5 Analytics of mabs and ADCs

Analytical SEC- and HIC-HPLC

Analytical size-exclusion chromatography (A-SEC) of the ADCs was conducted on a Vanquish Flex UHPLC System with a DAD detector, Split Sampler FT (4°C), Column Compartment H (25°C) and binary pump F (Thermo Fisher Scientific, USA) using a MAbPac SEC-1 300 Å, 4 x 300 mm column (Thermo Fisher Scientific, USA) with a flow rate of 0.15 ml/min. Separation of different ADC/mab populations have been achieved during a 30 minute isocratic gradient using a phosphate buffer at pH 7 (20 mM Na2HPO4/NaH2PO4, 300 mM NaCl, 5% v/v isopropyl alcohol as a mobile phase. 8 µg ADC/mab were loaded onto the column for A-SEC analysis. UV chromatograms were recorded at 220 and 280 nm. Quantification of monomer and HMWS was achieved after integration of the peak area at 220 nm. This method was performed in cooperation with AG Leonhardt, LMU and Tubulis GmbH.

MS-analysis

ADCs were deglycosylated and reduced prior MS analysis. 50 µl of a 0.2 mg/ml solution of the ADC were mixed with 0.5 µl PNGase-F solution (Pomega, Germany, Recombinant, cloned from Elizabethkingia miricola 10 u/µl) and 5 µl of a solution of 10 mM DTT (Merck, Germany) in PBS. The mixture was incubated at 37 °C for at least 2 hours before MS analysis. 2 µl were injected per analysis. Reduced and deglycosylated ADCs were analyzed using a Waters H-class instrument equipped with a quaternary solvent manager, a Waters sample manager-FTN, a Waters PDA detector and a Waters column manager with an Acquity UPLC protein BEH C4 column (300 Å, 1.7 µm, 2.1 mm x 50 mm). Proteins were eluted with a flow rate of 0.3 ml/min. The following gradient was used: A: 0.01 % FA in H_2O; B: 0.01 % FA in MeCN. 5-95 % B 0-6 min. Mass analysis was conducted with a Waters XEVO G2-XS QTof analyzer. Proteins were ionized in positive ion mode applying a cone voltage of 40 kV. Raw data was analyzed with MaxEnt 1 and deconvoluted until convergent. This method was performed by AG Hackenberger, FMP Berlin.

2.2.3 Protein biochemical methods

2.2.3.1 Lysate

To perform whole cell protein extraction, 4-6 x 10^6 suspension cells were spun down for 5 min at 300 g at 4°C and washed twice in cold PBS. Adherent cells (minimum one well of a 6-well plate) were scraped off the culture dish by using a cell scraper, spun down for 5 min at 300 g at 4 °C and washed twice in cold PBS. RIPA Lysis buffer was freshly supplemented 5 µl/ml aprotinin, 10µl/ml PMSF and 10 µl/ml orthovanadate. According to the cell pellet size, the cells were resuspended in lysis buffer (400 µl buffer for 1x10^7 cells). The cell lysates were incubated for 30 min on ice and

spun down at 13,000 rpm for 20 min at 4 °C. The supernatant was transferred into a pre-cooled tube and stored at -20 °C. For all further applications, the lysates were kept at 4 °C.

2.2.3.2 Determination of protein concentration

Cell lysate

The concentration of protein lysates was assessed by using the Bradford assay (Sigma-Aldrich B6916) according to manufacturer's protocol. Protein lysates were diluted 1:10 in PBS and 10 µl were pipetted in duplicates in a 96 well plate. For the calibration curve, a serial BSA dilution (200-1500 µg/µl) and a PBS blank were pipetted in duplicates as well. 200 µl of 1X Bradford solution was added and incubated for 5 min at RT. Absorption at 600 nm was measured in the GloMax plate reader. The blank control absorbance was subtracted, and the concentration was determined by using the calibration curve.

Antibodies and ADCs

To determine the concentration of antibody and ADC samples, the Bradford and the BCA assay were applied. Briefly, the antibody or ADC concentration was measured in nano Drop to roughly diluted the sample to 1 mg/ml in PBS. In a 96 well plate, 10 µl of the samples were pipetted in duplicates for each assay. For the calibration curve, pre-diluted BGG Protein Assay Standard and PBS control was also pipetted in duplicates. The Rapid Gold BCA reagent A was mixed with Reagent B (50:1 Reagent A:B) and 200 µl were added to the samples. As well, 200 µl Bradford solution was added to the second sample set.

The BCA assays was measured in the GloMax plate reader at 490 nm. The Bradford assay was measured at 600 nm. For each assay, the blank control absorbance was subtracted, and the concentration was determined by using the calibration curve. Afterwards, the mean of both methods was calculated.

2.2.3.3 Polyacrylamide gel electrophoresis and coomassie stain

To analyze the content of protein lysates or the purity of purified proteins SDS-polyacrylamide gel electrophoresis was used, which separates denaturized proteins based on their molecular weight. For separating high and low molecular weight proteins, an acrylamide concentration of 8 % to 15% was used, respectively.

Separating gel (e.g. 10 %): H_2O dest. 6.9 ml, 30 % acrylamide/bisacrylamide 4.0 ml, 1.5 M Tris-HCl buffer (pH 8.8) 3.8 ml, 10 % SDS in H_2O dest. 0.15 ml, 10 % APS in H_2O dest. 0.15 ml, TEMED 0.009 ml.

Stacking gel: H_2O dest. 3.4 ml, 30 % acrylamide/bisacrylamide 0.83 ml, 1.5 M Tris-HCl buffer (pH 6.8) 0.63 ml, 10 % SDS in H_2O dest. 0.05 ml, 10 % APS in H_2O dest. 0.05 ml, TEMED 0.005 ml.
After pouring the gels in gel-cassettes, a comb for 10, 12 or 15 wells was inserted and after polymerization, the gel was used or stored with wet tissue in the fridge up to several days. As well, precast gradient gels from Biorad were utilized. Samples containing equal amount of proteins (e.g. 30 µg for cell lysates, 1 µg for purified proteins) from lysates were mixed with water and 4:1 Lämmli buffer to a total volume of 12 or 17 µl followed by denaturation for 5 min at 95 °C. 10 or 15 µl of the samples and 5 µl of a molecular weight protein ladder were loaded in wells. Gels were run in a Xcell SureLock Mini Cell with 1x Electrophorese buffer at 70 V 15 min and 120 V 16 min.

For coomassie staining, the cassette was dissembled and the gel was stained for 1 h followed by short washing with water. The destain solution (100 ml ethanol and 75 ml acetic acid filled up to 1 l with water) was added for 1 h and changed several times until it stayed clear. The protein bands were visible in blue and were imaged using a scanner.

2.2.3.4 Immunoblotting

For detection of proteins, immunoblotting (western blotting) was applied. After a denaturating gel electrophoresis, the proteins on the gel were transferred to a nitrocellulose membrane using wet electroblotting system (Biorad Mini Protean Tetra system) according to manufacturer's protocol. Briefly, sponges, papers, the gel and a nitrocellulose membrane were assembled in a cassette, installed in the wet-blotting chamber and run over night at 100 mA at 4 °C. To protect the protein integrity, the blotting buffer was ice cold, ice packs were placed in the chamber and during the blotting, the solution was stirred constantly. Membranes were blocked with 5 % (w/v) non-fat dried milk or 5 % BSA (w/v) in Tris buffered saline (TBS-T) for 1h at RT and incubated with primary antibody solution (diluted antibody in 5 % (w/v) milk- or BSA-TBST) for 1 h at RT followed by three 5 min TBS-T washing steps. Further, the immunoblot was incubated for 1 h at RT with respective secondary HRP coupled antibody diluted 1:10000 in 5 % milk- or BSA-TBS-T. After washing with TBS-T, the immunoblot was incubated with Pierce ECL solution for 5 min and proteins were visualized on Fusion SL imaging system. Western blot signals were quantified using ImageJ and relative protein levels were normalized to loading control.

2.2.3.5 Antibody binding and internalization

Antibody binding and internalization by flow cytometry analysis

For antibody binding analysis, 0.5×10^6 cells were centrifuged at 200 g for 3 min, washed with ice cold PBS and incubated for 30 min on ice with 1 µg/100 µl primary antibody or ADC in FACS buffer

(PBS + 1 % FCS). After washing two times with cold FACS buffer, secondary antibody detecting the species of the first antibody was applied as 1:200 dilution in FACS buffer. The cells were incubated again for 30 min on ice in the dark followed by two washing steps with cold FACS buffer. The cells were resuspended in FACS buffer and transferred to FACs tubes filled with 300 µl buffer. The samples were kept on ice until analysis.

To analyze the internalization of the primary antibody, 0.5 × 10^6 cells were centrifuged at 200 g for 3 min, washed with PBS and incubated for 30 min on ice with 1 µg/100 µl primary antibody or ADC in FACS buffer. After washing, the samples were incubated for 30 min on ice or at 37 °C. Subsequently, all samples were kept on ice for further processing. Cells were washed twice with ice cold FACS buffer supplemented with 0.1 % NaN_3 to stop the internalization and stained with 1:200 secondary antibody in FACS buffer + 0.1 % NaN_3 for 30 min on ice in the dark. The samples were washed twice in FACS buffer + 0.1 % NaN_3, resuspended in 100 µl and transferred to a FACS tube containing 300 µl FACS buffer. The respective fluorescence of the cells was detected using a FACS Canto flow cytometer. The mean fluorescence intensity was evaluated using the Flow Jo software. The MFI of geometric mean of the respective antibody was normalized to a IgG1 control.

Antibody binding and internalization in Immunfluorescence Staining

Glass coverslips were cleaned with ethanol and coated with poly-lysine by incubating the glass slips carefully in 1 mg/ml poly lysin solution for 5 min and drying under sterile conditions over night. 2-3 x 10^6 cells were washed twice with PBS, at 700 rcf for 5 min and either used for internalization assay or directly proceed to the fixation.

For internalization, the cells were resuspended in 250 µl serum free media and primary antibody was added to final 1 µg/µl. The antibody treated and untreated samples were incubated for 30 min at 37 °C and 5 % CO_2. For staining of the membrane, 4 µl/ml Vybrant DiO is added for 5 min at 37 °C. Subsequently, the cells were washed twice with ice cold PBS.

For fixation, cells were resuspended in 3.7 % paraformaldehyde, 100 µl were seeded on coverslips and incubated at RT for 15 min. The cell suspension was washed three times with PBS followed by permeabilization with 0.2 % Triton-X in PBS for 10 min at RT. The cells were washed three times with PBS-T (PBS + 0.02 % Tween-20), blocked with 2 % BSA in PBS-T for 1 h at RT and if applicable, subsequently incubated with 100 µl primary antibody (10 µl/ml in PBS-T + 2 % BSA) for 1h at RT. The cells were washed three times with PBS-T before incubated with 100 µl secondary antibody (10 µl/ml in PBS-T + 2 % BSA) in the dark. After washing the cells three times with PBS-T, they were counterstained with DAPI (0.5 µg/ml in PBS) for 5 min at RT. A microscope glass slide was cleaned with ethanol, the cover slip was mounted on a drop of Vectashield and

sealed thoroughly with nail polish. Imaging was performed with a Leica TCS SP5 confocal scanning microscope.

2.2.3.6 Enzyme-linked immunosorbent assay

For ELISAs, half of a 96 well black Maxisorp plate was coated with 1 µg/ml human recombinant FLT3 protein in 100 µl PBS over night at 4 °C with gentle shaking on a rocking shaker. Then, the solution was removed, 250 µl/well blocking solution (5 % (v/v) IgG free BSA in PBS) was added to all wells and incubated at RT for 1 h. A 1:4 dilution row in blocking solution of each antibody was prepared with the highest concentration of 10 µg/ml. 100 µl of the antibody solution was added to the FLT3-coated and the BSA-control wells in duplicates. For control, only PBS was added to the wells. After incubation for 2 h at RT, the plate was washed five times with washing solution (0.05 % (v/v) Tween in PBS) and once with blocking solution. Then, 100 µl of anti-human alkaline phosphatase coupled antibody (1:10,000 diluted in blocking buffer) was added to each well. Again, after incubation for 1 h at RT, the plate was washed five times. 100 µl Attophos solution was added per well and incubated for 20 min at RT. The fluorescence was read in the GloMax plate reader with excitation of 405 nm and emission at 500-550 nm. The calculation of the dissociation constant K_d was performed in prism normalized to the BSA control wells.

2.2.3.7 Melting curve

To determine the melting temperature of the antibodies a thermal shift assay based on the fluorescence of Sypro Orange was performed. 15 µl sample with a concentration of 1 µM protein and 10X Sypro Orange dye in PBS was pipetted in triplicates in a 96 well qPCR plate on ice. After sealing the plate, it was centrifuged for 30 s at 2500 g at 4 °C to remove air bubbles. The following settings were programmed in a qPCR cycler (Light Cycler): equilibration 20 °C 5 min, temperature increase from 20 – 95 °C with ramp rate of 3.6 °C/minute. The fluorescence was read every cycle at 485 nm (Ex) and 510 nm (Em). The melting temperature was determined using the LightCycler® 480 Protein Melting Analysis sofware.

2.2.3.8 Deglycosylation of mabs

For the degycosylation of the ADCs, the enzyme Endo S (P0741S New England Biolabs) was used according to manufacturer's protocol. 10 µg ADC were incubated with 1 µl enzyme (=200 U) and 1 µl 10X reaction buffer in a total volume of 10 µl over night at 37 °C. Controls were ADC at 4 °C, ADC with buffer at 4 °C and ADC with buffer at 37 °C.

2.2.4 Molecular biological work

2.2.4.1 InFusion cloning

For cloning procedures, In-Fusion Cloning was applied according to manufacturer's protocol. The technique provides a ligation-independent and highly efficient cloning method, which is based on the annealing of complementary ends of an insert and linearized vector. The target vector was cut with desired enzymes (e.g. XhoI and EcoRI) by DNA restriction digest. The sequence of interest was amplified by specifically designed cloning primers (SnapGene) which contain 15 bp extensions (5') that were complementary to the ends of the linearized vector: 5 µl CloneAmp HiFi PCR Premix 2X, 1 µl primer FOR (10 µM), 1 µl primer REV (10 µM), 10 ng template vector and H_20 dest. to a total volume of 20 µl. The PCR program was 35 cycles with 98 °C for 10 sec, gradient 56-64 °C for 5 sec and 72 °C for 21 sec. After verification of the successful amplification of the DNA on an agarose gel, the amplicon was purified from the gel by the QIAQuick PCR Purification kit. To ligate the digested vector and the amplified insert, 2 µl 5x InFusion HD enzyme premix, 50 ng of amplified insert, 150 ng of linearized vector, and H_2O filled up to 10 µl in total were pipetted together and incubated for 15 min at 50 °C.

Stellar heat- shock competent cells were used for plasmid amplification. Therefore, cells were thawed on ice and 2.5 µl of the ligation mix was added. After 30 min on ice the cells were heat-shocked for 45 sec at 42 °C. Cells were cooled down on ice and after 2 min 500 µl SOC medium was added. After incubation at 37 °C and 210 rpm, cells were spun down and re-suspended in 100 µl fresh SOC medium. Several dilutions of bacteria suspension were spread out on LB-ampicillin agar plates and incubated at 37 °C overnight. The plasmid was purified in a plasmid mini preparation

2.2.4.2 Site directed mutagenesis

To introduce point mutation in the FLT3 epitope region, QuikChange II XL Site-Directed Mutagenesis Kit (Agilent Technologies, Santa Clara, US) was used according to the manufacturer`s instructions. Briefly, specific primers which both contain the desired mutation site were designed and used for plasmid amplification. Mutation inserting PCR was performed under following conditions: 5 µl 10X reaction buffer, 20 ng dsDNA template, 125 ng primer FOR, 125 ng primer REV, 1 µl dNTP mix with PfuUlta HF DNA polymerase, added up with H_20 dest. to 50 µl in total. Afterwards the DPNI endonuclease (target sequence: 5'-Gm6ATC-3') specifically digests the methylated and hemi methylated parental DNA strands. Transformation of the mutated vector is recommended in XL-10 blue super-competent E. coli cells, which were provided in the kit.

2.2.4.3 Chemical retransformation of bacteria with plasmid DNA

For a chemical retransformation of bacteria to multiply plasmid DNA, DH5α E. coli bacteria (Thermo Fisher Scientific, Waltham, US) were used. After slow thawing on ice, 25 µl of the bacterial suspension was gently mixed with 1 µl plasmid DNA, 10 µl 5X KCM and 14 µl H_2O. The suspension was incubated for 20 min on ice followed by 10 min at RT. 250 µl LB Ampicillin containing medium was added and the mixture was incubated for 45 min at 37 °C and 220 rpm. 50 - 200 µl of bacteria suspension were plated on a pre-warmed LB Ampicillin plates and incubated over night at 37 °C. Single colonies were picked the next day for further expansion and plasmid preparation.

2.2.4.4 Isolation of plasmid DNA

Maxi prep

For extraction of large amounts of plasmid DNA, a maxi plasmid preparation was performed using the Endofree Plasmid Maxi kit (Qiagen). A single colony was picked and incubated in 3 ml LB ampicillin/kanamycin media for 8h at 37 °C and 220 rpm. 100-200 LB ampicillin/kanamycin media in a 1000 ml Erlenmeyer flask were inoculated with the bacteria suspension and incubated over night at 37 °C and 220rpm. Plasmid DNA was extracted with Endofree Plasmid Maxi Kit according to the manufacturer's instructions. Briefly, bacteria were spun down at 6000 g for 15 min at 4 °C and supernatant was discarded. Bacteria were lysed, plasmid DNA was bound to a column, washed, eluted and precipitated. The pellet was air dried and dissolved in 200-500 µl H_2O dest. or TE buffer. Concentration and purity of plasmid DNA was determined using the Nanodrop. Aliquots of plasmid DNA were stored at -20 °C. The correct sequence was assessed by full length sanger sequencing

Mini prep

To extract small amounts of plasmid DNA of different bacterial colonies after cloning, single colonies were picked form LB agar plates and incubated in 2 ml LB Ampicillin or LB Kanamycin media for 8-10 h at 37 °C and 220 rpm. 1 ml of a single bacteria clone was used for mini preparation of plasmid DNA with QIAprep Spin Miniprep Kit according to the manufacturer's instructions. Briefly, Cells were spun down for 3 min at 6800 g and the supernatant was discarded, bacteria were lysed, plasmid DNA is bound in a column, washed, eluted in of 30-50 µl EB buffer and the concentration was determined by NanoDrop. Plasmid DNA was stored at -20 °C.

All new cloned plasmids from mini preps were screened for correctness by digestion with restriction enzymes and subsequent electrophoretic DNA separation. One mini prep was chosen and analyzed for the correct sequence by sanger sequencing.

2.2.4.5 DNA restriction digest

To prepare a vector for cloning or assess the correct cloning or mutagenesis, an enzymatic restriction digest was performed. All enzymes were purchased from New England Biolabs and applied as recommended by the manufacturer. 1 µg plasmid DNA, 1 µl of each restriction enzyme (10,000 u/µl or 20,000 u/µl), 2 µl of the recommended restriction buffer (10X) and H_2O dest. to obtain a total amount of 20 µl were pipetted together and incubated for 2 h at 37 °C.

2.2.4.6 Nucleic acid electrophoresis

To visualize RNA and DNA fragments of different size, nucleic acids were separated by gel electrophoresis. Depending on the fragment size, 0.7-1.5 % agarose gel was prepared by solving Agar in TAE buffer and supplemented with 0.1 µg/ml the fluorescent dye SYBR-Safe. The mixture was carefully heated in the microwave in 40 sec intervals until the agarose was dissolved, cooled down to 50 °C, poured in a gel tray and the comb was placed on the gel. The solidified gel was placed in the running chamber which was filled with 1x TAE buffer. DNA or RNA sample after PCR or restriction digest was mixed with 6x gel loading buffer and loaded to the gel. In the first lane, a molecular weight ladder was loaded. Gel was run at 80-120 V for 30-50 min and DNA fragments were visualized with UV light. In case that an extraction was needed from the gel, the specific band was cut out under UV light and cleaned up with the QIAquick Gel Extraction Kit according to the supplier's recommendations. Purified DNA was eluted in 30 µl of supplied elution buffer.

2.2.4.7 LB medium and LB agar plate preparation

LB plates were prepared by pouring 20 ml freshly autoclaved LB agar (35 g LB agar in 1 l H_2O dest) into 10 cm petri dish. After solidification, 40 µl ampicillin were mixed with 60 µl SOC medium and applied to the LB agar plate.

For LB medium, 10 g LB medium was dissolved in 500 ml H_2O dest and autoclaved. For selection, 200 µl ampicillin were added to 100 ml LB medium.

2.2.4.8 Sanger sequencing

Sanger sequencing was executed external by Sequiserve (Vaterstetten, Germany) or GATC for the validation of correct plasmid DNA fragments and PCR products.

3 Results

Current therapy in AML has reached its limits, the chances of cure are very low and therefore the need for new therapeutic options is immense. At the same time, science is gaining more and more insight into the mechanisms of tumorigenesis and evolution through large-scale sequencing and patient studies. Diagnostics are becoming more precise, and the entire body of knowledge makes it possible to develop and apply appropriately targeted therapies.

In this work, I describe the development of a FLT3-specific ADC for the treatment of AML. FLT3 specific antibodies were characterized, and the lead candidate was functionalized by a phosphonamidate-based conjugation with the drug MMAF. The efficacy of the FLT3 targeting ADC was evaluated in different cell models, AML cell lines and patient derived xenograft cells. Further, the hematotoxicity was assessed in CD34 positive cells. To explore how the effectivity of a FLT3 ADC-based therapy can be enhanced, a combination of the FLT3 specific ADC with already approved FLT3 inhibitors was tested.

3.1 General considerations for the generation and basic characterization of anti-FLT3 antibodies

For the generation of a FLT3 specific ADC for AML therapy, a target specific antibody, a toxin, a linker and a conjugation strategy must be selected. The antibody influences the disease specificity, effectivity and toxicity profile of an ADC drug and must be designed and chosen carefully regarding binding, affinity and internalization. Further, technical criteria regarding the producibility and storage stability must be considered. Cross reactivity with other species, especially with cynomolgus monkey, might simplify toxicity studies and is therefore desirable for further clinical development.

One approach for the generation of antibodies specific for a desired protein – in this case FLT3 –, is the hybridoma technique, for which an animal such as mice or rats are immunized with recombinant FLT3 protein and antibody-producing B-cells are isolated. To reduce immunogenicity in patients, the therapeutic antibody must be either partially or fully humanized. For the pre-clinical characterization of the FLT3-specific antibody described here, a partial humanization strategy for the antibody to a human native IgG1 immunoglobulin was selected, which will result in full effector function upon binding to Fc receptors such as CD64.

3.1.1 Expression analysis and rationale for targeting FLT3 in AML

Firstly, the expression of FLT3 and CD64 (FcγR1) in AML patient samples was validated. Analysis of available RNA sequencing data[112] (Bamopoulos et al. (GSE146173)), revealed expression of

FLT3 and CD64 isoforms in AML patient samples (n=261) (Figure 5A). A subsequent correlation analysis showed that many patients co-express both receptors simultaneously on AML cells (Figure 5B). Hence it was hypothesized, that a FLT3 specific ADC based on a human IgG1 backbone might be able to target the two receptors, FLT3 and CD64, on the cell surface of AML blasts which might result in higher cytotoxicity.

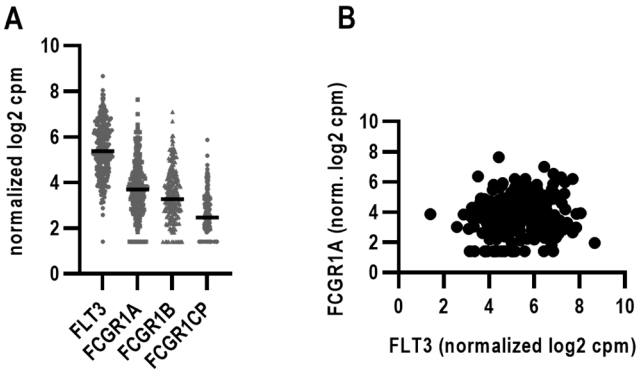

Figure 5 FLT3 and CD64 expression in AML patients. (A-B) Expression of FLT3 and FCGR1A of primary AML patient samples analyzed in scrbSeq presented as normalized log2 cmp. Patient data and RNASeq data was obtained from Bamopoulos et al. (GSE 146173) and provided by Dr. Tobias Herold, LMU Klinikum. (A) Expression of FLT3 and different isoforms of CD64 receptor. (B) Expression of FLT3 and FCGR1A receptor in AML patients.

3.1.2 Generation of chimeric anti-FLT3 antibodies

Monoclonal FLT3 specific antibodies were generated by immunization of mice and rats with a purified recombinant extracellular domain, comprising amino acids 27 to 541, of FLT3 in cooperation with Elisabeth Kremmer from the Monoclonal Antibody Core Facility at the Helmholtz Zentrum München. After isolation of B cells, the cells were fused to myeloma cells, obtaining hybridoma cells expressing murine and rat antibodies. Hybridoma clones were grown as single cell clones and after ELISA-based analysis of FLT3 binding, suitable monoclonal antibodies were selected. From these clones, mRNA was extracted, reversed transcribed and VL and VH sequences were PCR-amplified and sequenced. VL and VH sequences were further cloned to a human IgG1 sequence in pVITRO expression vectors (Figure 6A) by Andreas Stengl, LMU. By this, seven chimerized anti-FLT3 antibodies were obtained, transiently expressed in suspension HEK cells and purified by protein-A affinity chromatography and size-exclusion chromatography.

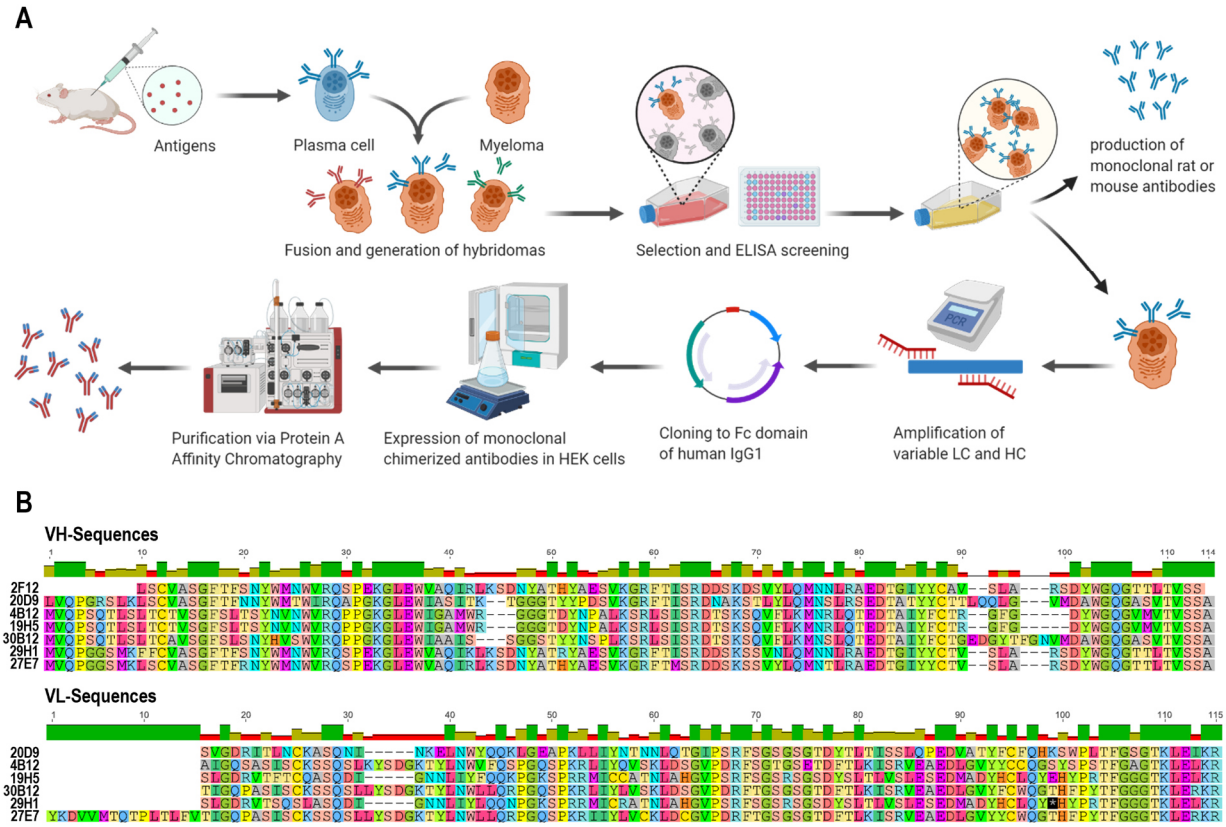

Figure 6 Generation of anti-FLT3 monoclonal antibodies. (A) Schematic workflow of generation and production of chimeric monoclonal antibodies using the hybridoma technology and chimerization to human IgG1 backbone. The figure was created with BioRender.com. (B) Amino acids sequences of variable regions of heavy (VH) and light (VL) chains of 7 anti-FLT3 antibody clones. Antibodies were generated by Dr. Elisabeth Kremmer, Helmholtz Zentrum München, and Dr. Harald Polzer, LMU Klinikum. Chimerization was performed by Dr. Andreas Stengl, LMU.

To verify the protein sequences after cloning and expression, the purified antibodies were analyzed by mass spectrometry (data not shown). The correct and validated amino acid sequences of the variable domains are displayed in Figure 6B. The variable, still murine or rat domains present 34 % of the antibody's protein sequence (VH: 120 of 449 amino acids and VL: 108 of 215 amino acids). The variable sequences of the seven antibody clones strongly differs in their similarity, which ranges from 47 % to 99 % identity (VH) and 43 % to 97 % identity (VL) with mean similarities of 62.77 % (VH) and 61.40 % (VL) (Supplementary Table 1). Overall, the antibodies have around 80 % sequence similarity.

A high producibility is critical to obtain sufficient antibody material needed for further analysis and characterization. The production efficiency varied strongly for the different mab clones. The 19H5 clone was barely expressed in HEK cells, while 20D9, 4B12 and 2F12 had satisfying yields with 50-70 µg purified protein per ml of cell culture supernatant (Figure 7A). One of the key features for the antibody's functionality is target binding. The affinities to recombinant FLT3 protein were assessed in enzyme-linked immunosorbent assay (ELISA) and the equilibrium

dissociation constant K_D varied from 11.5 ng/ml to 3981 ng/ml between the different clones (Figure 7B). Further, for handling purposes and reliability of the experimental results, the protein stability was analyzed. The antibody clones were tested in thermal shift assays to assess their denaturation temperature. All antibodies demonstrated equally good protein stabilities with melting temperatures of 67 °C to 75 °C (Figure 7C).

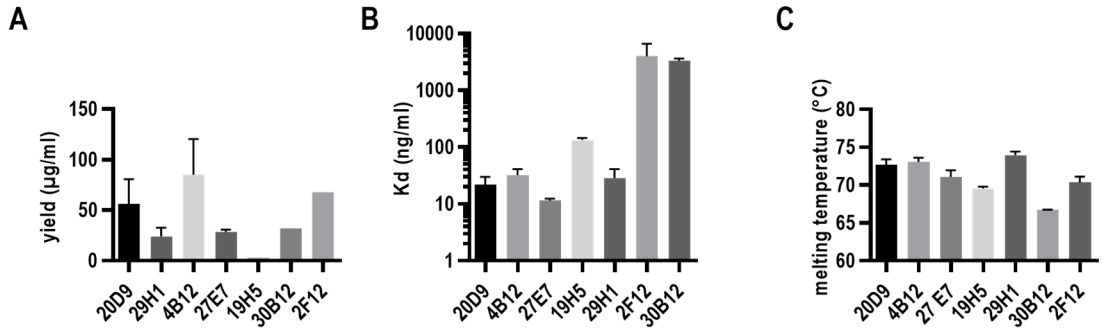

Figure 7 Basic characterization of anti-FLT3 monoclonal antibodies. (A) Production efficiency of seven anti-FLT3 antibody clones in 293F HEK suspension cell culture. Yield indicated as microgram antibody per millilitre culture. Mean ± s.d. of n=3. (B) Affinity of seven anti-FLT3 antibody clones to recombinant human FLT3 measured in ELISA and normalized to the binding of the antibodies to BSA control. Dissociation constant (K_D; mean ± s.d..; n=3) is depicted. (C) Melting temperature of seven anti-FLT3 antibody clones measured in thermal shift assay using Sypro Orange. Melting temperature in °C was calculated applying Roche thermal shift assay software. Mean ± s.d. of n=3.

3.1.3 Binding and internalization efficiency of anti-FLT3 antibodies

To identify their suitability for ADC development, the internalization upon FLT3 binding was evaluated for the different mabs. Ba/F3 cell line models stably expressing human wildtype FLT3 (Ba/F3- hFLT3wt) and the human AML cell lines MOLM-13, expressing wildtype FLT3 and mutant FLT3-ITD were tested. As control, Ba/F3 cells transduced with empty MSCV-IRES-YFP vector (pMIY) or FLT3 negative AML cell line HL-60 were used. The internalization was induced by 37 °C incubation and compared to a 4 °C incubated control. The analysis was based on two methods, flow cytometry for quantitative analysis, where the remaining amount of antibody at the cell surface was determined, and immunohistochemistry staining of intra- and extracellular FLT3 antibodies for qualitative analysis. In flow cytometry-based internalization assays, the clones 20D9, 4B12, 29H1 and 27E7 specifically bound to the Ba/F3-hFLT3wt cell line and were internalized after 37 °C incubation (Figure 8A) with an efficiency of around 80 % (Figure 8C). These observations could be confirmed in MOLM-13 cells (Figure 8B), which displayed an internalization rate of around 60 % (Figure 8D).

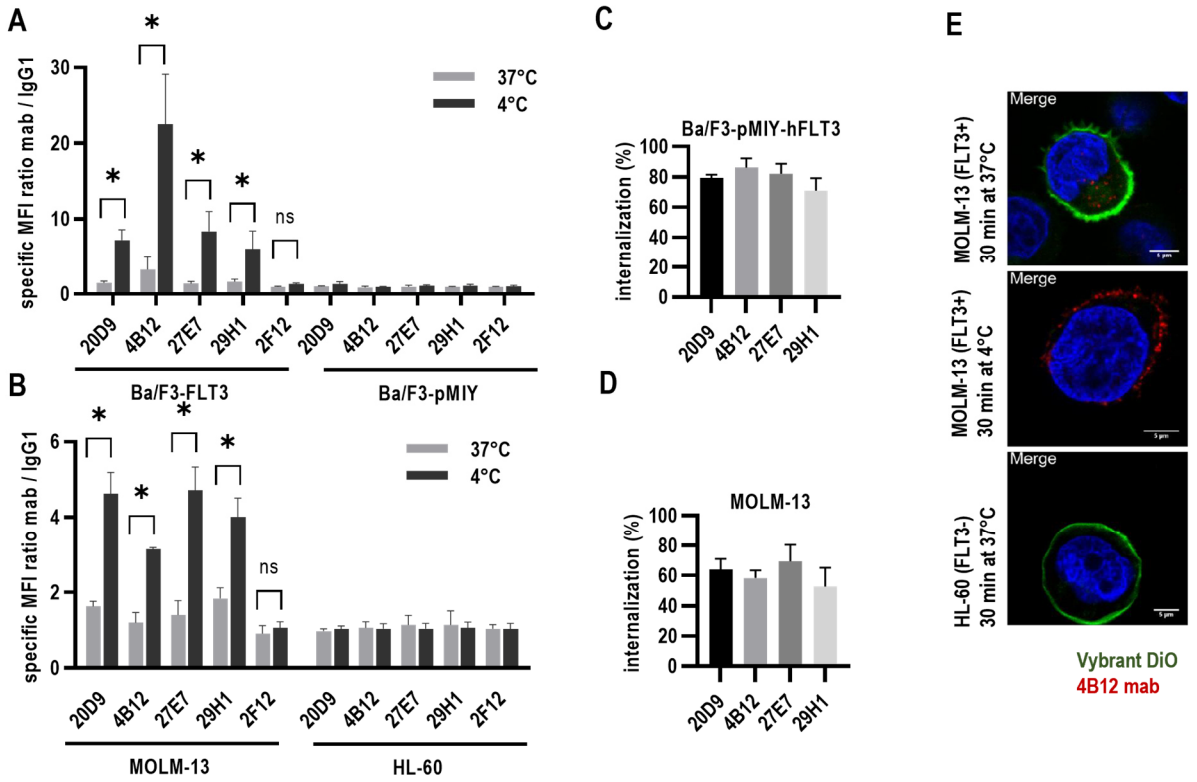

Figure 8 Evaluation of FLT3 binding and internalization of anti-FLT3 monoclonal antibodies. (A,B) Binding and temperature induced internalization of anti-FLT3 antibodies in Ba/F3 cells expressing human wildtype FLT3 or pMIY empty vector (A) or MOLM-13 and HL-60 cells (B). Internalization was induced by incubation for 30 min at 37 °C (grey) compared to 4 °C (black). Remaining surface-bound antibody was detected by flow cytometry. MFI was normalized to control human IgG1 binding. MFI= mean fluorescence intensity. Unpaired, two-tailed Student's t-test; *p<0.05; mean ± s.d. of n=3 is depicted. (C,D) Internalization rate in % calculated by MFI difference of 37 °C and 4 °C cell surface staining divided by 4 °C cell surface staining of different anti-FLT3 antibody clones in Ba/F3-hFLT3wt cells (C) and MOLM-13 cells (D). Mean ± s.d. of n=3. (E) Temperature induced internalization of 4B12 mab in MOLM-13 (FLT3 positive) cells after 30 min incubation at 37 °C compared to 4°C and HL-60 (FLT3 negative) after 37 °C incubation assessed in immunofluorescence staining. Red = FLT3 staining by 4B12, green = membrane staining by Vybrant DiO, blue = nuclear staining by DAPI. Scale bar 5 µm. Representative pictures are shown. Internalization experiments were done by Dr. Harald Polzer, LMU Klinikum (flow cytometry) and Verena Waller, LMU (IF).

Immunofluorescence staining of 4B12 antibody clone before and after temperature induced internalization in MOLM-13 is shown in Figure 8E (upper two pictures). The antibody was stained in red and was located as expected mainly at the cell membrane in the 4 °C conditions and inside the cell appearing as vesicles in the 37 °C condition, respectively. In the HL-60 FLT3 negative control cell line, the antibody was neither detectable at the cell membrane nor inside the cell. The internalized antibodies in MOLM-13 cells were further localized to early endosomes, which was demonstrated by the co-localization of the 20D9 antibody and EEA1 endosomal immunofluorescence staining (Supplementary Figure 1).

3.1.4 Epitope mapping of anti-FLT3 antibodies

For a detailed characterization, epitopes of FLT3 recognized by the different antibodies were determined. For this purpose, the antibodies were analyzed externally by PEPperPRINT© (Heidelberg, Germany). The linear epitope mapping to peptides derived from extracellular domain of FLT3 identified two main binding motifs KSSSYPM (bound by 30B12, 29H1, 27E7, 20D9) and SQGESCK (bound by 19H5, 4B12, 2F12) (Figure 9A). The rat 20D9 showed additional affinity to a third minor epitope DGYP. The two main epitopes were located at the N- terminus of the FLT3 extracellular domain, while epitope three was located close to the transmembrane domain (Figure 9B).

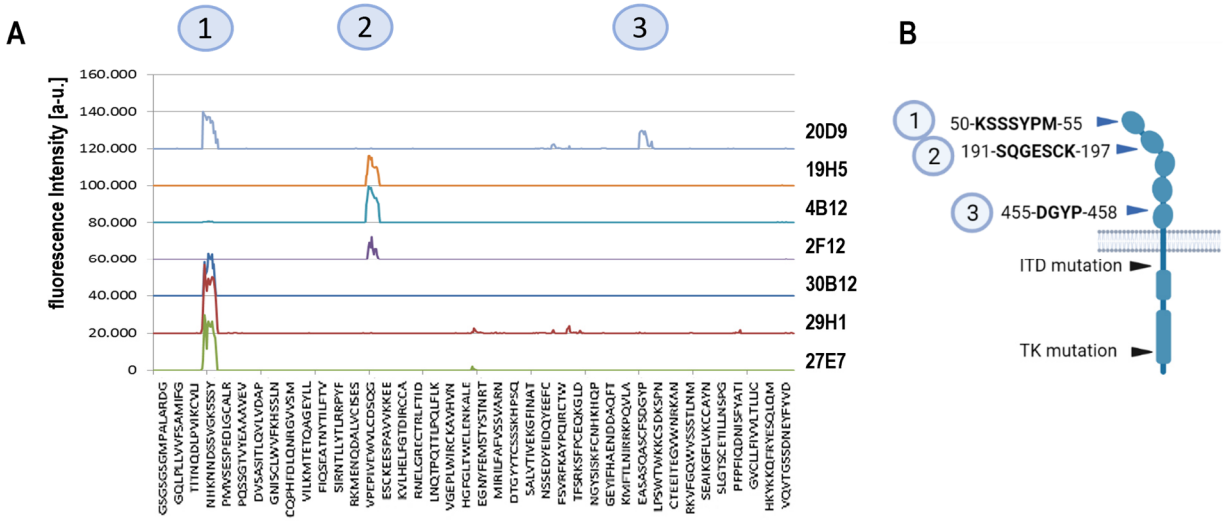

Figure 9 Epitope mapping of seven anti-FLT3 antibody clones. (A) Linear epitope mapping by PEPperPRINT© of different anti-FLT3 antibodies to peptide derived from the extracellular domain of FLT3. Numbers indicate the three identified epitopes. (B) Schematic FLT3 receptor. Black arrows indicate common mutations and blue arrows indicate the three identified epitopes of seven anti-FLT3 antibodies presented in A. Figure was created using BioRender.com.

The antibody binding to other species might be of interest and therefore, the amino acid sequences of the epitope regions identified in the human FLT3 were compared to FLT3 sequences of cynomolgus monkey (Macaca fascicularis), mouse (Mus musculus) and rat (Rattus norvegicus). The cynomolgus FLT3 showed identical sequences in all epitopes, while murine and rat sequences differed in epitope 1 and 2 (Figure 10A).

To verify the epitope analysis, the human FLT3 receptor sequence in the epitope region 1 was mutated to the murine sequence, which differs in two amino acids. The human double amino acid epitope mutant FLT3 S50P/P54R was expressed stably in Ba/F3 cells (Figure 10B). The 20D9 antibody, which recognizes the first and third epitope, was not binding anymore to the mutated FLT3 in flow cytometry analysis (Figure 10C), indicating that epitope 1 was the main binding epitope and epitope 3 was not essential. Western blot analysis of transiently transduced HEK293

cells showed that a single amino acid epitope FLT3 mutant (FLT3 P54R) was sufficient to abrogate the 20D9 antibody binding (Figure 10D). The 4B12 clone, which recognizes the epitope 2, still bound the epitope mutated variant (Figure 10D).

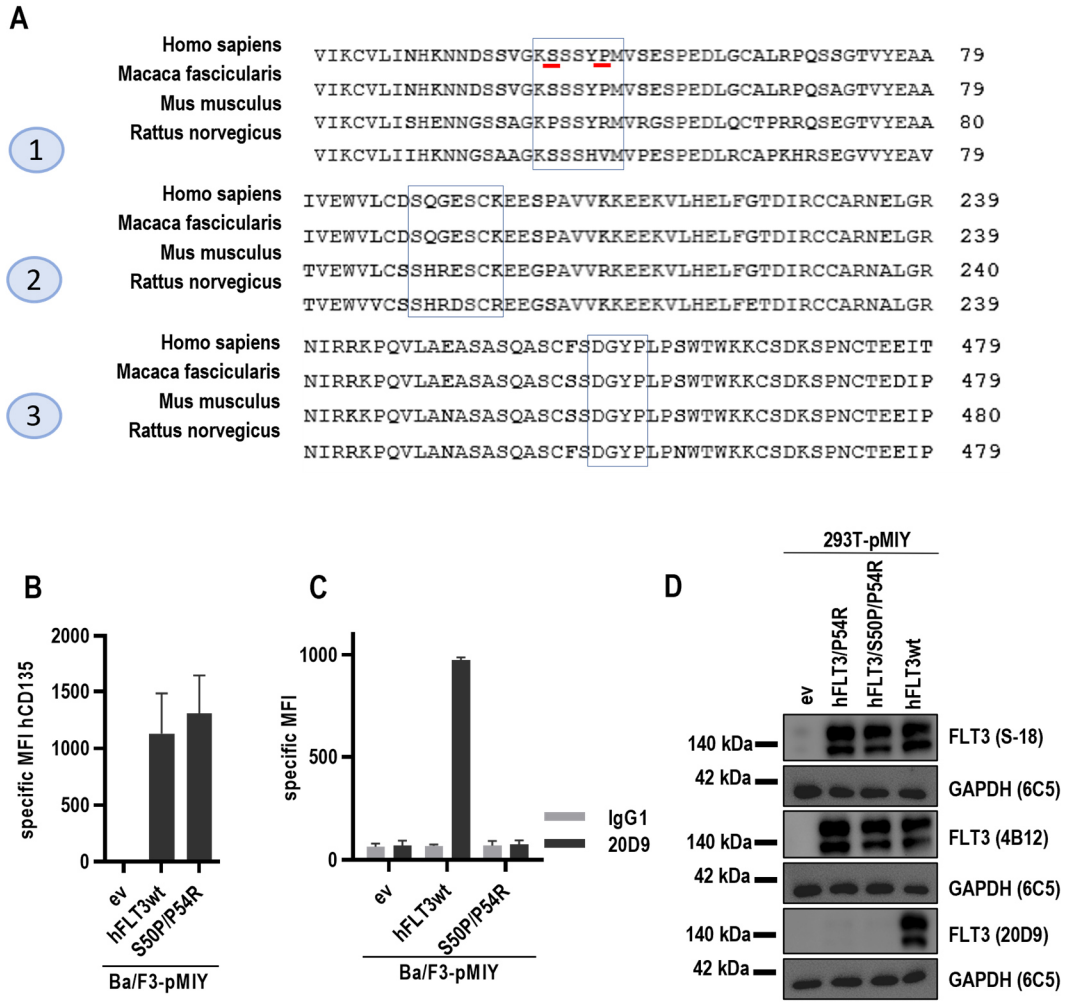

Figure 10 Evaluation of epitope specificity of anti-FLT3 monoclonal antibodies. (A) Amino acid sequence alignment of human (Homo sapiens, P36888), cynomolgus monkey (macaca fascicularis, XP015294593.1), murine (mus musculus, Q00342) and rat (rattus norvegicus, A0A0G2JW59) FLT3 receptor sequences. The blue rectangles represent the antibodies' epitopes identified from epitope mapping to human FLT3. Amino acids mutated for analysis of epitope specificity (hFLT3/S50P/P54R) are underlined in red. Alligned with https://blast.ncbi.nlm.nih.gov/. (B) Cell surface expression of human FLT3 receptor in Ba/F3-pMIY ev, hFLT3wt and epitope mutant FLT3 (hFLT3/S50P/P54R) measured by flow cytometry. Mean ± s.d. of n=3 is depicted. MFI= mean fluorescence intensity. (C) Cell surface binding of 20D9-mab or control hIgG1 antibody to Ba/F3-pMIY ev, hFLT3wt or hFLT3/S50P/P54R measured by flow cytometry. Mean ± s.d. of n=3. (D) FLT3 expression and 20D9 and 4B12 binding in HEK293T cells transiently transfected with pMIY ev, hFLT3wt or mutant FLT3 (hFLT3/P54R or hFLT3/S50P/P54R) analyzed by western blotting. GAPDH was used as loading control. The commercially available polyclonal S-18 anti FLT3 antibody recognizes all human FLT3 variants.

3.1.5 Binding analysis of anti-FLT3 antibody 20D9

As described above, FLT3 is often mutated in AML with FLT3-ITD being the most frequent and prognostically and therapeutically relevant mutation. Binding of the antibodies to FLT3-ITD is essential and unlikely to be altered compared to FLT3wt, since the FLT3-ITD mutation does not

affect the extracellular domain. To confirm binding specificity, a Ba/F3 cell line expressing human FLT3-ITD (hFLT3ITD) was used and binding of 20D9 was tested. The expression of the ITD mutant in Ba/F3 cells was only 35.9 % of the wildtype expression (Figure 11A). It is known, that FLT3-ITD has a lower surface expression[68]. The binding of 20D9 to FLT3-ITD was 20.6 % of the binding to the wildtype FLT3 (Figure 11B), probably due to the lower expression level in the cell model.

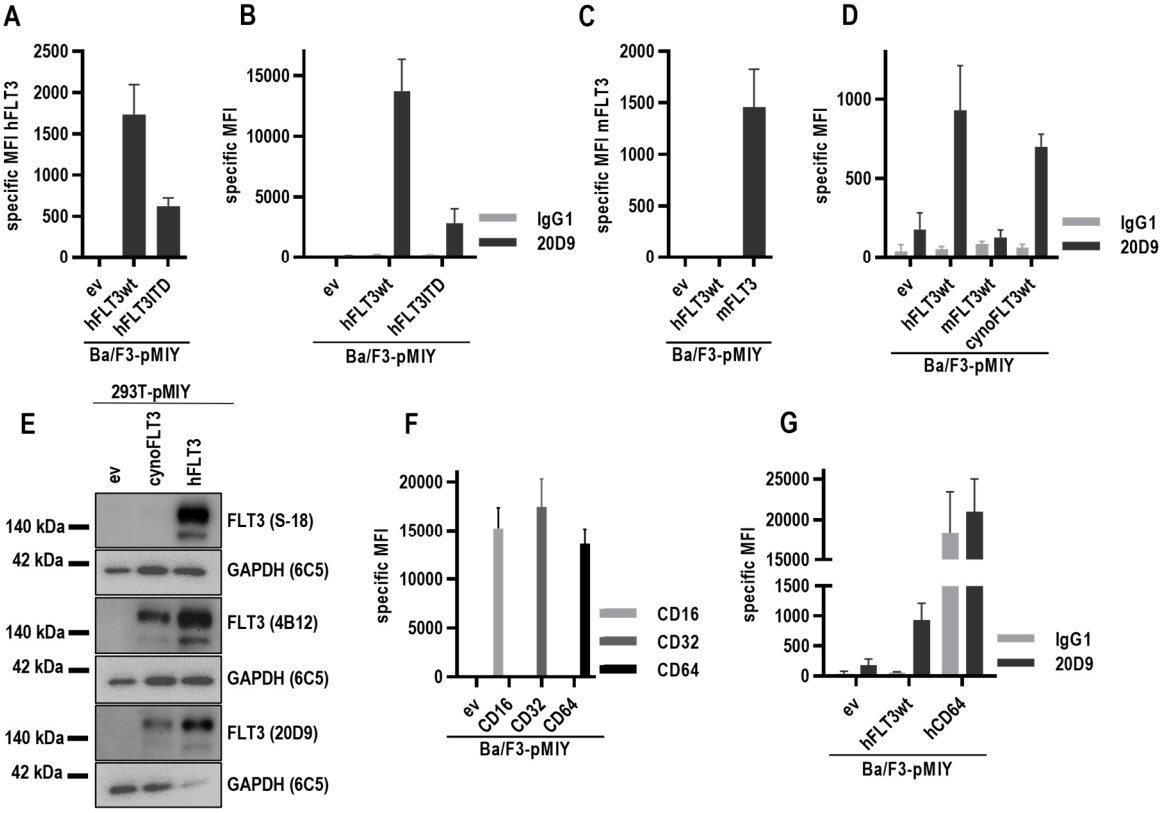

Figure 11 Binding of 20D9-mab to FLT3 variants expressed in Ba/F3 cells. Cell surface FLT3 in Ba/F3 cells stably expressing pMIY (Ba/F3-pMIY) empty vector (ev), wildtype (hFLT3wt) or ITD mutant human FLT3 (hFLT3ITD) measured by flow cytometry. Mean ± s.d. of n=3 is depicted. MFI= mean fluorescence intensity. (B) Cell surface binding of 20D9-mab or control human IgG1 antibody to Ba/F3-pMIY ev, hFLT3wt or hFLT3ITD was measured by flow cytometry. Mean ± s.d. of n=3. (C) Cell surface expression of murine FLT3 receptor in Ba/F3-pMIY ev, hFLT3wt and murine FLT3 (mFLT3) measured by flow cytometry. Mean ± s.d. of n=3 is depicted. (D) Cell surface binding of 20D9-mab or control hIgG1 antibody to Ba/F3-pMIY ev, hFLT3wt, mFLT3wt or cynomolgus monkey FLT3 (cynoFLT3wt) was measured by flow cytometry. Mean ± s.d. of n=3. (E) 20D9 and 4B12 binding in HEK293T cells transiently transfected with pMIY ev, hFLT3wt or cynoFLT3 analyzed by western blotting. GAPDH was used as loading control. (F) Cell surface human CD16, CD32 and CD64 receptor in Ba/F3-pMIY ev, Ba/F3 cells stably expressing human CD16, human CD32 or human CD64 analyzed by flow cytometry. Mean ± s.d. of n=3. (G) Cell surface binding of 20D9-mab or control IgG1 antibody to Ba/F3-pMIY ev, hFLT3wt or human CD64 (hCD64) measured by flow cytometry. Mean ± s.d. of n=3.

For future toxicity studies in animals, the binding of the antibodies to murine and cynomolgus monkey FLT3 orthologs is of importance. To evaluate the binding of the 20D9 clone to FLT3 orthologs from different species, Ba/F3 cell line models expressing murine or cynomolgus monkey were generated. Rat FLT3 was not included in the studies, since the antibody was derived from immunized rat, most likely excluding cross-reactivity with rat. Murine FLT3 was expressed in Ba/F3 cell line as verified by flow cytometry (Figure 11C) and as expected, 20D9-mab could not

bind the receptor (Figure 11D). In contrast to the murine FLT3 sequence, the protein sequence of the epitope 1 region of cynomolgus monkey FLT3 (cynoFLT3) is identical to the human FLT3 sequence. Thus, the cynoFLT3 expressing Ba/F3 cell lines bound the 20D9 antibody in flow cytometry (Figure 11D) and western blotting (Figure 11E). Here, it was also shown that the 4B12 clone could bind the cynomolgus monkey FLT3 (Figure 11E). Remarkably, the binding to cynomolgus FLT3 was weaker compared to human FLT3 for both antibody clones.

Finally, the binding of 20D9-mab to Fc receptors mediated via the IgG1 backbone was verified. Therefore, Ba/F3 cell lines stably transduced with either FCGR3a (CD16), FCGR2a (CD32) or FCGR1a (CD64, the human high affinity receptor for IgG1) were generated and the receptor expression was verified by flow cytometry (Figure 11F). As expected, Ba/F3-cells expressing CD64 bound 20D9 and IgG1 control antibody to a high extend (Figure 11G).

3.1.6 Choosing the lead candidates

After determining production efficiency, melting temperature, affinity, internalization capacity and binding epitopes for almost all antibody clones, lead candidates for ADC generation were chosen (Table 17). 30B12 and 2F12 were excluded due to low affinity, 19H5 due to low producibility and 29H1 due to low internalization.

mab	Original IgG type	Epitope	Affinity K_D (ng/ml)	Production efficiancy (µg mab/ml culture)	Internalization in MOLM-13	Internalization in Ba/F3-hFLT3
20D9	R-2a	1 (+3)	21.88	56	64 %	79 %
4B12	R-2a	2	31.91	85	58 %	86 %
27E7	M-2a	1	11.53	28	69 %	82 %
29H1	M-2a	1	28.4	24	53 %	71 %
2F12	R-2a	2	3981	68	12 %	26 %
19H5	R-2a	2	133.9	3	-	-
30B12	M-2b	1	3313	32	-	-

Table 17 Overview of antibody clone characteristics. Affinity, production efficiency and internalization were decision criteria for the lead candidate. R=rat, M=mouse.

20D9, 4B12 and 27E7 were the best candidates, representing both main epitopes (epitope 1: 20D9 and 27E7; epitope 2: 4B12) and originated from mice (27E7) and rat (20D9 and 4B12). Finally, the 20D9 clone was chosen for further ADC development as lead candidate.

3.2 Generation and characterization of 20D9 antibody-drug-conjugate

The 20D9 clone was most suitable for further development of an ADC and the 20D9-ADC was generated by applying a new conjugation method, the P5 conjugation, using phosphonamidates for coupling to the tubulin polymerization inhibitor monomethyl auristatin F. Further, the ADC stability was assessed, and the functionality was tested in cell line models.

3.2.1 P5 conjugation

Ethynylphosphonamidates have been previously described as stable alternatives for the widespread maleimide technology[90,91]. In cooperation with the Tubulis GmbH, this technique was applied to functionalize the IgG1-based 20D9 monoclonal antibody by MMAF conjugation. To obtain an IgG1-ADC only possessing the CD64 but no FLT3 binding, MMAF was conjugated to the IgG1 antibody palivizumab, which is specific for the glycoprotein F of the respiratory syncytial virus and is used for prevention of lower respiratory tract disease in pediatric patients[113].

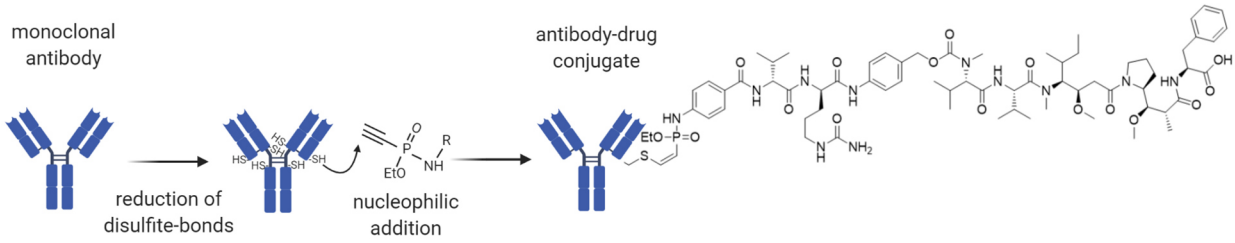

Figure 12 P5 conjugation. Schematic process of P5 conjugation technology[90] via disulfide bond reduction and Staudinger-induced Michael-addition. The final ADC consists of monoclonal antibody (20D9 or IgG1 antibody) coupled to monomethyl auristatin F toxin. The figure was created with BioRender.com. P5 conjugation was done in cooperation with Dr. Marc-Andre Kasper, Tubulis GmbH.

The disulfide bonds of native antibodies were reduced and the antibodies' cysteine residues were conjugated with a ethynylphosphonamidate molecule (P5-labelling; Figure 12A)[90,91]. Here, a cathepsin B cleavable monomethyl auristatin F - P5 conjugate was used (Supplementary Figure 2A). The product, mab-P5(OEt)-VC-PAB-MMAF (Supplementary Figure 2B) has been purified by size-exclusion chromatography.

After conjugation the ADCs were analyzed by a panel of analytical methods to determine the drug to antibody ratio, purity and identity. Mass spectrometry analysis revealed a DAR of 6.2 for the 20D9-MMAF conjugate and a similar DAR of 6.52 for the palivizumab control ADC (Supplementary Figure 2C). Quality analysis via HIC- and SEC-HPLC ensured conjugations and low aggregation (Supplementary Figure 2D,E). The HIC chromatography separates the molecules based on their hydrophobicity, which is higher the more toxin is conjugated to the antibody. Thus, the different ADC species were separated and the peaks were correlated to the toxin loading based on their

retention times. From the peak areas and the toxin loading, the average DAR could be calculated. In SEC chromatography, the ADCs were separated by the size, which allows for the assessment of unwanted high molecular weight species, indicative of ADC aggregation.

3.2.2 Storage and heat stability of the 20D9-ADC

It is important to know the stability of an ADC in regard to the stability of the toxin conjugation and its aggregation behaviour, since both influence the functionality and off-target toxicity of the drug. The P5 technology was described as a highly stable toxin to antibody linkage, which was verified for the 20D9-ADC in temperature incubation and long-term storage assays. The ADC was incubated for 1 or 2 weeks at 4 °C, 37 °C or 40 °C and additionally samples were taken at different timepoints for 1.5 years while the ADC was stored at 4°C. All samples were analyzed in HIC and SEC chromatography to determine the average DAR and amount of aggregates, respectively. As a result, the 37 °C and 40 °C incubation or a storage for 14 months at 4 °C did not significantly impact the 20D9-ADC DAR of 6.2, confirming the stable antibody-toxin conjugation (Figure 13A,B). The HMWS analysis showed that an incubation for 2 weeks at 40 °C or storage for 14 months at 4 °C and only slightly induced ADC aggregation from 1 % to 4.5 % or 2 %, respectively (Figure 13C,D).

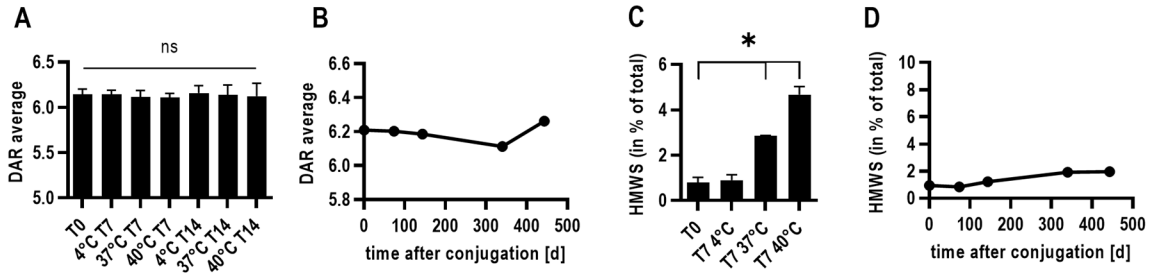

Figure 13 Heat and storage stability of 20D9-ADC. (A,B) Drug to antibody ratio (DAR) average of 20D9-ADC measured by hydrophobicity interaction chromatography (HIC). DAR average was calculated by division of the sum of peak areas multiplied with respective DAR by total peak area. (A) DAR of 20D9-ADC after heat incubation (37 °C and 40 °C) for 7 or 14 days compared to 4 °C stored sample. Mean ± s.d. of n=3. Unpaired, two-tailed Student's t-test; *p<0.05. (B) DAR of 20D9-ADC after long term storage at 4 °C. (C,D) High molecular weight species (HMWS) of 20D9-ADC measured by size exclusion chromatography (SEC) to assess the aggregation. Percent HMWS calculated relative to total ADC amount. (C) HMWS of 20D9-ADC after heat incubation (37 °C and 40 °C) for 7 days compared to 4 °C stored sample. Mean ± s.d. of n=3. Unpaired, two-tailed Student's t-test; *p<0.05. (D) HMWS of 20D9-ADC after long term storage at 4 °C. Analytical HIC and SEC analysis was done by Dr. Marcus Gerlach from Tubulis GmbH.

3.2.3 Cytotoxicity of 20D9-ADC to FLT3 in the Ba/F3 cell model

Proof-of concept cytotoxicity assays were carried out using a myeloid cell line model expressing the human proteins of interest. The cytotoxicity of the 20D9-ADC was tested in Ba/F3 cells expressing the human FLT3 either as wildtype or as ITD mutant. Both cell lines were sensitive to

the 20D9-ADC with IC_{50} values of 720.5 ng/ml and 1557 ng/ml (Figure 14A,B). The higher IC_{50} values of FLT3-ITD expressing Ba/F3 cells can be explained by the lower cell surface receptor expression.

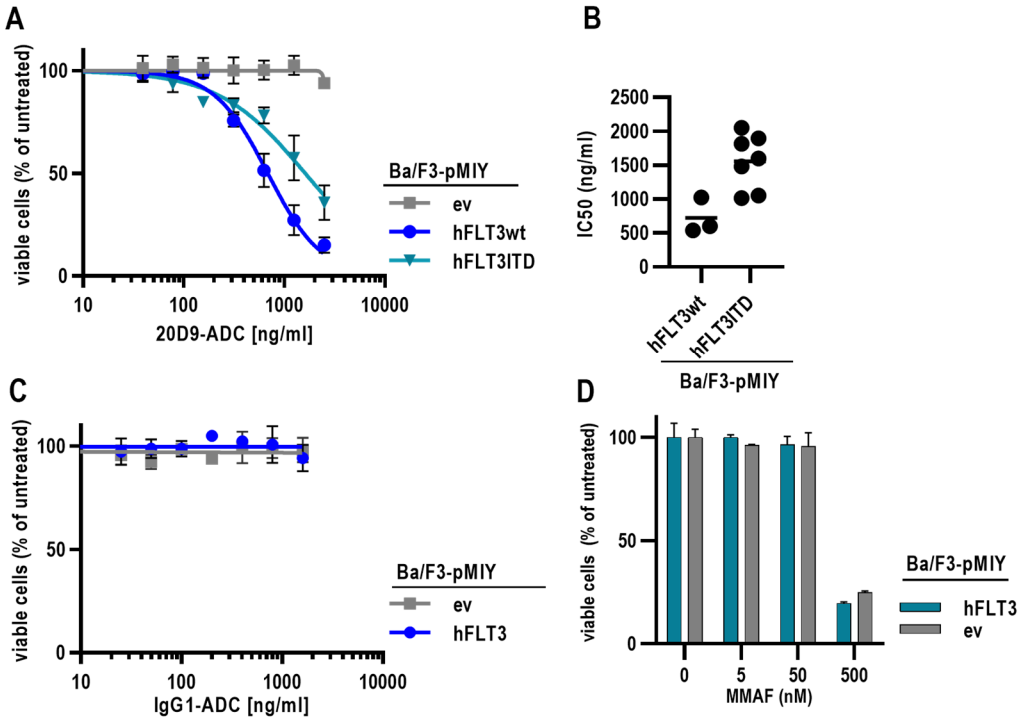

Figure 14 Analysis of cytotoxicity of 20D9-ADC to Ba/F3 cell lines expressing human FLT3. (A-D) Assessment of cytotoxicity of ADCs in different Ba/F3 cell lines. Viability was determined after 72 h treatment with different drug concentrations by trypan blue exclusion count and compared to untreated control. Mean ± s.d. of n=3 biological replicates. (A) Treatment of Ba/F3-pMIY ev, hFLT3wt and hFLT3ITD with 20D9-ADC. (B) IC_{50} values of 20D9-ADC in Ba/F3-hFLT3wt and Ba/F3-hFLT3ITD cell lines. Calculation based on data from A, calculated by GraphPad Prism. Unpaired, two-tailed Student's t-test; *p<0.05. Each dot represents a replicate, horizontal line indicates mean. (C) Treatment of Ba/F3-pMIY ev and hFLT3wt with IgG1-ADC. (D) Treatment of Ba/F3-pMIY ev and hFLT3wt with toxin MMAF. Mean ± s.d. of n=2 biological replicates.

As control, the FLT3 negative Ba/F3 cells expressing the empty vector were not affected even with high concentrations up to 2500 ng/ml of 20D9-ADC. Additionally, Ba/F3-hFLT3 and empty vector control were treated with the control IgG1-ADC. As expected, the IgG1-ADC had no effect, since no human Fc receptors were expressed (Figure 14C). Further, the cytotoxicity of uncoupled MMAF was tested in Ba/F3-hFLT3 and empty vector control cell line to ensure similar sensitivity to the toxin itself. As expected and due to its inability to cross cell membranes, MMAF killed Ba/F3 cells only at high concentrations of 500 nM and independent of FLT3 expression (Figure 14D). These assays verify a specific FLT3 cytotoxicity in the Ba/F3-hFLT3 cell model.

Next, the cytotoxicity against other FLT3 species and variants was tested. Cynomolgus monkey FLT3 expressing Ba/F3 cells were sensitive to 20D9-ADC treatment comparable to human FLT3

(Figure 15A). Consistent with the binding analysis, 20D9-ADC was not cytotoxic in Ba/F3-mFLT3 and the epitope mutant Ba/F3-hFLT3 S50P/P54R cells (Figure 15B).

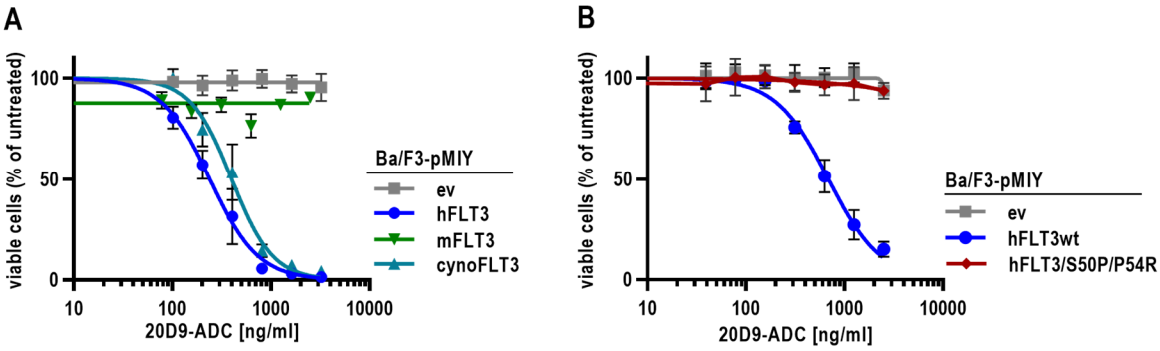

Figure 15 Analysis of cytotoxicity of 20D9-ADC to Ba/F3 cell lines expressing variants of FLT3. (A-B) Assessment of cytotoxicity of ADCs in different Ba/F3 cell lines. Viability was determined after 72 h treatment with different concentrations by trypan blue exclusion count and compared to untreated control. Mean ± s.d. of n=3 biological replicates. (A) Treatment of Ba/F3-pMIY ev, hFLT3wt, mFLT3wt and cynoFLT3wt with 20D9-ADC. (B) Treatment of Ba/F3-pMIY ev, hFLT3wt and hFLT3/S50P/P54R with 20D9-ADC.

3.2.4 FLT3 dependent and Fc receptor dependent cytotoxicity of 20D9-ADC

As described, besides the FLT3 specific binding, the 20D9-ADC could also bind CD64 receptor. The sensitivity of Ba/F3 cell lines expressing human Fc receptors CD64, CD32 or CD16 was tested in 20D9-ADC cytotoxicity assays. Only CD64 expression was sufficient to sensitize the Ba/F3 cell to 20D9-ADC treatment. Ba/F3 cells expressing CD16 or CD32 did not respond to 20D9-ADC treatment (Figure 16A).

These results indicated that the 20D9-ADC confers cytotoxicity via two different receptors, FLT3 and CD64. Based on these findings, it should be estimated if targeting both receptors is an advantage compared to targeting only one of them. Therefore, the FLT3 dependent and Fc receptor dependent cytotoxicity of 20D9-ADC was determined by using Ba/F3 cells expressing either CD64 or the combination of CD64 and human FLT3. The expression of both receptors was verified by western blotting (Figure 16B). In theory, 20D9-ADC and control IgG1-ADC should have similar cytotoxic efficacy in CD64 expressing Ba/F3 cells, since they target the same receptor. In Ba/F3 cells expressing both receptors, 20D9-ADC was expected to be more potent based on the additional binding to the FLT3 receptor. Confirming the hypotheses, Ba/F3 cells expressing CD64 were sensitive to 20D9-ADC and control IgG1-ADC with similar IC_{50} values of 37.3 ng/ml and 31.8 ng/ml, respectively (Figure 16C,E). Ba/F3 cells expressing both hFLT3wt and CD64 were significantly more sensitive to 20D9-ADC compared to IgG1-ADC ((IC_{50} = 0.5 ng/ml versus 78.3 ng/ml), indicating the advantage of targeting both antigens *in vitro* (Figure 16D,E).

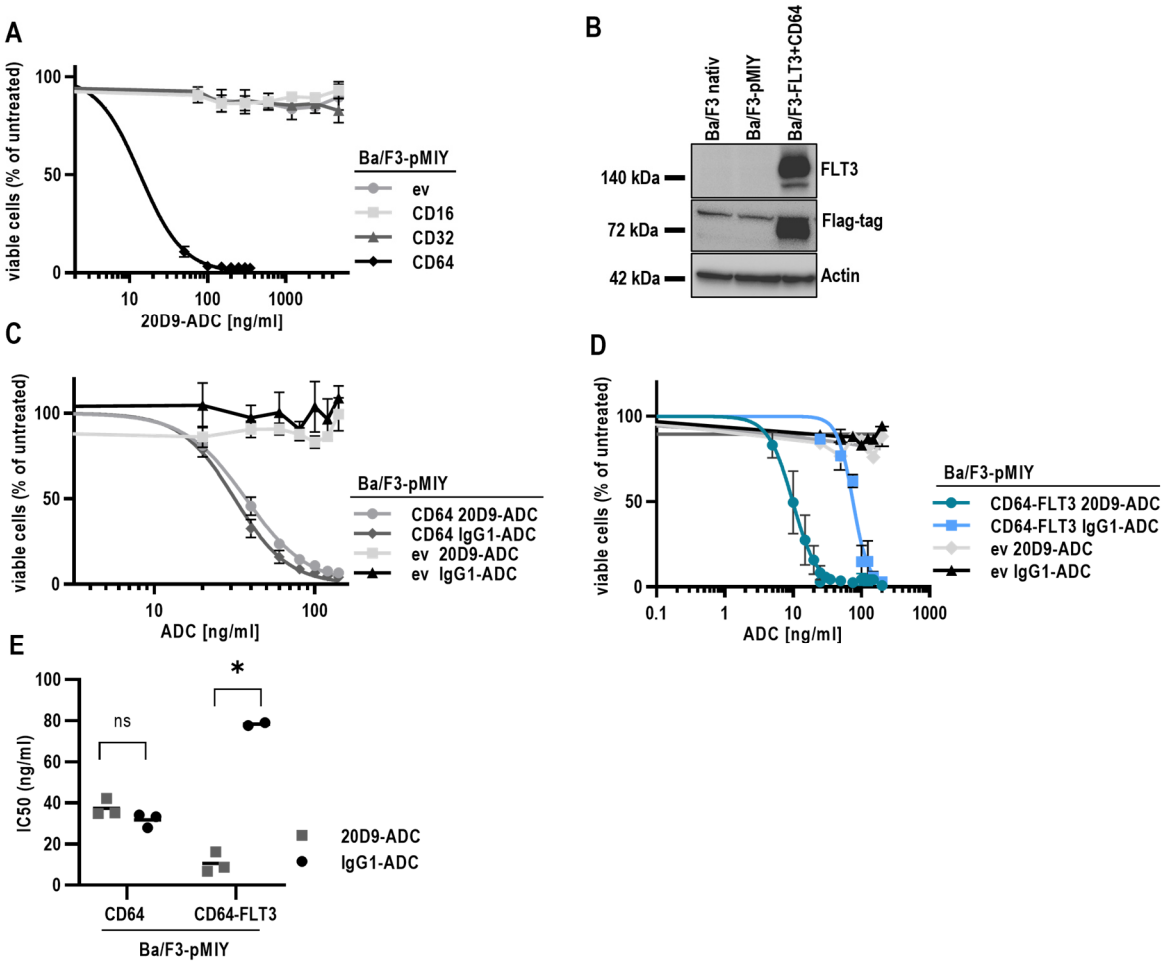

Figure 16 Analysis of cytotoxicity of 20D9-ADC to Fc receptor expressing Ba/F3 cells. (A,C-D) Assessment of cytotoxicity of ADCs in different Ba/F3 cell lines. Viability was determined after 72 h drug treatment by trypan blue exclusion count and compared to untreated control. Mean ± s.d. of n=3 biological replicates. (A) Treatment of Ba/F3-pMIY ev, human FCGR3A (CD16), human FCGR2A (CD32) or human FCGR1A (CD64) with 20D9-ADC. (B) Expression of FLT3 and CD64 in native Ba/F3 cells (native) or Ba/F3 cells transduced with either empty vector (ev) or FLT3 and FLAG-tagged CD64 (FLT3-CD64) analyzed by western blotting. Loading control stained with anti-β-actin. (C) Treatment of Ba/F3-pMIY ev or CD64 with either 20D9-ADC or IgG1-ADC. (D) Treatment of Ba/F3-pMIY ev or CD64-FLT3 with either 20D9-ADC or IgG1-ADC. (E) IC_{50} values of 20D9-ADC and IgG1-ADC in Ba/F3-CD64 and Ba/F3-CD64-FLT3 cell lines. Calculation based on data from C and D using GraphPad Prism. Unpaired, two-tailed Student's t-test; *p<0.05. Each dot represents a replicate, horizontal line indicates mean.

Taken together, an antibody-drug-conjugate of 20D9-mab was successfully generated and showed good stability characteristics. The ADC specifically bound and confered cytotoxicity to Ba/F3 cells expressing human wildtype FLT3, human FLT3ITD mutant and cynomolgus monkey FLT3. Further, it was shown that the 20D9-ADC was cytotoxic via FLT3 and via CD64 binding.

3.3 *In vitro* cytotoxic activity of 20D9-ADC in AML cell lines

Next, the cytotoxicity of the 20D9-ADC in human AML cell lines endogenously expressing FLT3 and Fc receptors was evaluated. It was investigated if there is a correlation between expression levels and IC_{50} values of 20D9-ADC and IgG1-ADC. Further, the Fc receptor and FLT3 mediated cytotoxicity was characterized.

3.3.1 Target receptor expression in leukemia and lymphoma cell lines

First, the expression levels of FLT3 and CD64 in different leukemia and lymphoma cell lines were determined (Figure 17A,B). As expected HL-60, K-562, Karpas-422, KG-1a, L428 and U-937 cells did not show any detectable FLT3 expression. Kasumi-1 showed minimal expression, NOMO-1 and MV4-11 cells a weak expression, PL-21, THP-1, OCI-AML3 and -5 a moderate expression, MM-1 and MOLM-13 a strong expression and MM-6 a very strong FLT3 expression. CD16 was not expressed at detectable levels in the investigated cell lines and CD32 and CD64 were expressed in a range of very low to very high levels. Interestingly, a significant correlation of FLT3 and CD64 cell surface expression levels in the AML and lymphoma cell lines could be detected (Figure 17C).

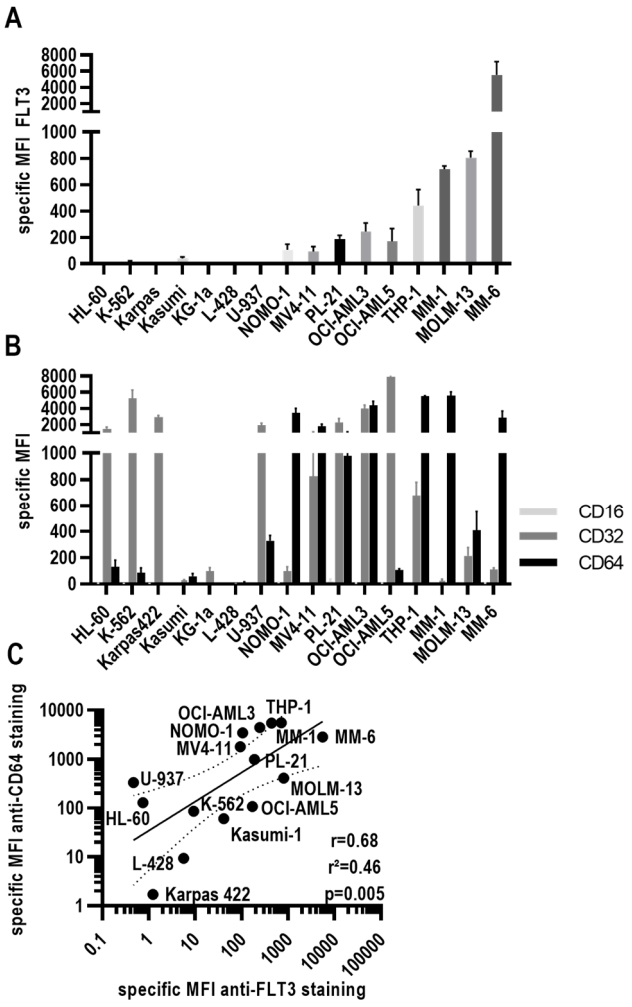

Figure 17 Expression of FLT3 and CD64 in AML cell lines. (A) Cell surface expression of human FLT3 receptor on different leukemia and lymphoma cell lines measured by flow cytometry. Mean ± s.d. of n=3. MFI= mean fluorescence intensity. (B) Cell surface expression of human CD16, CD32 or CD64 receptor on different leukemia and lymphoma cell lines measured by flow cytometry. Mean ± s.d. of n=3. (C) Correlation of MFI of CD64 cell surface expression and MFI of FLT3 cell surface expression of myeloid human cell lines measured by flow cytometry, presented in A and B. Black line indicates simple linear regression with error interval. r = Pearson correlation coefficient; r^2= Coefficient of determination; p = p value from two tailed test with confidence interval of 95%. MFI = mean fluorescence intensity.

3.3.2 Cytotoxicity of 20D9-ADC in leukemia and lymphoma cell lines

Further, the cytotoxicity of 20D9-ADC in leukemia and lymphoma cell lines was investigated. Since the chimeric 20D9-mab also binds to Fc receptors via its human Fc-backbone, the binding analysis were carried out using the rat monoclonal 20D9 antibody and compared to control rat IgG (Figure 18A). Binding of the rat 20D9 antibody could be shown in all FLT3 positive cell lines, whereas the FLT3 negative cell lines did not bind the 20D9 antibody.

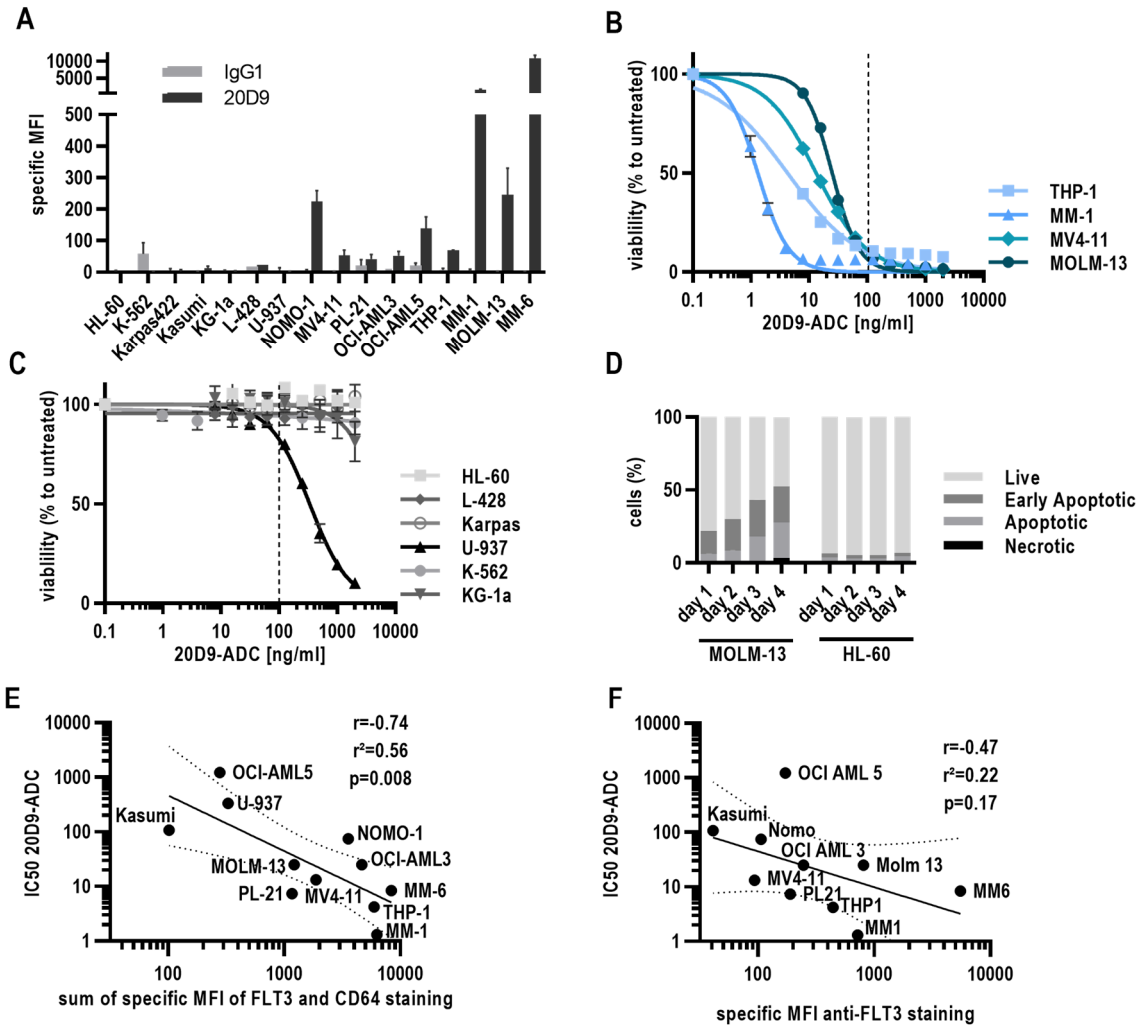

Figure 18 Binding and cytotoxicity of 20D9-ADC to leukemia and lymphoma cell lines. (A) Cell surface binding of rat 20D9 antibody or control rat IgG1 antibody to leukemia and lymphoma cell lines measured by flow cytometry. Mean ± s.d. of n=3. (B,C) Assessment of cytotoxicity of ADCs in different human cell lines. Viability was determined after 96h treatment with different concentrations of ADCs by resazurin fluorescence and normalized to untreated control. Dashed line indicates 100 ng/ml drug concentration. Mean ± s.d. of n=3 biological replicates. (B) Treatment of FLT3 positive human cell lines with 20D9-ADC. (C) Treatment of FLT3 negative human cell lines with 20D9-ADC. (D) Apoptosis in MOLM-13 and HL-60 cells after treatment with 30 ng/ml 20D9-ADC for 1, 2, 3 and 4 days analyzed by flow cytometry after annexin V-APC and propidium iodid staining. Double negative (live), annexin stained (early apoptotic), Iodid stained (necrotic) and double positive (late apoptotic) cells are presented in percent of all cells. Mean of n=3 is depicted. (E,F) Correlation of IC_{50} values of 20D9-ADC and receptor cell surface expression of myeloid human cell lines measure by flow cytometry. Black line indicates simple linear regression with error interval. r = Pearson correlation coefficient; r^2 = Coefficient of determination; p = p value from two tailed test with confidence interval of 95%. (E) Correlation of IC_{50} values of 20D9-ADC and sum of MFI of FLT3 and CD64 cell surface expression. (F) Correlation of IC_{50} values of 20D9-ADC and MFI of FLT3 cell surface expression.

Cytotoxicity of the 20D9-ADC could be shown in all FLT3 positive cell lines with IC_{50} values varying between 1.3 ng/ml and 107.33 ng/ml (Figure 18B, Table 18). Further, no cytotoxicity of 20D9-ADC was observed in 5 out of 6 FLT3 negative AML cell lines. The FLT3 negative, CD64 positive cell line U-937 showed an IC_{50} value of 334 ng/ml (Figure 18C). The 20D9-ADC acts via apoptosis induction, which was demonstrated in FLT3-ITD positive MOLM-13 cells treated with 30 ng/ml compared to FLT3 negative HL-60 cells using annexin-V/PI staining (Figure 18D). Consistently, there was a correlation of the expression of both CD64 and FLT3 receptors and the 20D9-ADC IC_{50} values (Figure 18E). For the FLT3 expression and the 20D9-ADC IC_{50} values, there was a weak correlation (Figure 18F).

As control, all cell lines were incubated with unconjugated 20D9-mab, which did not result in reduced cell proliferation. For the cell lines MM-1 and MV4-11 even an enhanced cell proliferation was observed (Figure 19A). As well, the unconjugated control IgG1 antibody did not impair cell proliferation (data not shown). Further, FLT3 positive MOLM-13 and FLT3 negative HL-60 cell lines showed similar sensitivity towards the ADC payload MMAF (Figure 19B).

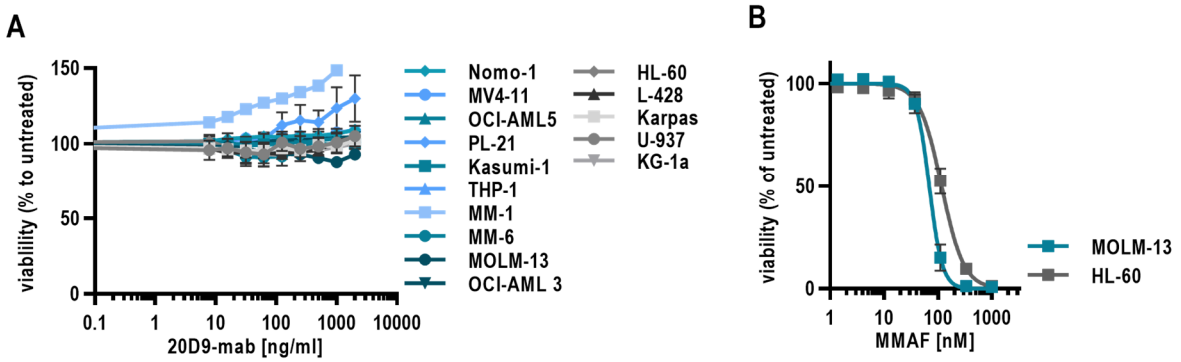

Figure 19 Cytotoxicity of 20D9-mab and toxin MMAF to leukemia and lymphoma cell lines. Cytotoxicity of 20D9-mab (A) and MMAF (B) in AML cell lines. Viability was determined after 96 h treatment with different concentrations of indicated drug by resazurin fluorescence and normalized to untreated control. Mean ± s.d. of n=3 biological replicates.

To analyze CD64 mediated cytotoxicity, the cell lines were treated with the control IgG1-ADC, which showed cytotoxic activity with IC_{50} values ranging from 12.82 ng/ml to around 2000 ng/ml (Figure 20A,B; Table 18). Confirming the results of the Ba/F3 cell model, the cytotoxic activity of IgG1-ADC *in vitro* seemed to be dependent on CD64, but not on CD32. For example, the weak CD64 expression in HL60-60 and K-562 cells was not sufficient to reduce cell proliferation. However, some cell lines did not show the correlation of CD64 expression and IgG1-ADC sensitivity. In Kasumi-1 cells, which had a very weak CD64 expression, the IgG1-ADC had intermediate IC_{50} values around 200 ng/ml. Furthermore, the MM6 cell line expresses CD64 at high levels as detected by flow cytometry, but did not respond to IgG1-ADC treatment. Thus, a correlation

between IgG1-ADC IC_{50} and CD64 cell surface expression was not significant (Figure20 C). Compared to 20D9-ADC, IgG1-ADC showed in general higher IC_{50} (Figure 20D, Table 18).

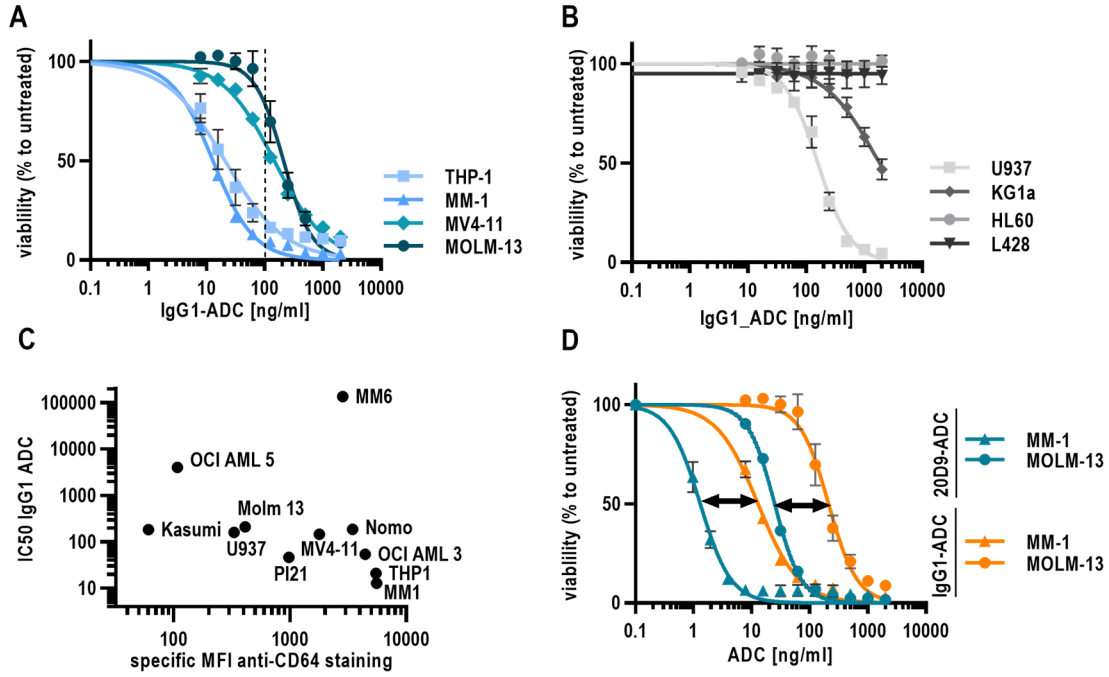

Figure 20 Analysis of cytotoxicity of control IgG1-ADC in leukemia and lymphoma cell lines. (A-B,D) Assessment of cytotoxicity of ADCs in different human cell lines. Viability was determined after 96 h treatment with different concentrations of ADCs by resazurin fluorescence and normalized to untreated control. Dashed line indicates 100 ng/ml drug concentration. Mean ± s.d. of n=3 biological replicates. (A) Treatment of FLT3 positive human cell lines with IgG1-ADC. (B) Treatment of FLT3 negative human cell lines with IgG1-ADC. (C) Correlation of IC_{50} values of 20D9-ADC and MFI of CD64 cell surface expression of myeloid human cell lines measure by flow cytometry. (D) Comparison of cytotoxicity of 20D9-ADC and IgG1-ADC in MOLM-13 and MM-1 cells. Arrows emphasize the sensitivity difference of the respective cell line to the drugs.

Name	FLT3 status	IC_{50} IgG1-ADC (ng/ml)	IC_{50} 20D9-ADC (ng/ml)
MM-1	V592A	12.82	1.3
THP-1	wt	20.8	4.23
PL-21	ITD het.	46.14	7.4
MM-6	V592A	> 5000	8.42
MV4-11	ITD LOH	146.53	13.17
MOLM-13	ITD het.	211.47	24.91
OCI-AML3	wt	54.07	25.03
NOMO-1	wt	186.12	74.92
KASUMI-1	wt	182.39	107.33
U-937	wt	159.29	334.14
OCI-AML5	wt	4026.47	1221.38
KG-1a	wt	1821.2	-
HL-60	wt	-	-
L-428	wt	-	-
Karpas-422	wt	-	-
K-562	wt	-	-

Table 18 IC_{50} values of 20D9-ADC and IgG1-ADC in leukemia and lymphoma cell lines.

3.3.3 FLT3 dependent and Fc receptor dependent cytotoxicity of 20D9-ADC in AML cell lines

To investigate the impact of CD64 on the efficacy of IgG1 based ADCs, the CD64-IgG1 binding was disrupted. This was done by removing the N-linked glycans of 20D9-ADC and IgG1-ADC, which are essential for the interaction of IgG1 and Fc receptors[79]. The effective deglycosylation of the protein is shown by the lower molecular weight of the heavy chains of 20D9-ADC and IgG1-ADC after treatment with the enzyme Endo S (Figure 21A). The binding of deglycosylated 20D9 and IgG1 antibody was reduced in Ba/F3 cells expressing human CD64 compared to the native controls. Remarkably, there was no complete loss of the binding capacity. In Ba/F3-hFLT3wt cells, the binding affinity of the deglycosylated 20D9 to FLT3 was unaffected (Figure 21B), as expected. In the cytotoxicity assay in MOLM-13 and HL-60 cells, the deglycosylated IgG1-ADC showed no activity on MOLM-13 cells in the tested concentration range. Since there was no complete abrogation of the CD64- FcγR binding, it might be that the remaining binding was too weak to induce internalization. Compared to the native 20D9-ADC, the IC_{50} value of deglycosylated 20D9-ADC shifted from 15.7 ng/ml to 473.7 ng/ml reflecting the proportions of FLT3 and CD64 specific effects (Figure 21C).

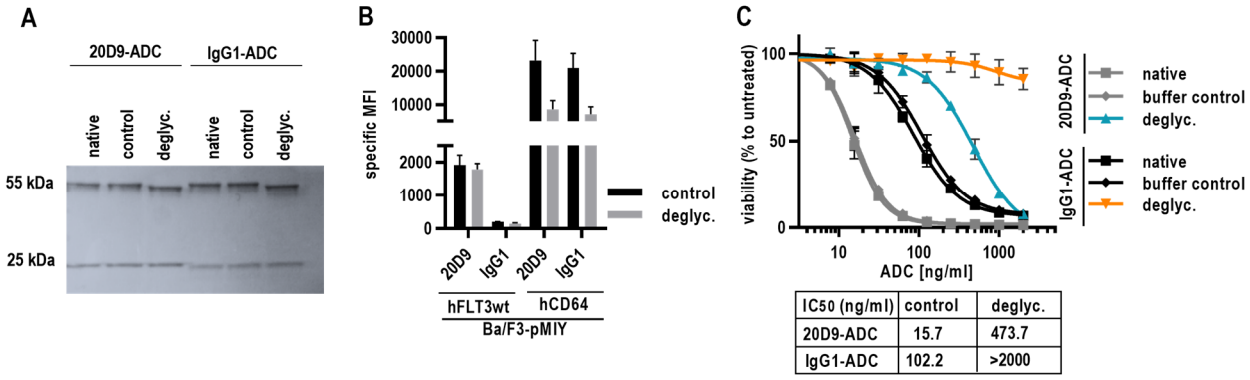

Figure 21 Cytotoxicity of deglycosylated 20D9-ADC and control IgG1-ADC in leukemia and lymphoma cell lines. (A) native 20D9-ADC and IgG1-ADC (native), buffer-incubated control (control) or deglycosylated by Endo-S treatment (deglyc.) were analyzed in SDS-PAGE and Coomassie staining confirming the successful degylcosylation by the decreased weight of the heavy chain. (B) Assessment of binding of 20D9-ADC or IgG1-ADC either buffer - incubated control or deglycosylated to Ba/F3-pMIY hFLT3wt or hCD64 was measured by flow cytometry. Mean ± s.d. of n=3. (C) Assessment of cytotoxicity of ADCs in different human cell lines. Viability was determined after 96 h treatment of MOLM-13 cells with 20D9-ADC or IgG1-ADC either native, buffer - incubated control or deglycosylated by resazurin fluorescence and normalized to untreated control. Mean ± s.d. of n=3 biological replicates.

Another approach to discriminate between the FLT3 and the CD64 mediated cytotoxicity was the saturation of Fc receptor binding sites with immunoglobulins (IGs). Therefore, Flebogamma®, an approved immunoglobulin substitute, was used. Flebogamma consists of 66.6 % IgG1, 28.5 % IgG2, 2.7 % IgG3 and 2.2 % IgG4 prepared from human plasma[114].The applied concentration was

derived from the immunoglobulin level in healthy human sera, which range from 7 to 12 g/l. 75 % of the immunoglobulins are IgG, which means 5.25 to 9 g/l [115]. So, 8 g/l flebogamma were added to the assays to mimick the IgG concentration in human plasma. MOLM-13 cells, which express CD64 and FLT3, were treated with 20D9-ADC and IgG1-ADC together with 8 mg/ml IGs. The cytotoxic effect of IgG1 was completely inhibited after Flebogamma incubation while 20D9-ADC was still active but with reduced efficacy (Figure 22A). Presumably, the remaining cytotoxicity was conferred by FLT3 receptor binding. Further, the U-937 cell line, which expressed only CD64 and no FLT3 receptor, was tested. In line with the expression, 20D9-ADC and IgG1-ADC showed similar cytotoxicity in U-937 cell line and immunoglobulin supplementation inhibited both ADCs similarly (Figure 22B). HL-60 cells were used as control and showed no sensitivity to the ADCs with or without Flebogamma supplementation.

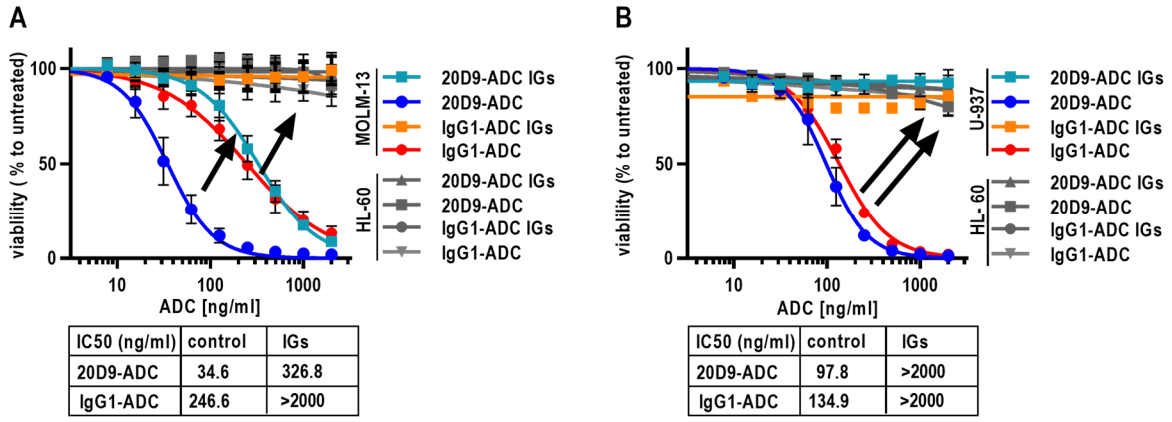

IC50 (ng/ml)	control	IGs
20D9-ADC	34.6	326.8
IgG1-ADC	246.6	>2000

IC50 (ng/ml)	control	IGs
20D9-ADC	97.8	>2000
IgG1-ADC	134.9	>2000

Figure 22 Cytotoxicity of 20D9-ADC and control IgG1-ADC with immunoglobulin supplement. Assessment of cytotoxicity of ADCs in different human cell lines. Viability was determined after 96 h treatment with different concentrations of ADCs by resazurin fluorescence and normalized to untreated control. Mean ± s.d. of n=3 biological replicates. IC_{50} values are indicated below. (A) Treatment of MOLM-13 and HL-60 cell line with IgG1-ADC or 20D9-ADC with or without 8 mg/ml immunoglobulin supplementation. (B) Treatment of U937 and HL-60 cell line with IgG1-ADC or 20D9-ADC with or without 8 mg/ml immunoglobulin supplementation.

In conclusion, the 20D9-ADC has significant cytotoxic activity in human AML cell lines and it was possible to discriminate between the FLT3 and the CD64 mediated toxicity using deglycosylated ADCs and immunoglobulin supplementation in the cytotoxicity assays.

3.4 Antileukemic activity of 20D9-ADC *in vivo* in AML mouse models

To determine the *in vivo* antileukemic activity of 20D9-ADC, xenograft mouse models of AML were used. In this method, cells stably transduced with luciferase expressing vectors were injected into immunodeficient NOD SCIDγ (NSG) mice. This allowed *in vivo* monitoring of the disease during treatment with bioluminescence imaging (BLI). Once or twice per week, the animals were anesthetized, injected with the luciferase substrate and imaged for bioluminescence, which was detected with high sensitivity through the skin. For this purpose, either AML cell lines or primary patient samples can be applied. Particularly, this method is useful for investigation of patient samples, since they do not grow well in cell cultures. Primary AML patient samples were isolated and transplanted in NSG mice. After engraftment, cells were reisolated and transduced with luciferase and fluorescent protein expressing vector, that allows for fluorescent activated cell sorting (FACS) of positive cells. The cells were retransplanted, isolated and enriched by FACS for positivity (Figure 23). For AML cell line based *in vivo* experiments, cells were stably transduced with luciferase and fluorescent marker protein expressing vector. All *in vivo* experiments were conducted in kind cooperation with Prof. Irmela Jeremias, Helmholtz Zentrum München.

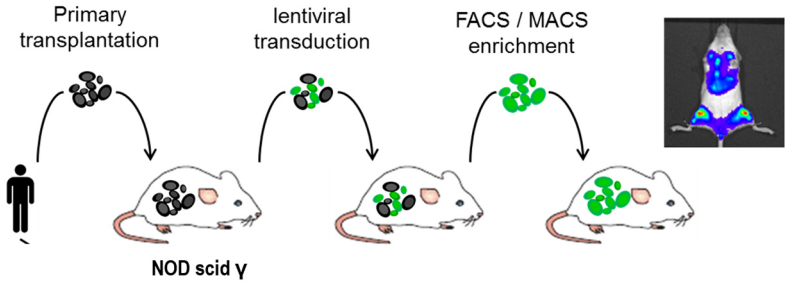

Figure 23 Schematic process of patient derived xenograft generation in NSG mice. Primary human AML cells are transplanted in mice and tumor burden in mice can be monitored by bioluminescence imaging. This technique is established in the laboratory of Prof. Irmela Jeremias, Helmholtz Zentrum München.

3.4.1 Evaluation of *in vivo* activity of 20D9-ADC in MOLM-13 mouse model

First, the efficacy of ADCs in the MOLM-13 xenograft model was analyzed *in vivo*. Mice were injected with transgenic MOLM-13 cells and treated once per week intravenously with 1 mg/kg 20D9-ADC (6 weeks) or 3 mg/kg 20D9-ADC (4 weeks) and compared to PBS treated mice. While repetitive administration of 1 mg/kg 20D9-ADC decelerated the increase of BLI signal compared to PBS treated control mice, 3 mg/kg of 20D9-ADC led to a strong reduction of the tumor burden below BLI detection limit for at least 154 days (Figure 24A). To simulate a very high leukemic burden, the PBS treated animals with fully grown leukemia were treated with 3 mg/kg 20D9-ADC weekly intravenously for three weeks. The anti-tumor effect of 20D9-ADC at advanced tumor

burden was comparable to therapy started at intermediate tumor burden (Figure 24B). After three applications, the tumor cells were strongly reduced but still detectable and the MOLM-13 cells regrew after treatment stop.

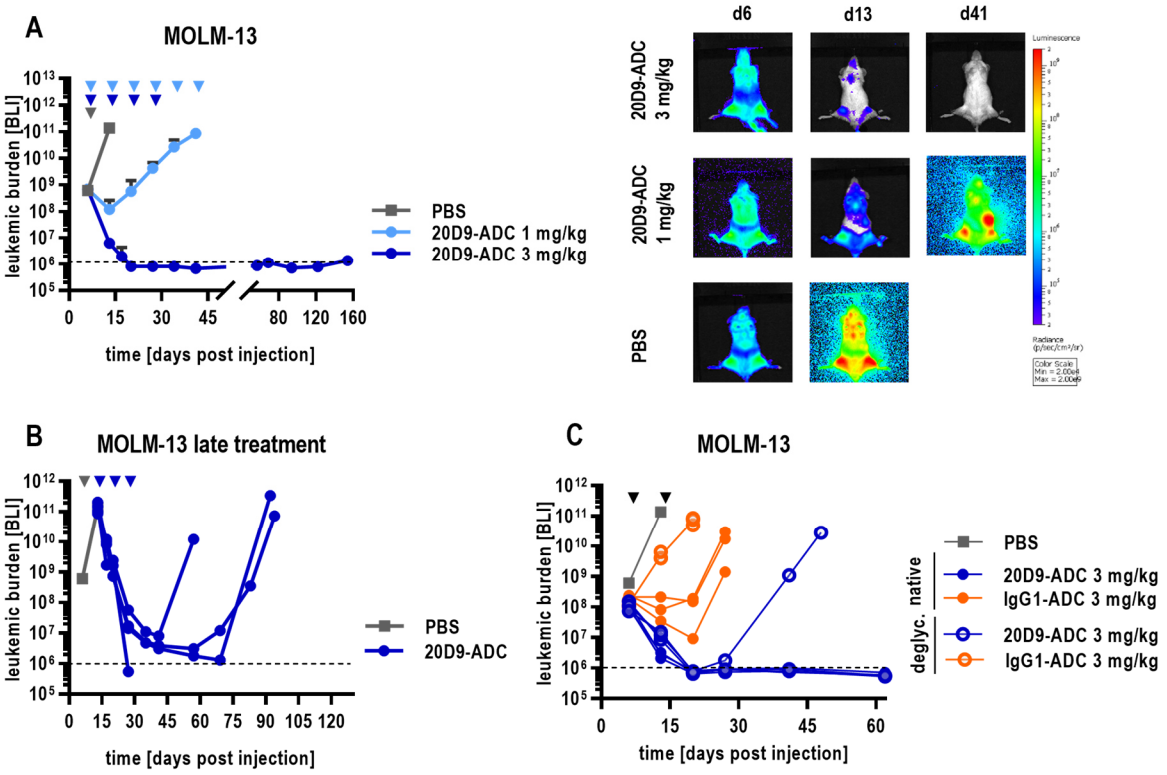

Figure 24 Evaluation of *in vivo* activity of 20D9-ADC in MOLM-13 xenograft mouse models. NSG mice were injected intravenously (i.v.) with $1x10^5$ luciferase expressing MOLM-13 cells. Leukemic burden was monitored once or twice a week by bioluminescence imaging (BLI), and total flux was quantified. Mean ± standard deviation is depicted. Treatment is indicated with rectangles in dark blue (20D9-ADC, 3 mg/kg), light blue (20D9-ADC, 1 mg/kg), grey (PBS) or black (all groups). (A) One week after transplantation, mice were treated with 20D9-ADC (1 mg/kg or 3 mg/kg, i.v.) or PBS as control (n=4/group) once a week for six weeks (1 mg/kg) or for four weeks (3 mg/kg). BLI pictures of one representative mouse per group are shown. (B) Two weeks after transplantation, PBS treated control mice from Figure A were treated at advanced tumor burden with 20D9-ADC (3 mg/kg, n=4) once a week for three weeks. One mouse died in inhalation narcosis 27 days after transplantation. (C) One week after transplantation, mice were treated with native or glycosylated 20D9-ADC or with native or glycosylated IgG1-ADC (3 mg/kg; n=3/group) once a week for two weeks. PBS control mice of experiment shown in A are included as control. *In vivo* experiments were planned in cooperation with Dr. Binje Vick and performed by Maike Fritschle and Anette Frank at the HelmoltzZentrum München.

To define CD64-related effects of the 20D9-ADC *in vivo*, 3 mg/kg of either native or deglycosylated IgG1-ADC or 20D9-ADC were applied once per week intravenously for two weeks in a MOLM-13 transplanted mouse model (Figure 24C). Interestingly, the deglycosylated 20D9-ADC showed a strong cytotoxicity in a range that is comparable to the native 20D9-ADC, although only FLT3 and not CD64 was targeted. This indicates that FLT3 targeting was sufficient to elicit a long-lasting response. In contrast, the anti-tumor effect of native IgG1-ADC was much lower compared to native 20D9-ADC underlining that CD64 targeting alone was not sufficient *in vivo.* The

deglycosylated IgG1-ADC had only a minimal effect compared to PBS control mice, confirming the successful abrogation of FcR mediated cytotoxicity (Figure 24C).

3.4.2 Evaluation of *in vivo* activity of 20D9-ADC in patient derived xenograft mouse models

Next, the effect of 20D9-ADC on patient derived xenograft (PDX) samples engrafted in NSG mice should be determined[103]. PDX samples recapitulate the phenotype and stem cell hierarchy of primary human AML samples and are therefore a good pre-clinical tool to assess cytotoxicity in a setting resembling the patients disease. Several AML–PDX samples were analyzed for their FLT3 expression level and compared to primary AML samples. AML-415, AML-640, AML-573 and AML-579 samples with FLT3-ITD mutations and moderate to high FLT3 expression were selected, representing the AML patient conditions[116] (Figure 25A, Supplementary Table 2). *Ex vivo*, these four AML-PDX cells were sensitive to 20D9-ADC treatment (Figure 25B). The sensitivity was much lower compared to the AML cells, which was due to the slow proliferation of AML-PDX cells *in vitro* (data not shown) since the toxin MMAF is a cell cycle dependent drug. As control, treatment with 20D9-mab had no effect on cell viability (Figure 25C).

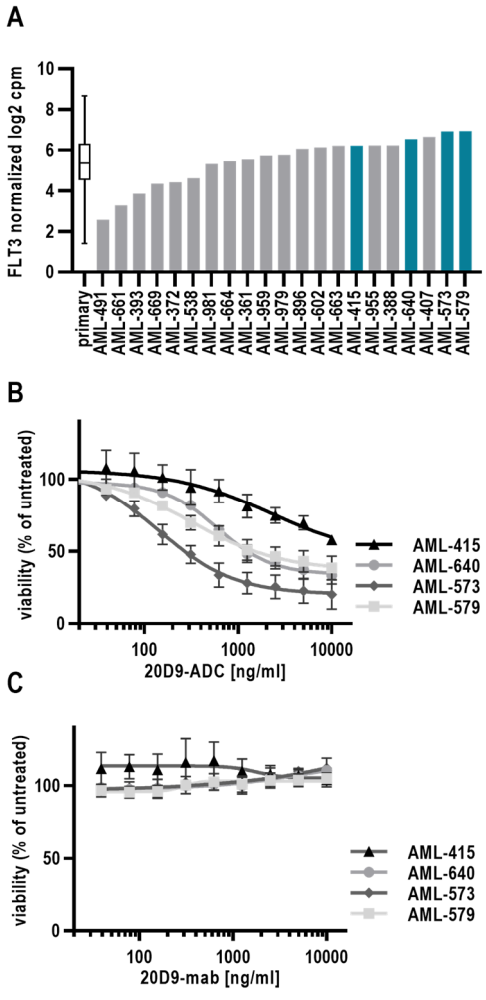

Figure 25 Evaluation of activity of 20D9-ADC in patient derived xenograft samples *ex vivo*. (A) FLT3 RNA expression of AML PDX samples (n=21) and primary patient samples[116] (n=261) analyzed by SCRB sequencing[117]. Data presented as normalized log2 counts per million (cpm). Samples selected for *ex vivo* and *in vivo* analysis are marked in blue. Data was kindly provided by Dr. Tobias Herold, LMU Klinikum. (B,C) Cytotoxicity of 20D9-ADC (B) or 20D9-mab (C) in four FLT3-ITD positive PDX samples *ex vivo*. Viability was determined after 96 h treatment by resazurin fluorescence and normalized to untreated control. Mean ± s.d. of n=3 biological replicates.

AML-640, AML-573 and AML-579 samples were further evaluated *in vivo* in NSG mice. PDX samples were transplanted in mice and after engraftment at day 20, mice were treated with either 3 mg/kg 20D9-ADC or PBS once per week intravenously for three or five weeks as indicated (Figure 26A). In AML-640 and AML-579 transplanted mice, treatment with 3 mg/kg 20D9-ADC for three weeks led to a strong tumor reduction followed by a tumor outgrowth after treatment stop (Figure 26A). Treatment of AML-573 transplanted mice with 3 mg/kg 20D9-ADC for five weeks led to a strong tumor reduction followed by stably low tumor burden up to 150 days.

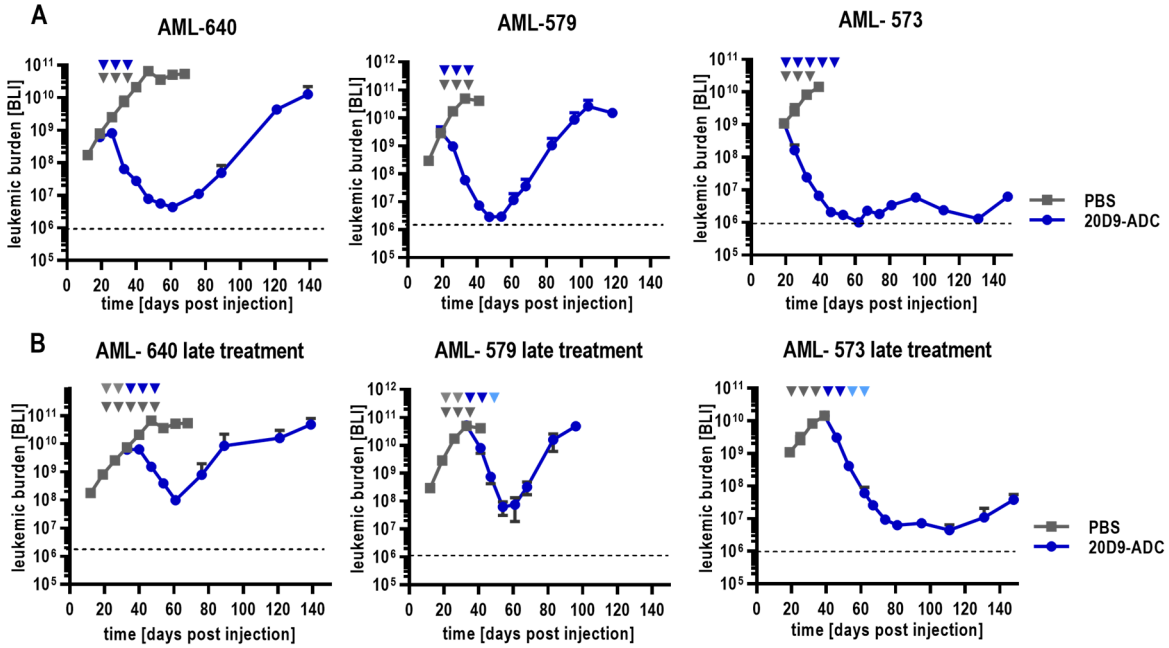

Figure 26 Evaluation of *in vivo* activity of 20D9-ADC in patient derived xenograft mouse models with intermediate and advanced tumor burden. NSG mice were injected intravenously (i.v.) with $2x10^6$ luciferase expressing AML-640, AML-579 or AML-573 PDX cells. Leukemic burden was monitored once or twice a week by bioluminescence imaging (BLI), and total flux was quantified. Mean ± standard deviation is depicted. Treatment is indicated with rectangles in dark blue (20D9-ADC, 3 mg/kg), light blue (20D9-ADC, 1 mg/kg) or grey (PBS). (A) 20 days (AML-573) or 21 days (AML-640 and AML-579) after transplantation, mice were treated at intermediate tumor burden with 20D9-ADC (3 mg/kg) or PBS as control (n=3/group) once a week for up to four or five weeks as indicated. (B) PBS-treated control mice from A (n=3) were treated at day 41 (AML-573) or day 35 (AML-640 and AML-579) after transplantation at advanced stage leukemia (>$1x10^{10}$ photons/sec) with 20D9-ADC once a week for three or four weeks as indicated. In vivo experiments were planned in cooperation with Dr. Binje Vick and performed by Maike Fritschle and Anette Frank at the Helmholtz Zentrum München.

As described in the MOLM-13 *in vivo* experiments, the ADC activity at advanced tumor burden was examined, mimicking a clinical scenario with advanced disease state. When PDX transplanted and PBS treated control mice showed a fully grown leukemia with a BLI of $1x10^{10}$ photons/sec, they were treated intravenously with 20D9-ADC (1 or 3 mg/kg) for three or four weeks as indicated. Three weeks treatment of advanced AML-640 and AML-579 leukemia with 20D9-ADC led to strong tumor reduction followed by a tumor outgrowth after treatment stop (Figure 26B). The

five weeks treatment of advanced AML-573 leukemia also strongly reduced the tumor burden, which was stably low up to 150 days (Figure 26B).

The animal's weight was controlled regularly and after treatment, a decrease of body weight <10% was observed in most of the animals, which quickly returned to normal (Supplementary Figure 3). The weight decrease seemed to be dependent on ADC type and dosage, as it was slightly stronger for higher dosage and stronger for the native compared to deglycosylated variants. Apart from this, the mice were in good physical conditions. Only one ADC treated mouse was sacrificed showing clinical signs of illness or weight loss above 15 % under therapy. One ADC treated mouse died in inhalation narcosis which reflects a typical complication of the procedure and was excluded from further analysis.

To assess the ADC hematotoxicity in mice, blood counts during 20D9-ADC treatment in AML-640 *in vivo* mouse experiments were analyzed in cooperation with the central laboratory, LMU Klinikum. A moderate thrombocytopenia on day 27 in 20D9-ADC (3 mg/kg) treated animals compared to PBS treated control mice (364 G/l and 1736 G/l respectively) was found (Figure 27). Further, the leukocyte count was increased from 1.8 to 4.78 G/l after one administration 20D9-ADC. Both levels were recovered at day 48. The haemoglobin levels did not change significantly during treatment.

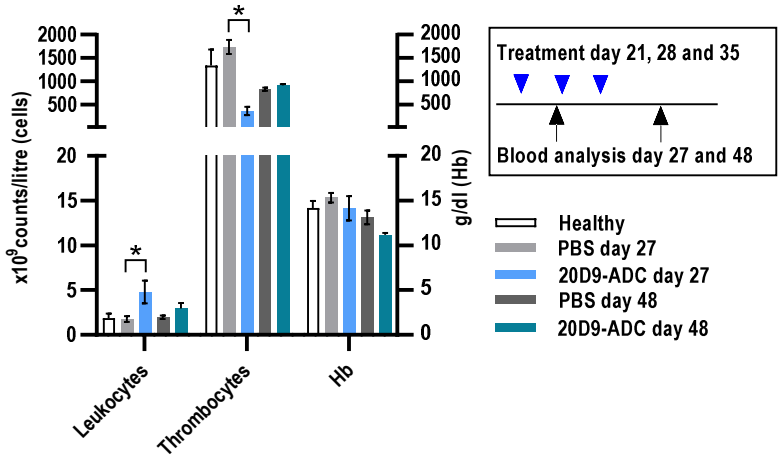

Figure 27 Blood counts of AML-640 transplanted and 20D9-ADC treated NSG mice. Blood analysis of NSG mice during treatment with 20D9-ADC. NSG mice were injected i.v. with AML-640 cells and treated with 20D9-ADC (3 mg/kg) or PBS once a week for 3 weeks. 6 days after the first dose (d27) or 13 days after the last dose (d48), 100 µl of peripheral blood was collected. Blood cell counts (thrombocytes, leukocytes, and hemoglobin levels) were compared to NSG mice without cell transplantation or treatment. 2way ANOVA; *p<0.05; Mean ± s.d. of n=3. Blood analyzes were kindly performed by the Institut für Laboratoriumsmedizin, LMU Klinikum.

In summary, the 20D9-ADC showed high *in vivo* activity in MOLM-13 and PDX mouse model independent from tumor burden at treatment start. In the MOLM-13 cell line model, a long-lasting complete elimination of the tumor cells was observed.

3.5 Hematotoxicity of 20D9-ADC in human CD34 positive cells

The 20D9-ADC did not bind the murine FLT3, therefore the information regarding on-target toxicity in the mouse model was limited. Since FLT3 is expressed on human hematopoietic progenitor cells, the hematotoxicity of 20D9-ADC and IgG1-ADC on normal human CD34 positive hematopoietic cells was investigated *in vitro* in cooperation with the group of Prof. Katharina Götze, MRI. Bone marrow cells from healthy donors were isolated and enriched for CD34 expressing cells (Figure 28A). As expected, FLT3 expression could be detected in 18.9 % of CD34 positive cells, while CD64 was barely expressed on 1 % of cells (Figure 28B). The CD34 positive cells were treated for four days, the viability and differentiation were assessed and additionally, the treated cells were seeded for CFU-assays for analysis of colony forming capacity (Figure 28A).

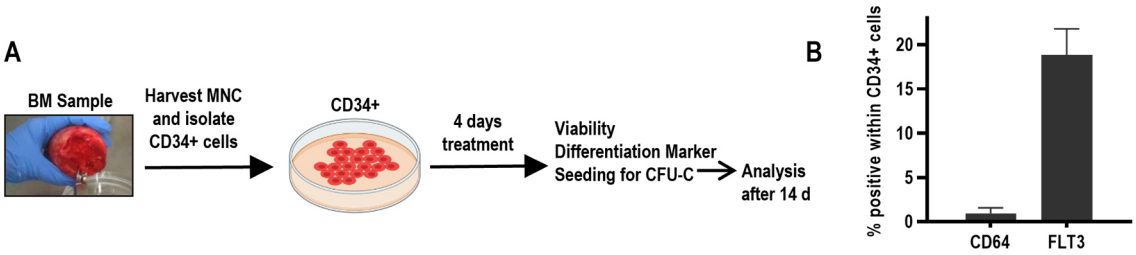

Figure 28 Workflow of hematotoxicity analysis in human CD34 positive cells. (A) Schematic workflow of experiments assessing hematotoxicity in CD34 positive bone marrow (BM) cells of healthy donors (without known hematologic disease). CD34 positive BM cells were treated for 4 days *ex vivo* with 20D9-ADC (0.04 µg/ml, 0.2 µg/ml or 1 µg/ml), IgG1-ADC (1 µg/ml) or PBS. (B) Expression of FLT3 and CD64 in CD34 positive healthy BM cells measured by flow cytometry. Mean ± s.d. of n=3 donors. Experiments were performed by Dr. Judith Hecker in the laboratory of Prof. Katharina Götze, MRI.

Cells were treated with ADC concentrations within the range of the observed IC_{50} values in AML cells (40 and 200 ng/ml) and with a high dose (1000 ng/ml), and cell viability and multilineage differentiation potential were investigated by flow cytometry. Only treatment with the high dose of both 20D9-ADC and IgG1-ADC led to a significant decrease in cell viability (Figure 29A) and might indicate IgG1 dependent toxicity that induced a significant reduction of CD64 positive cells after treatment (Figure 29B). Accordingly, an effect on the differentiation capacity could only be seen after treatment with high dose 20D9-ADC, which revealed a significantly decreased proportion of hematopoietic stem cells (HSC), CD34+CD38-, CD34+CD38+, multi-lymphoid progenitor (MLP), common myeloid progenitor (CMP), and granulocyte-monocyte progenitor (GMP) cell populations (Figure 29C). After treatment with high dose IgG1-ADC, significantly decreased counts of MLPs, CMPs, and GMPs were observed. Nevertheless, this was to a lower extent compared to the 20D9-ADC. The application of 40 ng/ml and 200 ng/ml 20D9-ADC showed no significant reduction of differentiation capacity.

Furthermore, clonogenic capacity was assessed by colony forming unit (CFU) assay of healthy CD34 positive cells. Again, only high dose treatment with 20D9-ADC and IgG1-ADC revealed significantly reduced granulocytic, monocytic and granulocytic-macrophagic colony formation. Both lower concentrations did not alter the colony forming capacity. The erythroid progenitors were unaffected (Figure 29D).

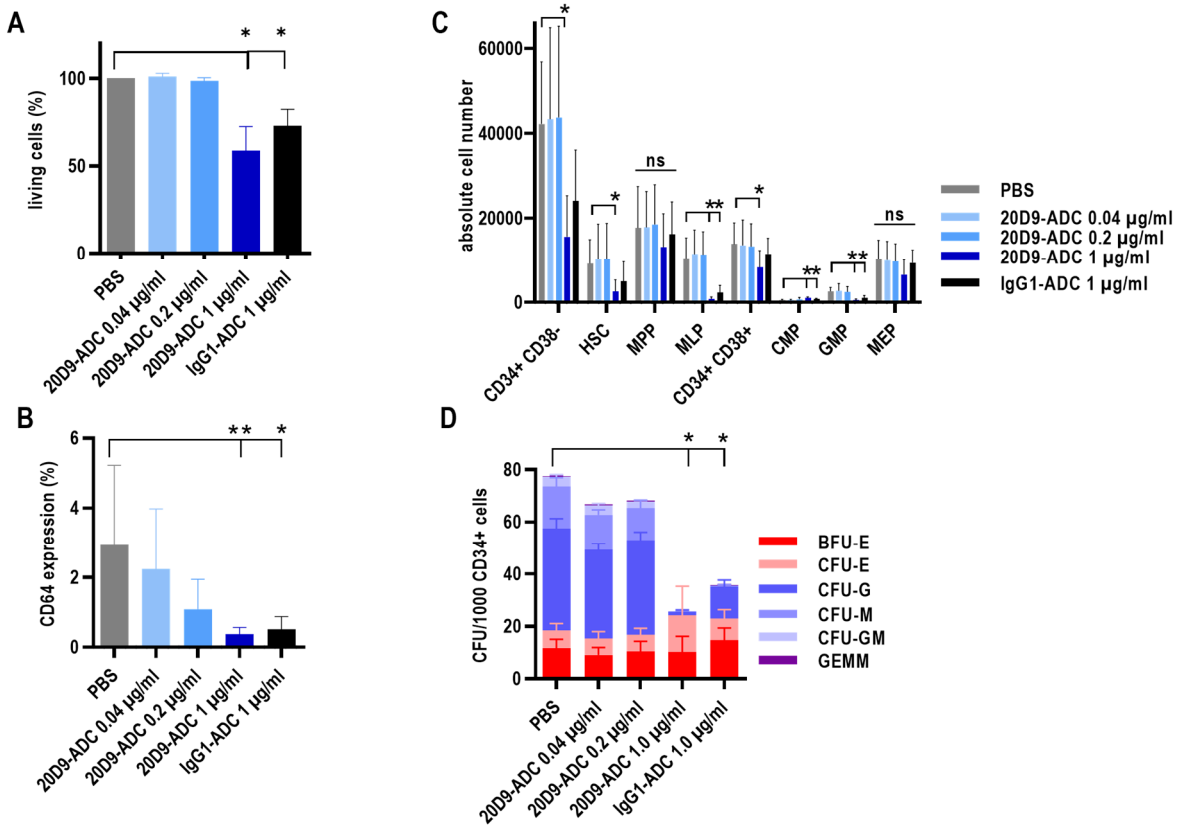

Figure 29 Hematotoxicity of 20D9-ADC in human CD34 positive cells *in vitro*. (A-C) CD34 positive cells were treated with 0.04 µg/ml, 0.2 µg/ml or 1 µg/ml 20D9-ADC, 1 µg/ml IgG1-ADC or PBS and analyzed by flow cytometry after 4 days. Kruskal-Wallis test; *p<0.05; **p<0.01; ***p<0.001; Mean ± s.d. of n=5. (A) Percentage of living cells measured with Annexin V/PI staining and normalized to PBS. (B) Differentiation assessment after staining to differentiation markers. CMP: common myeloid progenitors; GMP: granulocyte-monocyte progenitors; MEP: megakaryocyte/erythroid progenitors; MLP: multilymphoid progenitors; MPP: multipotent progenitors; hematopoietic stem cells (HSC). (C) CD64 expression after treatment analyzed by flow cytometry. Proportion of CD64 positive cells within all CD34 positive cells is shown. (D) Assessment of clonogenic capacity of healthy CD34+ BM cells. Cells were treated with 0.04 µg/ml, 0.2 µg/ml or 1 µg/ml 20D9-ADC, 1 µg/ml IgG1-ADC or PBS for four days and plated afterwards for colony forming unit (CFU) assay. After 14 days, colonies were counted. GEMM: granulocyte, erythrocyte, macrophage, megakaryocyte. GM: granulocyte, macrophage. M: macrophage. G: granulocyte. E: erythrocyte. BFU-E: burst-forming unit erythrocyte. CFU: colony forming unit. 2way ANOVA; *p<0.05; Mean ± s.d. of n=5. These experiments were performed by Dr. Judith Hecker, TUM.

3.6 Treatment combination of 20D9-ADC and TKIs

The FLT3-ITD mutant shows spontaneous autophosphorylation and a prominent intracellular localization compared to the wildtype receptor which is mainly expressed at the cell surface. The groups of Prof. Karsten Spiekermann and Dr. Philipp Greif have previously shown that TKI treatment increased the surface expression of FLT3 on FLT3-ITD positive AML cells[68]. TKI treatment leads to upregulation and stronger glycosylation of FLT3-ITD, which enhance the localization of FLT3 to the membrane. This increased accessibility of FLT is an advantage for cell surface targeting drugs. This was exploited by a bispecific FLT3 × CD3 antibody construct, which increased T cell-mediated cytotoxicity in TKI treated FLT3-ITD-positive AML cell lines, PDX cells and primary patient samples[68]. Thus, in this project, the 20D9-ADC was combined with kinase inhibitors to increase the cytotoxic activity of the ADC *in vitro* and *in vivo*.

3.6.1 Upregulation of FLT3 after TKI treatment

First, the FLT3 upregulation upon TKI treatment seen by Reiter et al[68] were confirmed in MOLM-13 cell line using the FLT3-targeting TKIs midostaurin, quizartinib (AC220) and sorafenib. Incubation of MOLM-13 cells with different concentrations of the inhibitors led to an increase of FLT3 cell surface expression after 48 h, confirming the previously published data (Figure 30A).

To proof that this was a FLT3-TKI specific effect and not attributed to the influence of TKIs on the cell viability, the FLT3 expression was determined in response to the control TKI dasatinib, that targets BCR-ABL, c-KIT, EPH and PDGFβ and is used in CML, ALL and AML therapy[118]. Even though dasatinib exhibits similar effects on cell viability compared to FLT3 TKIs (data not shown) in MOLM-13 cells, dasatinib does not upregulate FLT3 expression (Figure 30B).

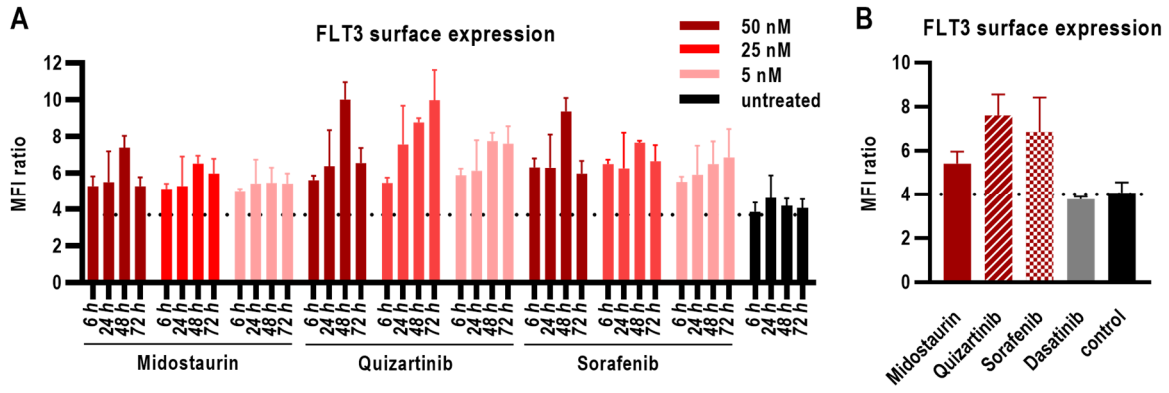

Figure 30 FLT3 cell surface upregulation after treatment combination of 20D9-ADC and tyrosine kinase inhibitors. Upregulation of FLT3 cell surface expression in MOLM-13 cells after treatment with kinase inhibitors compared to untreated control. Cells were analyzed by flow cytometry after treatment. Dotted line represents MFI ratio of untreated cells. Mean ± s.d. of n=2 is depicted. (A) Cells were treated with 5, 25 or 50 nM midostaurin, quizartinib and Sorafenib for 6, 24, 48 or 72 h. (B) Cells were treated with 5 nM midostaurin, 1 nM quizartinib, 5 nM Sorafenib or 1 µM dasatinib for 72 h. These experiments were performed by Dr. Saskia Schmid, Tubulis GmbH.

3.6.2 Combination treatment of cell lines *in vitro* with FLT3 ADC and TKI

Based on these results, the 20D9-ADC was combined with midostaurin, a multi-kinase inhibitor approved for treatment of FLT3-ITD positive AML patients, or AC220, a FLT3-ITD specific kinase inhibitor in clinical studies, to increase the cytotoxic activity of the ADC. Different dose combinations of 20D9-ADC and TKI were applied in a cross scheme to MOLM-13 cells *in vitro*. While midostaurin as single drug had no effect on cell viability at low doses, combination treatment with the 20D9-ADC was significantly beneficial compared to 20D9-ADC treatment alone (Figure 31A). To calculate synergistic effects, two different calculation methods were utilized: the Combination Index (CI)[106] or the ZIP method using the Synergy Finder[108,109]. The CI values are indicated in Figure A, a value of CI < 1 indicates synergy (underlined), CI = 1 indicates additive effects of the two drugs and CI > 1 indicates antagonism. The Synergy Finder analysis calculates a synergy delta score which is depicted in a 3D graph. Values > 0 indicate synergisms.

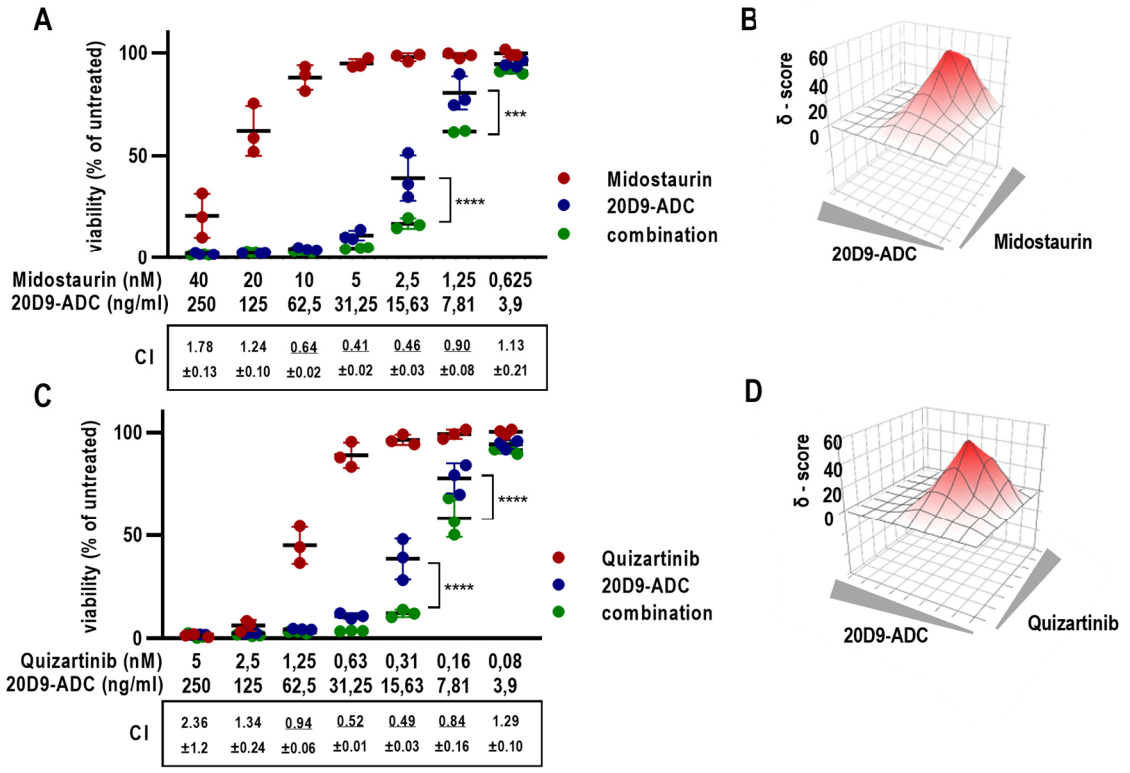

Figure 31 Treatment combination of 20D9-ADC and TKIs in cell lines *in vitro*. Treatment combination of 20D9-ADC and midostaurin (A,B) or quizartinib (C,D) in MOLM-13 cells compared to treatment with 20D9-ADC, midostaurin or quizartinib as single agent. Viability was determined after 96 h by resazurin fluorescence and normalized to dimethyl sulfoxide (DMSO) treated control. (A,C) Each dot represents one biological replicate, the horizontal line indicates the mean. two-way ANOVA; *p<0.05; **p<0.01; ***p<0.001. Combination indices (CIs) with standard deviation were determined using CompuSyn software; CI < 1 indicates synergy and is underlined; CI = 1 additivity; CI > 1 antagonism. (B,D) The synergy score was calculated by 'Synergy Finder' software using zero interaction potency (ZIP) modelling. Grey triangles indicate increasing drug concentrations. A positive synergy score value δ and the red colouring indicate synergism.

Both methods show that a combination using lower drug concentrations of 20D9-ADC and midostaurin were synergistic (Figure 31B). The same effects could be observed for the combination of 20D9-ADC and quizartinib (Figure 31C,D).

3.6.3 Combination treatment of cell lines *in vivo* with FLT3 ADC and TKI

The observations in the *in vitro* assays were validated *in vivo* using MOLM-13 cells transplanted in NSG mice, as described above. After engraftment, mice were treated with either 50 mg/kg midostaurin per os five days a week, 1 mg/kg 20D9-ADC intravenously once per week, both treatment regimens or PBS for three weeks. Treatment with midostaurin or 20D9-ADC 1 mg/kg as single agents only led to modest growth delay *in vivo* (Figure 32A,B). Strikingly, combination of 20D9-ADC and midostaurin treatment led to drastic tumor reduction and probably cure in 2 out of 3 tumor-bearing animals. Thus, these results indicate a high synergistic potential of the FLT3 specific ADC when combined with FLT3 TKIs.

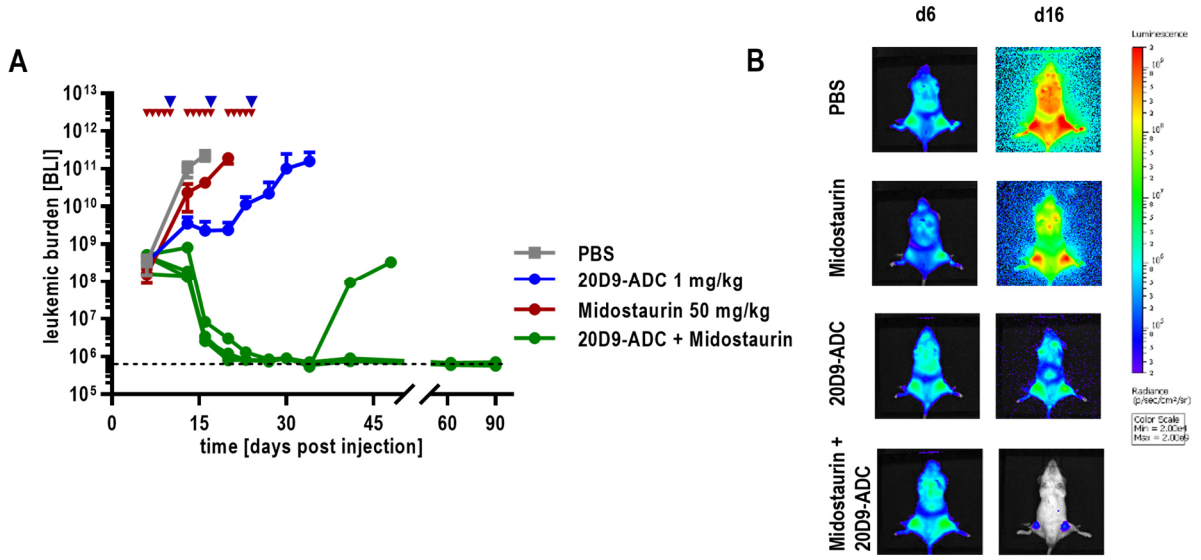

Figure 32 Treatment combination of 20D9-ADC and tyrosine kinase inhibitor *in vivo*. (A) Treatment combination of 20D9-ADC and midostaurin *in vivo*. NSG mice were injected i.v. with 1e5 luciferase expressing MOLM-13 cells. Leukemic burden was monitored once or twice a week by BLI, and total flux was quantified. Mean ± standard deviation is depicted. One week after transplantation, mice were treated for three weeks with 20D9-ADC (1 mg/kg i.v., once per week), midostaurin (50 mg/kg p.o. 5 days a week), a combination of both or PBS as control (n=4/group). (B) Bioluminescence imaging of one representative mouse of each group at day 6 and 16. *In vivo* experiments were planned in cooperation with Dr. Binje Vick and performed by Maike Fritschle and Anette Frank at the Helmholtz Zentrum München.

In conclusion, the combination of TKIs and 20D9-ADC *in vitro* revealed a strongly increased efficiency, probably due to the FLT3 receptor upregulation. The observed effects were even stronger in the *in vivo* setting. The enhanced effectivity may allow for dose reduction, resulting in lower side effects, while retaining the therapeutic effect.

4 Discussion

In this study, I described the development and preclinical characterization of the novel FLT3 targeting ADC 20D9-ADC. FLT3 specific antibodies were generated, chimerized with human IgG1 and the lead candidate was selected based on superiority in binding, affinity, internalization, epitope specificity and stability. By choosing the IgG1 backbone for the partial humanisation, the antibody was designed for double targeting FLT3 and the Fc receptor CD64, which is also expressed on AML cells. For ADC generation, a phosphonamidite based conjugation technology was successfully applied to conjugate the 20D9-mab with the cytotoxic agent MMAF. The 20D9-ADC showed strong and selective cytotoxicity in FLT3 positive cell lines *in vitro.* A clear advantage of FLT3 and CD64 targeting was detected *in vitro* by comparison of native 20D9-ADC with a deglycosylated 20D9-ADC, which is deficient in CD64 binding. *In vivo*, aggressive AML cell lines and AML patient derived xenograft responded effectively to 20D9-ADC treatment independent from the tumor burden at start of treatment. Interestingly, *in vivo*, the deglycosylated 20D9-ADC achieved almost the same efficacy compared to the native 20D9-ADC, showing that double targeting of FLT3 and CD64 had no advantage in the mouse model. Further, hematotoxicity was evaluated in human CD43 positive cells, which were not affected by 20D9-ADC in concentrations in the range of IC_{50} values of AML cell lines, indicating a favourable toxicity profile. Moreover, it was shown that the combination of the FLT3 specific ADC with FLT3 TKIs benefits from the TKI induced FLT3 upregulation and an enhanced cytotoxic effect by synergistic mechanisms was identified. In conclusion, these results show that FLT3 is a clinically promising target for ADC application.

In the following paragraph, the 20D9-ADC is discussed in the context of current state of knowledge.

4.1 The FLT3 targeting ADC is an urgently needed therapy for AML

The 5-year survival rate of AML is still low and shows the high medical need to improve therapy. Approaches to increase the efficacy of the standard 7+3 chemotherapy with the TKIs midostaurin and gilteritinib targeting FLT3 and the reapproved CD33 specific gemtuzumab-ozogamicin improved the outcome but still face problems like development of resistance[20]. Overall, a personalized medicine based on targeted therapy is the most promising strategy to increase therapy efficacy and improve patient's outcome in the next decades. Today this can be realistically implemented, as scientists gain more and more insight into the molecular mechanisms of AML and there is already sound experience in technology and design of different targeted therapy

approaches. Now, it is essential to develop precisely tailored drugs for all known vulnerabilities of AML, aiming for patient - specific combination therapies[119].

Here, FLT3 has a very important role to play. Mutated FLT3 has already been proven as a safe and efficient target for inhibitors in AML treatment. Wildtype FLT3 is not constitutively activated and therefore, cannot be effectively targeted with FLT3 tyrosine kinase inhibitors. Importantly, wildtype FLT3 presents an excellent target in AML therapy. Compared to other possible targets like CD33, CD123 and CLL1, FLT3 provides the largest therapeutic index, which is predicted by an AML specific overexpression, restricted and low expression in a subset of healthy hematopoietic cells and low abundance in non-hematopoietic tissue. Thus, agents targeting FLT3 in AML are expected to have little to no healthy tissue toxicity beyond potential hematologic toxicities[73]. Another advantage of low expression in non-AML tissue is that the ADC efficacy is not decreased by specific off-site ADC binding, which can reduce the ADC concentration. FLT3 is also a particularly appealing drug target because it is additionally expressed on leukemic progenitor cells and could therefore be used to target tumor stem cells for relapse prevention[120]. Nevertheless, for targeting leukemic stem cells, other targets like CD33 und TIM3 are currently focused[121].
The up-coming class of antibody-drug-conjugates unites the specificity of an antibody with the toxicity of a drug, targeting only antigen-positive cells and thus opening the therapeutic window[78]. ADCs are ideally suited for liquid tumors, as tissue penetration does not play a major role there. Following, the therapeutic class of ADCs has greatest potential in AML and antibody-based FLT3-specific therapies could offer a new approach for many FLT3 positive AML patients, regardless of their mutation status[54,122].

One weak point of FLT3 as target might be the absolute expression level. Even though the antigen density of FLT3 on AML cells is low compared to CD33, the expression threshold level for immunotherapy is described to be optimal for recognition by engineered T-cells[75] and monoclonal antibody therapy[69]. Additionally, the difference of FLT3 molecule density on AML cells to normal cells is more important. It is reported that FLT3 expression levels on AML cells varied between 300 and 4600 molecules/cell and, in most cases, were substantially higher than those detected on normal hematopoietic precursor cells and dendritic cells (approximately 300 molecules/cell)[69]. For ADCs, there is no description of a required antigen density level since the efficacy also depends e.g. on internalization rate and potency of drug[102].
Further, there are some other therapy strategies beside ADCs addressing the need for FLT3 targeting independent of mutation. But every type of drug is facing several problems concerning the balance of effectivity and safety. So, it is important that a bunch of different drug entities is in

development to ensure the progress of combatting cancer in the future. FLT3-specific CAR T-cells[76] are very promising and currently evaluated in clinical trials. The main issues in CAR-T cell therapy is minimizing the "off-tumor" toxicity and risk of life-threatening graft-versus-host disease[120,123]. Further, some attempts to target FLT3 only with naked antibodies have failed and there are new FLT3 targeting monoclonal antibodies in development[69,71]. But it is reported, that antibodies conferring primarily ADCC or CDC might be ineffective in AML, due in part to the qualitative defects of natural killer cells in these patients[20]. Moreover, therapies with FLT3 specific T cell engager BiTE®s are under successfull investigation[56,73]. Nevertheless, there might be a limitation of effectiveness since both CD8+ T and CD4+ T cells from patients with AML exhibit features of senescence and exhaustion[124]. So, an ADC based therapy whose mechanism does not primarily depend on immune cells, is a good strategy to target FLT3 in AML.

4.2 20D9-mab is suitable as lead candidate

As requirement for a good effectivity and toxicological profile of an ADC, the antibody must be carefully chosen. Humanization, good target affinity, cross-reactivity, binding and internalization are important aspects for the development of an antibody suitable for ADC generation[79]. In this project, mice and rats were immunized with human FLT3 protein Asn27-541 for antibody generation and after raising single cell clones of the hybridoma cells, monoclonal antibodies were first selected for FLT binding. Afterwards, the antibodies were chimerized to reduce immunogenicity. Prospectively, a full humanization using complementarity determining region grafting (CDR grafting) could be applied to diminish the risk of anti-mouse or anti-rat reactions[125]. On the other hand, a full humanization may reduce the antibody's clinical effectiveness and it needs to be evaluated based on both biochemical characteristics and the targeted therapeutic indication if a humanization is suitable[126]. For the present work, the chimerization is sufficient, but for further development, a full humanization could be considered.

The 20D9 mab was chimerized with a IgG1 backbone, as it is applied in many therapeutic antibodies like rituximab, trastuzumab, cetuximab and for almost all ADCs for example brentuximab vedotin (CD30), trastuzumab emtansine(Her2) and polatuzumab vedotin (CD79b)[77]. IgG1 provides several advantages compared to IgG2, 3 and 4. Very important was the number of disulfide linkages, since the conjugation will take place at reduced cysteine residues. The antibody should possess 4 interchain disulfide bridges to achieve a maximum DAR of 8. Following, the isotypes IgG1 and IgG4 could be used, since IgG2 and IgG3 have six and thirteen interchain disulfide bonds, respectively. Further, the IgG1 has a good serum half-life of 21 days, which is also true for IgG2 and IgG4. But the most important difference of IgG1 compared to IgG2 and IgG4 is

the strong engagement of the immune system by FcR interactions, which triggers CDC, ADCC and ADCP[82,127]. IgG1 has the strongest affinity to CD64, which is expressed in mature hematopoietic cells like granulocytes, monocytes, dendritic cells and the brain[128]. Especially in AML, many blasts express also Fc receptors, in particular CD32 and CD64, while the latter was already mentioned as therapeutic target in therapy[129]. As mentioned, the ADC should target Fc receptors additionally to the FLT3 specificity, thus it was decided to use a native IgG1 as backbone for the 20D9-ADC. The concept of targeting two receptors is aiming to reduce the dosage while maintaining the effectivity. The choice of IgG1 for most therapies based on naked antibodies is clear, since ADCP, ADCC and complement activation is the main mechanism of action. For an ADC, the advantage of the effector function must be evaluated in relation to the toxicity, that may be conferred through binding to Fc receptors expressed on healthy immune cells[127], which is discussed later.

From the chimerization process, seven antibody clones were obtained. The seven monoclonal antibodies were evaluated regarding FLT3 affinity, epitope specificity, internalization as well as producibility and stability.

The K_D concentrations were determined by ELISA assays and were identified between 11.5 ng/ml and 3981 ng/ml. Compared to the literature, the K_D for a FLT3/CD3 bispecific antibody by Yeung et al. was 49 pM[73] and the affinity of the FLT3 specific antibody IMC-EB10 was determined to be 158 pM[130]. The clones 20D9, 4B12, 27E7 and 29H1 show K_D concentrations similar to the literature and are therefore suitable as antibodies for ADC generation. The lead candidate 20D9 clone possessed an K_D of 21.88 ng/ml which is equivalent to 145.87 pM. However, high antigen-binding affinity does not always result in a more efficacious therapeutic antibody, since induction of internalization is also crucial.

Further, the epitopes of the FLT3 protein targeted by the antibody clones were analyzed by PEPperPRINT as external service. Two main epitopes responsible for the FLT3 binding were identified, independent of the species where the antibody was generated. A cross reactivity to the cynomolgus monkey FLT3 for both epitope was very likely, since epitopes 1 and 2 were identical in the human and cynomolgus monkey sequences. As expected, clones 20D9 (recognizes epitope 1) and 4B12 (recognizes epitope 2) were both cross reactive to the cynomolgus monkey FLT3 receptor. This cross reactivity will be an advantage if toxicological studies are carried out in the future. Cross-reactivity with mouse and rat FLT3 was not found, which was probably because the antibodies were generated in these species and both have a high degree of homology. Furthermore, an epitope 3 was identified in peptide mapping studies which was not sufficient for binding since mutation of epitope 1 in 20D9 completely prevented binding.

To evaluate the internalization that is exclusively triggered by FLT3 receptor, the Ba/F3 cell model expressing human wildtype FLT3 was used. Here an internalization rate of about 80 % was

detected. In MOLM-13 cells, the internalization rate was about 50 % to 70 % for the different clones, which is comparable to internalization rates of 50 % to 75 % reported for Mylotarg in different AML cell lines[131]. Thus, I assumed that binding and internalization of the clones 20D9, 4B12, 27E7 and 29H1 was sufficient for ADC development.

One major concern is the producibility, which is substantial for drug development. Approximately, 100 µg 20D9-mab were produced in 100 ml culture volume and after the purification around 50-70 µg were obtained. In optimized expression of antibodies in CHO cells, the highest yield for transient expression is around 1 g/l and 12 g/l can be obtained by stable expression. So, the production of the FLT3 antibodies in HEK cells was by far not optimized. Cell culture media, gene delivery reagents, host cell line, and expression vector are the decisive factors for yield and have to be improved for the antibody expression process if larger amounts are needed[132].

Moreover, the folding stability was analyzed, which is critical for maintaining long-term activity. The melting temperature of all antibody clones was calculated between 67 °C to 75 °C based on thermal shift assays. This is comparable to antibody melting temperatures described in the literature of 63 °C to 80°C for thermal denaturation of monoclonal antibodies measured by differential scanning calorimetry[133]. The highest stabilities were obtained for the clones 20D9, 4B12, 27E7and 29H1. Further, the melting stability can also be improved by optimized formulation, since the antibodies and ADCs were simply stored in PBS.

Taken all parameters together in a final evaluation, the 20D9 clone convinced with the best characteristics and was used for ADC generation.

4.3 Design of the components for 20D9-ADC generation

The generation of safe and effective drug conjugates is particularly challenging because of the risk of reduced bioactivity of conjugated drugs, reduced binding affinity or specificity of modified antibodies, premature release of the conjugated drug, short circulation times and poor biodistribution[134]. These issues should be circumvented by optimal design of the 20D9-ADC regarding conjugation site and strategy, toxin, and linker selection.

For the toxin conjugation, the novel P5 conjugation via reduced disulfide residues was applied. The P5 conjugation technology was recently patented by Tubulis GmbH and is simple and inexpensive, which is advantageous for the quick and efficient evaluation of an antibody-drug-conjugate[90]. As already described, the conjugation technology and linker design are essential as they influence the stability of the antibody-toxin linkage. The P5 method is based on ethynylphosphonamidates which leads to outstanding serum stability characteristics. Kapser et

al. analyzed commercially available Adcetris® that targets CD30 in comparison to the analog brentuximab-P5-MMAE. They investigated serum stability after 7 days at 37°C and found a drastic DAR decrease of Adcetris compared to the P5 ADC. Maleimide conjugated ADCs, like Adcetris, are prone to hydrolysis and unwanted thiol exchange might result in attachment of the drug to endogenous proteins, promoting toxicity[92].

Between the reactive P5 group and the toxin, a cleavable linker was established. This protease sensitive linker type facilitates efficient intracellular release of the toxin and is successfully applied in approved ADCs[85,90,91]. Additionally, tumors can present a higher expression of proteases like cathepsin B than normal cells[85], which enhances the tumor specific activity.

Further, the toxin of choice was MMAF, which is a highly potent agent with an IC_{50} in the subnanomolar range. MMAF belongs, like monomethyl auristatin E (MMAE), to the microtubule-targeting agents which are used as payloads in two-thirds of all clinical stage ADCs[127]. It is more hydrophobic compared to MMAE, which leads to impaired diffusion through the cell membrane. This results in lower bystander killing effects in comparison to MMAE, which is an advantage in hematologic malignancies[135,136]. Different ADCs based on MMAF in clinical studies reported toxicities like corneal depositis, thrombocytopenia, ocular toxicity, hemorrhage, epistaxis and keratophathy. Most of the described side effects occur for many ADC toxins, but the ocular toxicity seems to be associated with the toxin MMAF. It is unclear why the eye is particularly sensitive to MMAF, but it was reported that an optimized linker chemistry could reduce the ocular toxicity[87]. For the 20D9-ADC, the toxicological profile was not yet evaluated and might raise the question to use another toxin.

The 20D9 monoclonal antibody was successfully conjugated to the toxin MMAF via a cleavable linker obtaining a mean drug to antibody ratio of 6.2 ranging from 4 to 8. As expected, the conjugation did not alter the binding to the FLT3 receptor. A very good heat and long-term storage stability of 20D9-ADC diluted in PBS was observed, as the DAR remained stable at all condition. Additionally, the aggregation was very low even after long term storage, where only 1 % aggregates were detected. Following, the different DAR species varying from DAR 4 to 8 did not influence the stability as far it was analyzed. The pharmacokinetic and serum stability was not tested for the 20D9-ADC yet but has to be considered for further development.

To evaluate the ADC design, the 20D9-ADC can be compared to two related ADCs: first to the preclinical FLT3 specific ADC (AGS62P1) and second, to the CD33-ADC approved for AML therapy. The FLT3-ADC AGS62P1 was developed from Astellas Pharma[55] and is an IgG1-based, AGL-0182-30 linked ADC with a DAR of 2. AGL-0182-30 is a variation of MMAF and is connected with a non-cleavable alkoxyamine linker to p-acetyl phenylalanine residue at position 124 of each heavy

chain by oxime-conjugation. Further, they used a D356E/L358M IgG1 variation, which should provide lower immunogenicity but still has effector functions. The clinical study NCT02864290 in R/R AML was recently terminated due to lack of efficacy without providing further details[35,74]. So, there is no evidence if the design of AGS62P1, the study design, samples size or other issues led to the termination of the study. Following, it is not possible to draw any conclusions about the effectiveness of the 20D9-ADC.

Mylotarg (Gemtuzumab ozogamicin, GO) is the only approved ADC for AML therapy until now[53,54]. GO is a humanized anti-CD33 IgG4 mab conjugated to a cytotoxic agent N-acetyl gamma calicheamicin via an acid-labile hybrid 4-(4′-acetylphenoxy)butanoic acid linker by lysin based conjugation. Only about 50% of the antibody is linked to the toxin with an average loading of 4–6 molecules. In 2000, Mylotarg was voluntarily withdrawn due to liver toxicity, veno-occlusive disease and increased mortality rate in a randomized study. Problems like an unstable conjugation and the heterogeneous product most probably contributed to the toxicity. However, 2017 it was reapproved after dose regime modifications and improved toxicity profile[137–139]. Now, Mylotarg therapy faces problems like the susceptibility of calicheamicin to be shuttled by multi drug resistance transporter 1 (MRD1), which leads to drug resistance. Other ADCs targeting CD33 were in development, using improved and state-of-the-art coupling techniques. AVE9633 is a second generation CD33-ADC coupled to a DM4 derivate. Unfortunately, this construct was ineffective in clinical studies. Vadastuximab talirine is a third generation CD33-ADC, comprising of an IgG1 antibody and PBD toxin. A phase 3 study evaluating vadastuximab talirine was stopped 2017 due to high mortality[78].

All in all, it is difficult to predict the efficacy and toxicity of an ADC even if all components are known. The design and the components of the 20D9-ADC were chosen with the greatest care and based on available evidence. The linker and the toxin are well known, applied and proven components. Noteworthy is the significantly stable conjugation method, which will certainly make a positive contribution to reducing side effects and provide a solid basis for the success of this therapeutic molecule.

4.4 20D9-ADC shows effectivity *in vitro* and *in vivo*

The effectivity of the generated ADC was tested in several *in vitro* and *in vivo* AML models to evaluate its potency to kill AML cells.

First, Ba/F3 cell line models expressing the human FLT3 and/or CD64 receptors was used to conduct cytotoxicity assays, allowing for specific and exclusive analysis of the targeting. A FLT3

dependent activity of 20D9-ADC for human wildtype FLT3, human ITD mutated FLT3 and cynomolgus monkey FLT3 was detected, which was in accordance with the binding analysis. Based on the cytotoxicity curves, IC_{50} values displaying the half-maximal effectivity, were calculated. The IC_{50} values for the FLT3 expressing cell lines were relatively high, pointing to the assumption that targeting FLT3 may not be sufficient to eradicate AML cells. Due to the IgG1 backbone, the 20D9-ADC and the IgG1-ADC were highly active in CD64 expressing Ba/F3 cells with low IC_{50} values. As expected, the 20D9-ADC was even more effective in the Ba/F3 cell line expressing FLT3 and CD64. The greater sensitivity of the 20D9-ADC in comparison to the IgG1-ADC in the Ba/F3-FLT3-CD64 cell line highlights the advantage of double targeting in cell culture. Remarkably, the expression of FLT3 in Ba/F3 cells was relatively low compared to the expression of CD64. Overall, the analysis of 20D9 in an experimental cell model system provides a proof of concept for the cytotoxic activity of 20D9-ADC to FLT3 and CD64 receptors.

Further, the cytotoxic activity of 20D9-ADC in established AML cell lines were evaluated. Most AML cell lines showed a simultaneous FLT3 and CD64 expression, comparable to primary AML cells. This underlined the suitability of the AML cell lines as experimental tools and emphasized the potential benefit of FLT3-CD64 double targeting. In AML cells with endogenous FLT3 expression, the 20D9-ADC had strong cytotoxic activity *in vitro*. The IC_{50} values in the most sensitive cell lines were 1.3 ng/ml for MM-1, 24.91 ng/ml for MOLM-13 and 13.17 ng/ml for MV4-11 cells. Compared to Mylotarg, which showed an IC_{50} of 0.3 ng/ml in the cytotoxicity assays (own data, not shown) for MOLM-13 cell line, significantly higher concentrations of 20D9-ADC were needed to achieve similar cytotoxicity. But a direct comparison of both ADCs cannot be made, since CD33 is much higher expressed, the toxin calicheamicin is also more potent and the backbone of Mylotarg is IgG4. More convenient is the comparison to the FLT3-ADC AGS62P1 from Astella Pharma, which showed approximately an IC_{50} value of 100 ng/ml for MOLM-13 and 300 ng/ml for MV4-11 cells[74]. Here, the cytotoxicity of 20D9-ADC was higher in comparison but in a similar range.

Furthermore, the advantage of targeting CD64 and FLT3 *in vitro* was demonstrated. This can be shown by comparing the cell lines to each other and by comparing the activity of 20D9-ADC and IgG1 ADC. The cell line OCI-AML 3 had similar FLT3 expression level compared to OCI-AML 5 but a strongly higher level of CD64 receptor. Consistently, the IC_{50} value of 20D9-ADC in OCI-AML 3 was 25.03 ng/ml and about 50-fold lower compared to OCI-AML 5. The IgG1-ADCwas active in most of the FLT positive cell lines with IC_{50} values about 10-fold higher compared to the 20D9-ADC IC_{50}. One exception was the THP-1 cell line, which showed a relatively low expression of FLT3 but high CD64 expression and the IC_{50} value for the IgG1-ADC was only 4-fold higher than 20D9-ADC.

Additionally, the cytotoxicity of deglycosylated 20D9-ADC and IgG1-ADC in the cell lines also demonstrated the proportions of efficacy of FLT3 and CD64 targeting. The IC_{50} of the deglycosylated 20D9-ADC was 30-fold higher compared to the native 20D9-ADC in the MOLM-13 cells, indicating the advantage of double targeting. As well, the supplementation of immunoglobulins demonstrated the proportions of CD64 and FLT3 mediated cytotoxicity. The immunoglobulin supplement flebogamma was used, mimicking the IgG concentration in human plasma. Adding Immunoglobulins to the ADC treatment in MOLM-13 cells could abrogate any cytotoxic activity of native IgG1-ADC. The activity of deglycosylated 20D9-ADC was reduced about 9-fold compared to the 20D9-ADC.

The analysis of the ADC cytotoxicity *in vitro* gives first hints, but the effectivity *in vivo* is much more important for evaluating the potential of a new drug, since solubility and bioavailability, as well as pharmacokinetic of the drug play an important role. So, the ADC was applied in an *in vivo* setting and the effectivity was analyzed by continuous measurement of tumor burden during the treatment and the tolerability of the ADC was assessed by weight and blood analysis and visual examination.

For this purpose, the 20D9-ADC was tested in a preclinical NSG mouse *in vivo* model after transplantation of MOLM-13 cells using repetitive BLI as monitoring read out. After weekly treatment, a dose dependent response to 20D9-ADC was observed. A dose of 3 mg/kg was very effective with a 10-fold reduction of the BLI signal per week leading to a complete eradication of the tumor cells for up to 120 days after treatment. The reduction of the BLI signal was independent from the tumor burden at start of treatment, showing that also treatment of an advanced tumor state was possible.

A direct comparison of the 20D9-ADC to the already developed FLT3 ADC of Astellas Pharma AGS62P1 is not possible since the latter was tested in a solid tumor model[74]. AGS62P1 was described to have an effective dose of 1 and 2 mg/kg *in vivo*, which is a comparable concentration range to the effective dose of 20D9-ADC, validating the effectivity of the 20D9-ADC. The dosage necessary for effective killing is among others depending of the antigen density of the cell surface. The CD33 specific Mylotarg at a dose of 0.03 mg/kg resulted in a 10-fold reduction of BLI signal per week in MOLM-13 transplanted NOD-SCID mice (data not shown). Compared to the 20D9-ADC, the dosage is much smaller but the CD33 receptor expression and the more potemt toxin can explain this high difference. Further, the 20D9-ADC activity can be compared to FLT3 inhibitors. The efficacy of gilteritinib, a FLT3 selective protein tyrosine kinase (PTK) inhibitor is shown by Mori et al. to completely inhibit the tumor growth with 6 mg/kg assessed in MV4-11 intra-bone transplantation model[140], which is comparable to 20D9-ADC effectivity. Moreover, midostaurin was tested by Göllner et al. in cooperation with Prof. Irmela Jeremias, thus allowing for direct

comparison since the same xenograft tumor model was used[141]. Here, Midostaurin could only inhibit the tumor growth MV4-11 leukemic cells engrafted in NSG mice, but no eradication of the tumor cells was observed. Following, compared to Midostaurin, the 20D9-ADC has a higher cytotxic potential *in vivo.*

Moreover, a cytotoxic activity of FLT3 ADC against AML patient derived xenograft models was shown *in vivo*. These PDX samples recapitulate the phenotype and stem cell hierarchy of primary human AML samples and therefore, an effectivity in this model is of high significance. The 20D9-ADC showed cytotoxic activity in three different AML-PDX samples independent from tumor burden at treatment start. Compared to the MOLM-13 transplanted animals, the tumor reduction per time was lower with approximately 10-fold BLI reduction in two weeks. For AML-640 and AML-579 PDX *in vivo* samples, three treatment cycles with 20D9-ADC could only reduce the tumor burden and after treatment was stopped, the AML samples grew out again. Here, dose and schedule optimizations might result in a stronger reduction of tumor burden. Further, an explanation for the weaker activity of 20D9-ADC could be the cell cycle dependency of the toxin, which results in reduced activity rate in the slowly proliferating patient derived cells. But compared to other treatment regimens applied in PDX xenograft models, 20D9-ADC treatment efficacy was particularly high in comparison to the conventional AraC and Daunorubicin treatment of the PDX-AML 491 sample, which shows a 10-fold reduction of BLI intensity after approximately 6 weeks[142].

In addition, the interplay of double targeting of FLT3 and CD64 was assessed *in vivo* in a MOLM-13 transplanted NSG model. Interestingly, the deglycosylated 20D9-ADC targeting exclusively FLT3 achieved almost the same efficacy compared to the native 20D9-ADC *in vivo*. Applying IgG1-ADC was much less effective than 20D9-ADC, both deglycosylated and native, indicating, that CD64 targeting alone in the NSG mouse model was not sufficient to effectively reduce MOLM-13 cells and therefore CD64 seems not suitable as target for AML cell eradication. In conclusion, the advantage of dual targeting *in vitro* could not be confirmed as the dual targeting of FLT3 and CD64 had no advantage in the *in vivo* setting in NSG mice using MOLM-13 cells. The question, why this discrepancy between the *in vivo* and *in vitro* data was found cannot be answered. However, it underscores how critical *in vivo* experiments are in drug development. Since NSG mice are deficit for B, T, and functional NK cells, immunoglobulin levels should not play a role in this model[103], but an altered binding modality of the antibody due to any other molecular interference might be the reason.

In the *in vivo* studies, the ADCs were well tolerated as single agents and in combination with FLT3 TKIs while showing high effectivity. In general, the mice appeared healthy and the blood analysis

showed no greater defects expect a slight reduction of thrombocytes. Nevertheless, one observation in the *in vivo* experiments was a short-time dose dependent weight loss after administration of the 20D9-ADC. This was avoided by dose reductions, when the 20D9 was combined with a FLT3 PTK inhibitor. Moreover, the weight loss after treatment was higher for the native 20D9-ADC and IgG1-ADC variants compared to deglycosylated variants. So, this toxic effect might be related to the CD64 targeting, but there is not enough data to finally draw a conclusion. In addition, the mouse model has major limitations in determining the toxicology profile of 20D9. The antibodies were derived from rat and there was no cross reactivity to the murine FLT3 receptor as both species have high sequence homology. Further, the murine homologue for CD64 does not bind the human IgG1 in a comparable manner and is moreover expressed differently[143,144]. Thus, another system is needed to evaluate the specific side effects.

In summary, a high effectivity of 20D9-ADC in both *in vitro* and *in vivo* was proven, which provides a strong basis for further development of 20D9-ADC. Importantly, it seemed that the FLT3 specificity is sufficient and no dual targeting is necessary for effective treatment of the AML xenograft mouse model.

4.5 Toxicity of 20D9-ADC

To evaluate the toxicity profile of 20D9-ADC in healthy human tissue, hematopoietic stem and progenitor cells were of interest, since FLT3 is mainly expressed in lymphoid organs, hematopoietic stem cells, early progenitors and dendritic cells[128]. FLT3 expression in the brain, pancreas and lung tissue seems to be limited to the cytoplasm or to be very low[73] and can therefore be neglected. Moreover, the large molecular weight of ADCs will probably prevent crossing of the intact blood brain-barrier. As well, the CD64 receptor is also mainly expressed in the hematopoietic tissue[128]. Thus, the toxicity of 20D9-ADC to normal human CD43 positive hematopoetic cells was analyzed in cell viability and differentiation assays after treatment.
20D9-ADC at concentrations of 40 ng/ml and 200 ng/ml, which represents the range of IC_{50} values of AML cell lines, did not induce apoptosis in healthy human CD34 positive cells in vitro suggesting a favourable toxicity profile. Only at high concentrations, the 20D9-ADC shows cytotoxicity towards myelomonocytic and lymphoid progenitors, which can be expected from the physiological expression pattern of FLT3. Compared to 20D9-ADC, high concentrations of IgG1-ADC showed weaker but also significant toxicity. This might indicate that there was an unspecific toxicity due to high concentration or that CD34 positive cells are susceptible to IgG1 based ADCs. But the expression of CD64 in undifferentiated CD34+ cells at day 0 was very low and cannot explain the toxicity that was observed after IgG1-ADC treatment. One explanation could be an

upregulation of CD64 during differentiation towards MLP, CMP and GMP. To answer this question, Fc silenced 20D9-ADC should be generated and tested in the described assays to distinguish FLT3 and CD64 mediated cytotoxicity.

A good estimation of the toxicity profile of 20D9-ADC could be made from experiments using other FLT3 targeting agents. Based on the FLT3 expression pattern, toxicity towards hematopoietic progenitor cells could be expected and was reported by *in vivo* studies in cynomolgus monkey with FLT3 x CD3 bispecific antibodies. In this study, Brauchle et al. showed a favourable toxicity profile but detected a reversible depletion of dendritic cells, HSPCs and monocytes without any major clinical signs of toxicity[73]. Furthermore, it was reported that a FLT3 specific CAR-T cell (AMG 553) only affected a percentage of normal hematopoietic stem and progenitor cells in preclinical toxicity assessment[76]. In this publication, they hypothesize that the unaffected fraction of FLT3-negative stem cells might be sufficient to repopulate the bone marrow after treatment with FLT3 targeting agents. More information about the hematotoxocity can be derived from clinical studies with FLT3 PTK inhibitors. For the FLT3 inhibitor quizartinib, neutropenia and thrombocytopenia are described as side effects[145]. In the RADIUS-X study, midostaurin was applied as single agent in maintenance therapy to gain insights into the safety profile. The rates of adverse events were generally low and included few cases with platelet count and neutrophil count decreased, anemia, leukocytosis, pancytopenia, thrombocytopenia, and white blood cell count decreased[146].

The second binding affinity of the 20D9-ADC is the CD64 receptor, which is expressed on mature macrophages and monocytes[128]. An IgG1-based ADCs could trigger a target-independent, FcγR–dependent internalization in these cells resulting in unwanted side toxicity. But IgG1-based ADCs targeting CD30 in Hodgkin lymphoma or HER2 in breast cancer, showed manageable tolerability and safety profiles in clinical studies[147] suggesting that hematotoxicty is not a major problem. Nevertheless, it was reported that IgG1-based anti-HER2 ADC trastuzumab emantisine might confer toxicity towards megakaryocytes resulting in thrombocytopenia[100]. However more sophisticated and detailed analyzes of the toxicity of the 20D9-ADC have to be performed in appropriate model systems and finally in clinical studies.

For the generation of ADCs, antibodies are coupled to highly potent toxins. Therefore, it is important to evaluate the toxicity profile of ADCs also with respect to the toxicity profile of the respective toxin. Certain toxicities are expected for the immunoconjugates as they target either tubulin and the mitotic spindle (auristatins and maytansinoids) or DNA (calicheamycin and PBD). These include bone marrow toxicity up to grade 4, sensitive neurological and vegetative toxicities[137]. For MMAE and the derivate MMAF conjugated ADCs, the following toxicities are

reported in patients, respectively[86]: Anemia (7 %; no data), neutropenia (16 %; no data), thomocytopenia (10 %; 15 %), leukopenia (10 %; no data), peripheral neuropathy (7 %; 0 %) and ocular toxicity (0 %; 16 %). The ocular toxicity reported for MMAF might be a challenge for the clinical use of 20D9-ADC. But this exceptionally important characteristic is hard to predict because the whole design of the ADC and especially the conjugation strategy influence strongly the toxicity profile. Until now, the 20D9-ADC seems to have low toxicity, but a full toxicity study is needed.

4.6 Final considerations for IgG1 as basis for the FLT3 targeting ADC

Summarized, the studies have shown a superior cytotoxic activity of targeting FLT3 and CD64 by the 20D9-ADC compared to the single receptor targeting *in vitro*. However, this could not be confirmed *in vivo*. On the other hand, there might be a IgG1 dependend hematotoxicity, which was seen *in vitro* in the presented experiments and reported in literature. Following, it is unclear whether the FcγR binding of the 20D9-ADC will be beneficial in AML patients with respect to toxicity and efficacy.

While unconjugated antibody therapies rely on antibody effector functions like ADCC, the role of these functions in ADC therapy is unclear[97,98,148]. For the development of Mylotarg, the IgG4 isotype was chosen because it has the longest circulating half-life of all isotypes and is least likely to participate in immune-mediated mechanisms via Fc receptor, that may result in target-independent, FcγR–dependent toxicity. In contrast, a functional IgG1 Fc region of an ADC might also have advantages since it was reported that the capacity of trastuzumab to induce ADCC of breast cancer cells was not affected by conjugation to the toxin DM[78] and brentuximab vedotin has been described to induce ADCP *in vivo* contributing to its anti-tumor efficacy [127].

Another important aspect is, that it is not clear which role the human immunoglobulins in serum play in the context of CD64 targeting in ADC therapy. The *in vitro* cell line experiments using an immunoglobulin supplement could abrogate the IgG1-ADC activity. But since Fc interactions are one of the main mechanisms of action of common antibody-based therapy, the binding of therapeutical IgG1 to Fc receptors in the presence of serum immunoglobulin must be sufficient to induce e.g. ADCC. But it is not clear if an antibody-antigen interaction in the presence of immunoglobulins in human blood would also lead to sufficient internalization of the ADC. The *in vitro* assays just give a hint but cannot replace *in vivo* experiments analyzing the efficiency of 20D9-ADC in the presence of immunoglobulins.

Taken all arguments together, the advantage of CD64 targeting seems to be smaller and not reliable enough to rule out the arising toxicity issues. Following, Fc silencing of the ADC should be strongly taken into consideration. There are several possibilities to diminish the effector function capacity. Mutations of IgG1 in the lower hinge region to the IgG2 equivalents, in particular E233P, L234A/L235A (LALA-mutation), and G236Delta, abrogate binding to FcγRI. Another commonly used method to reduce their ability to recruit immune cells is antibody glycoengineering and afucosylation, which impairs FcR-IgG interaction[82,149]. Of course, further studies comparing 20D9-ADC and a Fc-engineered 20D9-ADC will be necessary to finally evaluate the advantages or disadvantages of IgG1-based ADCs.

4.7 Combination treatment of 20D9-ADC with TKIs increases effectivity

As described elswhere, FLT3 is expressed at medium levels on the cell surface that is further downregulated by activating mutations[68]. FLT3-ITD mutations are associated with a poor prognosis and a high medical need for improved therapy[67]. Therefore, it was aimed to increase the FLT3 expression thereby enhancing the potency of 20D9-ADC. As reported previously by our group, the treatment of FLT3-ITD mutated AML cell lines with the FLT3 PTK inhibitor quizartinib led to an increase in FLT3 expression, which potentiates the therapeutic efficacy of a bispecific FLT3 x CD3 antibodies *in vitro*[68]. It is hypothesized that a combinational treatment of 20D9-ADC and TKI in FLT3-ITD positive AML could also improve the treatment efficacy of 20D9-ADC. Further, due to the cell's dependency of FLT3 survival signalling, the FLT3-ITD+ AML is a preferred AML subset for anti-FLT3 immunotherapy because the risk of clonal evolution leading to low FLT3 expression or loss of FLT3 expression is low[75].

The combination of 20D9-ADC and TKI treatment showed significantly higher cytotoxicity *in vitro* compared to single drug treatment. The *in vivo* experiments resulted in even more striking benefit of the combination therapy of low dose 20D9-ADC and midostaurin and the animals stayed leukemia-free up to 2 months until the end of the experiment. Importantly, the dosage of 20D9-ADC could be reduced to 1 mg/kg in the combination therapy compared to 3 mg/kg in the single agent therapy. This indicates that the combination can widen the therapeutic window and has the potential to reduce dose related side effects. Here, it is hypothesized that the remarkable treatment efficacy of the drug combination of 20D9-ADC and midostaurin was due to a FLT3 dependent synergy. The upregulation of the FLT3 receptor on the cell surface of FLT3-ITD cells treated with TKIs was reported previously by our lab[68] and these findings could be reproduced for midostaurin, quizartinib and sorafenib treatment. Importantly, dasatinib, an TKI not targeting FLT3 was not able to upregulate the FLT3 cell surface level. Since midostaurin is a multi-kinase

inhibitor targeting FLT3, but also VEGFR-2, PDGFR and KIT[150], it cannot be excluded that the enhanced effectivity of 20D9-ADC might be based on a FLT3 independent effect.

The hypothesis of FLT3 upregulation followed by drug synergism is supported by other research reports. Increased FLT3 cell surface levels after midostaurin treatment[151] and after lestaurtinib treatment[152] (another FLT3 inhibitor) were reported. An upregulation of FLT3 is an advantage for FLT3 targeting drugs, who's potency is dependent on the amount of FLT3 on the cell surface. So, there are also studies for synergy in the context of CAR T-cell treatment that act synergistically with the FLT3-inhibitor crenolanib[75]. Crenolanib induces increased FLT3 surface protein expression in FLT3-ITD+ AML cells and CAR T-cells targeting FLT3 had potentiated activity against FLT3 - ITD + AML.

Interestingly, synergistic activity was also reported for the combination of tyrosine kinase inhibitors with drugs not targeting FLT3. Fu Li et al described an anti CD123-ADC to be more efficient in combination with quizartinib in FLT3 mutant cells, without explaining this phenomenon in more detail[34]. Further, a CD33-targeting ADC (IMGN779) showed increased effectivity in combination with quizartinib[153,154]. This synergy may result from a quizartinib mediated reduction of the anti-apoptotic protein Mcl-1 levels, which were elevated after IMGN779 treatment. A decreased cell's DNA damage response and pro-survival signalling might be responsible for the increased cell killing by IMGN779 when combined with quizartinib.

In conclusion, there is strong evidence that combination of 20D9-ADC with TKIs can synergistically enhance its cytotoxic activity which might result in a favourable toxicity profile of the combination treatment in FLT3-ITD positive AML. Here, we could show this phenomenon for the 20D9-ADC in combination with midostaurin.

4.8 Positioning of the 20D9-ADC in the landscape of AML treatment and outlook for further development

The increasing knowledge of AML biology will lead to more subset-specific and personalized AML therapies, ideally tailored to each patient's disease. Prospectively, there is the need of many therapeutic options targeting efficiently all known vulnerabilities of AML. In the presented study, I described the development of a novel IgG1-based FLT3-targeting P5-conjugated ADC that demonstrated potent antileukemic activity in preclinical models of AML as single drug or in combination with tyrosine kinase inhibitors. FLT3 targeting using the 20D9-ADC could contribute to personalized medicine, having the potential to eradicate FLT3 positive leukemic cell populations (Figure 33).

Therefore, the 20D9-ADC should be put in context of current and future AML therapies. Since 2017, FLT3 targeting drugs are routinely used in the clinic for patients carrying FLT3 mutations. The tyrosine kinase inhibitor midostaurin is applied in induction, consolidation, and maintenance therapy, while relapsed patients can be treated with the TKI gilteritinib. The 20D9-ADC should not be a replacement but rather a complementation and extension of the approved PTK inhibitor therapy. The therapeutic benefit of FLT3 inhibition, particularly as a monotherapy, frequently results in the development of treatment resistance and disease relapse[155], which could potentially be prevented by a combinational therapy with 20D9-ADC. Patients with mutant FLT3 could benefit from the synergism of the combination treatment of TKIs and 20D9-ADC in addition to 7+3 induction therapy to eradicate FLT3 mutant clones and improve survival.

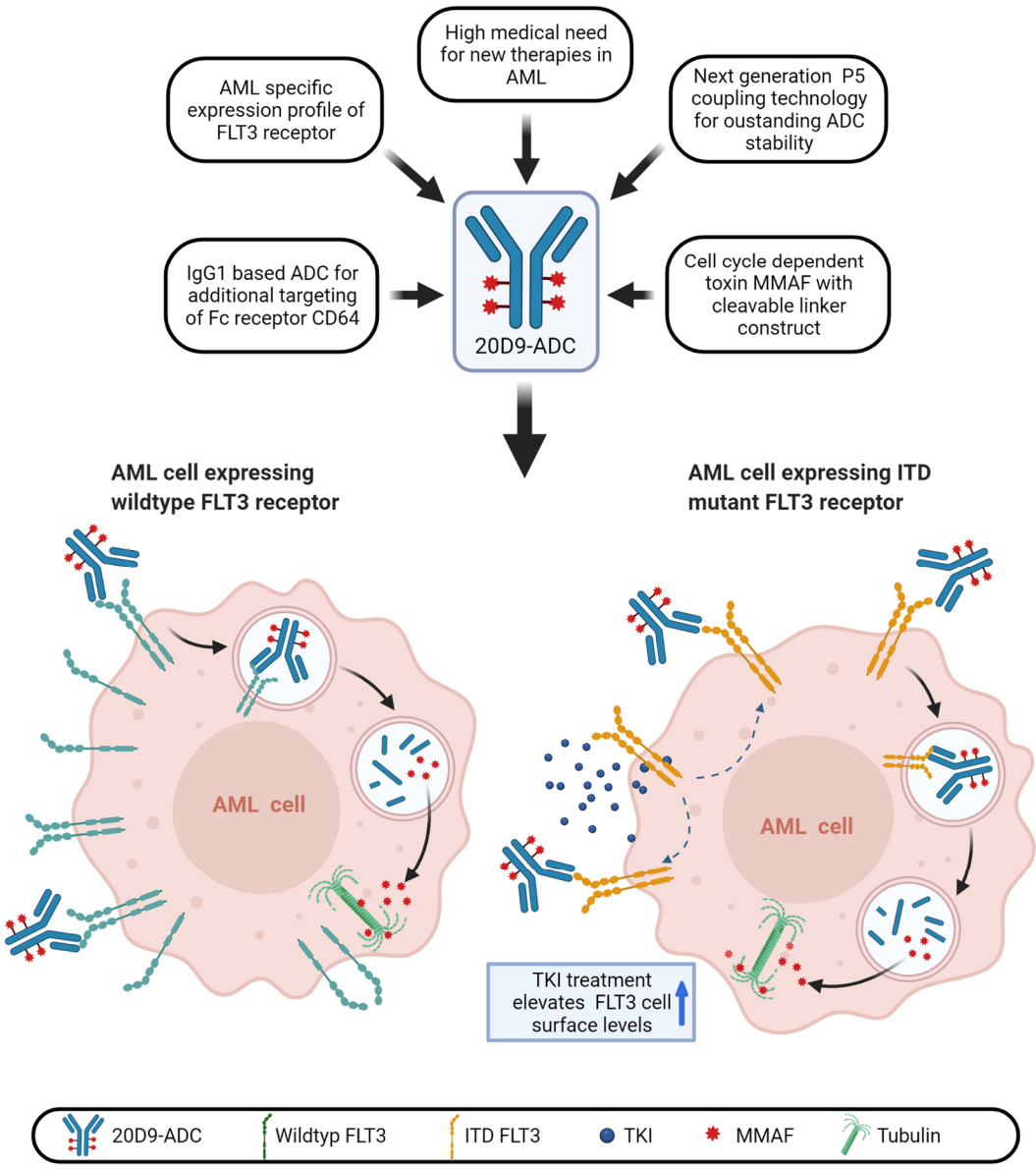

Figure 33 Schematic project summary. Summarized overview of 20D9-ADC rational and design and proposed mechanism of 20D9-ADC in AML expressing either wildtype FLT3 receptor or mutant FLT3-ITD receptor.

The 20D9-ADC would also be applicable in combination with the 7+3 induction chemotherapy for patients expressing wildtype FLT3, which cannot be targeted with the current available TKI therapies that rely on a constitutively activated receptor. Assessment of FLT3 expression can be easily implemented in the standard diagnostic workup using flow cytometry. Specific AML subgroups, like the FAB M5a and M5b could show an even greater benefit from this therapy, since these patients show higher FLT3 expression levels in the leukemic cells[57]. Further, an combination of 20D9-ADC and Mylotarg or any other ADC targeting CLL-1, CD-123, IL3RA and CXCR4, that are currently under investigation[156] for AML therapy might be also possible and may open the therapeutic window for patients with FLT3 and CD33 or another overexpressed target, respectively.

To date, there is currently no FLT3-ADC in clinical development. 20D9-ADC has great potential, and for an effective AML therapy in the future, a FLT3 specific agent targeting wildtype and mutant FLT3 is urgently needed. There are some other therapy strategies beside ADCs addressing wildtype FLT3, for example CAR-T cells and bispecific antibodies, but their development also faces problems. To improve patient's outcome, several therapeutic classes for FLT3 targeting must be evaluated to find the best options.

For further development of the 20D9-ADC, a central point is the Fc receptor engagement. The generation and characterization of a Fc engineered LALA mutated variant, which has reduced effector functions, is indispensable. The *in vivo* data suggest that the effectiveness will be sufficient, and it is important to keep the potential side effects as small as possible.

Prospectively, some variations of 20D9-ADC could diversify the scope of application of the 20D9 antibody. The expression pattern of FLT3 provides the possibility of targeting AML stem cells during induction therapy or in setting of minimal residual disease (MRD). The described 20D9-ADC is conjugated to the cell cycle-depending toxin MMAF, which is perfectly active in eradicating proliferative cells. But MMAF might not be suitable for targeting of slow-dividing AML stem cells and for this purpose, toxins forming covalent interactions with DNA like duocarmycines could be coupled to the well characterized 20D9 monoclonal antibody.

In this study, I discussed that a FLT3 specific therapy independent of the mutational status has great potential to improve AML therapy and presented the highly effective FLT3 specific 20D9-ADC as possible candidate for such application in the future. The 20D9-ADC was effective *in vitro* and *in vivo* and remarkably active even in low concentrations in combination with midostaurin, suggesting a treatment concept with possibly favourable toxicity profile. FLT3 is a clinically promising target for ADC application and the 20D9-ADC could be further evaluated in clinical studies in the future.

5 References

1. Papavramidou N, Papavramidis T, Demetriou T. Ancient greek and greco-Roman methods in modern surgical treatment of cancer. *Ann Surg Oncol*. 2010;17(3):665-667. doi:10.1245/s10434-009-0886-6
2. Boveri T. Concerning the origin of malignant tumours by Theodor Boveri 1902. Translated and annotated by Henry Harris. *J Cell Sci*. 2008;121(SUPPL. 1):1-84. doi:10.1242/jcs.025742
3. Hanahan D, Weinberg RA. Hallmarks of cancer: The next generation. *Cell*. 2011;144(5):646-674. doi:10.1016/j.cell.2011.02.013
4. Hanahan D, Weinberg RA. The hallmarks of cancer. *Cell*. 2000;100(1):57-70. doi:10.1007/s00262-010-0968-0
5. World Health Organisation. Latest global cancer data: Cancer burden rises to 19.3 million new cases and 10.0 million cancer deaths in 2020. *Int Agency Res Cancer*. Published online 2020. Accessed May 28, 2021. https://www.iarc.who.int/news-events/latest-global-cancer-data-cancer-burden-rises-to-19-3-million-new-cases-and-10-0-million-cancer-deaths-in-2020/
6. Siegel RL, Miller KD, Fuchs HE, Jemal A. Cancer Statistics, 2021. *CA Cancer J Clin*. 2021;71(1):7-33. doi:10.3322/caac.21654
7. World Health Organization. Cancer. Published online May 31, 2021. Accessed May 31, 2021. https://www.euro.who.int/en/health-topics/noncommunicable-diseases/cancer/cancer
8. Shallis RM, Wang R, Davidoff A, Ma X, Zeidan AM. Epidemiology of acute myeloid leukemia: Recent progress and enduring challenges. *Blood Rev*. 2019;36:70-87. doi:10.1016/j.blre.2019.04.005
9. Deschler B, Lübbert M. Acute myeloid leukemia: Epidemiology and etiology. *Cancer*. 2006;107(9):2099-2107. doi:10.1002/CNCR.22233
10. Abelson S, Collord G, Ng SWK, et al. Prediction of acute myeloid leukaemia risk in healthy individuals. *Nat 2018 5597714*. 2018;559(7714):400-404. doi:10.1038/s41586-018-0317-6
11. Hiddemann W, Bartram C. *Die Onkologie*. Springer Medizin Verlag Heidelberg 2010; 2010. doi:10.1007/978-3-540-79725-8_80
12. Kayser S, Döhner K, Krauter J, et al. The impact of therapy-related acute myeloid leukemia (AML) on outcome in 2853 adult patients with newly diagnosed AML. *Blood*. 2011;117(7):2137-2145. doi:10.1182/BLOOD-2010-08-301713
13. Weinberg OK, Seetharam M, Ren L, et al. Clinical characterization of acute myeloid leukemia with myelodysplasia-related changes as defined by the 2008 WHO classification system. *Blood*. 2009;113(9):1906-1908. doi:10.1182/BLOOD-2008-10-182782
14. Visser O, Trama A, Maynadié M, et al. Incidence, survival and prevalence of myeloid malignancies in Europe. *Eur J Cancer*. 2012;48(17):3257-3266. doi:10.1016/j.ejca.2012.05.024
15. Bonnet D, Dick JE. Human acute myeloid leukemia is organized as a hierarchy that originates from a primitive hematopoietic cell. *Nat Med*. 1997;3(7):730-737. Accessed May 1, 2017. http://www.ncbi.nlm.nih.gov/pubmed/9212098
16. Döhner H, Estey E, Grimwade D, et al. Diagnosis and management of AML in adults: 2017 ELN recommendations from an international expert panel. *Blood*. 2017;129(4):424-447. doi:10.1182/blood-2016-08-733196
17. Estey EH. Acute myeloid leukemia: 2019 update on risk-stratification and management. *Am J Hematol*. 2018;93(10):1267-1291. doi:10.1002/ajh.25214
18. Metzeler KH, Herold T, Rothenberg-Thurley M, et al. Spectrum and prognostic relevance of driver gene mutations in acute myeloid leukemia. Published online 2016. doi:10.1182/blood-2016-01
19. Taylor J, Xiao W, Abdel-Wahab O. Diagnosis and classification of hematologic malignancies on the basis of genetics. *Blood*. 2017;130(4):410-423. doi:10.1182/blood-2017-02-734541

20. Short NJ, Konopleva M, Kadia TM, et al. Advances in the treatment of acute myeloid leukemia: New drugs and new challenges. *Cancer Discov*. 2020;10(4):506-525. doi:10.1158/2159-8290.CD-19-1011
21. Medinger M, Passweg JR. Acute myeloid leukaemia genomics. *Br J Haematol*. 2017;179(4):530-542. doi:10.1111/BJH.14823
22. Barbui T, Thiele J, Gisslinger H, et al. The 2016 WHO classification and diagnostic criteria for myeloproliferative neoplasms: document summary and in-depth discussion. *Blood Cancer J*. 2018;8(2):15. doi:10.1038/s41408-018-0054-y
23. Kantarjian H, Kadia T, DiNardo C, et al. Acute myeloid leukemia: current progress and future directions. *Blood Cancer J*. 2021;11(2):41. doi:10.1038/s41408-021-00425-3
24. Herold T, Rothenberg-Thurley M, Grunwald V V., et al. Validation and refinement of the revised 2017 European LeukemiaNet genetic risk stratification of acute myeloid leukemia. *Leukemia*. 2020;34(12):3161-3172. doi:10.1038/s41375-020-0806-0
25. Greaves M. Leukaemia "firsts" in cancer research and treatment. *Nat Rev Cancer*. 2016;16(3):163-172. doi:10.1038/nrc.2016.3
26. Amjad MT, Kasi A. Cancer Chemotherapy. *Fundam Pharm Nanosci*. Published online November 24, 2020:401-427. Accessed July 19, 2021. https://www.ncbi.nlm.nih.gov/books/NBK564367/
27. Ellison RR, Holland JF, Weil M, et al. Arabinosyl cytosine: a useful agent in the treatment of acute leukemia in adults. *Blood*. 1968;32(4):507-523. doi:10.1182/blood.v32.4.507.507
28. Wei AH, Döhner H, Pocock C, et al. Oral Azacitidine Maintenance Therapy for Acute Myeloid Leukemia in First Remission. *https://doi.org/101056/NEJMoa2004444*. 2020;383(26):2526-2537. doi:10.1056/NEJMOA2004444
29. Pollyea DA, Amaya M, Strati P, Konopleva MY. Venetoclax for AML: Changing the treatment paradigm. *Blood Adv*. 2019;3(24):4326-4335. doi:10.1182/bloodadvances.2019000937
30. Cortes JE, Dombret H, Merchant A, et al. Glasdegib plus intensive/nonintensive chemotherapy in untreated acute myeloid leukemia: BRIGHT AML 1019 Phase III trials. *Futur Oncol*. 2019;15(31):3531-3545. doi:10.2217/fon-2019-0373
31. Stanchina M, Soong D, Zheng-Lin B, Watts JM, Taylor J. Advances in acute myeloid leukemia: Recently approved therapies and drugs in development. *Cancers (Basel)*. 2020;12(11):1-32. doi:10.3390/cancers12113225
32. Burnett A, Stone R. AML: New Drugs but New Challenges. *Clin Lymphoma, Myeloma Leuk*. 2020;20(6):341-350. doi:10.1016/j.clml.2020.02.005
33. Kovtun Y, Jones G, Harvey L, et al. IMGN632: A novel antibody-drug conjugate (ADC) of a CD123-targeting antibody with a potent DNA-alkylator is highly active in preclinical models of AML with poor prognosis. *Haematologica*. 2016;101:222.
34. Li F, Sutherland MK, Yu C, et al. Characterization of SGN-CD123A, APotent CD123-directed antibody-drug conjugate for acute myeloid leukemia. *Mol Cancer Ther*. 2018;17(2):554-564. doi:10.1158/1535-7163.MCT-17-0742
35. Rudra-Ganguly N, Lowe C, Virata C, et al. AGS62P1, a Novel Anti-FLT3 Antibody Drug Conjugate, Employing Site Specific Conjugation, Demonstrates Preclinical Anti-Tumor Efficacy in AML Tumor and Patient Derived Xenografts. *Blood*. 2015;126(23):3806-3806. doi:10.1182/blood.v126.23.3806.3806
36. Jiang YP, Liu BY, Zheng Q, et al. CLT030, a leukemic stem cell-targeting CLL1 antibody-drug conjugate for treatment of acute myeloid leukemia. *Blood Adv*. 2018;2(14):1738-1749. doi:10.1182/bloodadvances.2018020107
37. Büchner T, Schlenk RF, Schaich M, et al. Acute Myeloid Leukemia (AML): Different treatment strategies versus a common standard arm - Combined prospective analysis by the German AML Intergroup. *J Clin Oncol*. 2012;30(29):3604-3610. doi:10.1200/JCO.2012.42.2907
38. Dombret H, Gardin C. An update of current treatments for adult acute myeloid leukemia. *Blood*. 2016;127(1):53. doi:10.1182/BLOOD-2015-08-604520
39. Rashidi A, Weisdorf DJ, Bejanyan N. Treatment of relapsed/refractory acute myeloid leukaemia in adults. *Br J Haematol*. 2018;181(1):27-37. doi:10.1111/BJH.15077

40. Landau DA, Carter SL, Getz G, Wu CJ. Clonal evolution in hematologic malignancies and therapeutic implications. *Leukemia*. 2014;28(1):34. doi:10.1038/LEU.2013.248
41. Thol F, Ganser A. Treatment of Relapsed Acute Myeloid Leukemia. *Curr Treat Options Oncol*. 2020;21(8). doi:10.1007/s11864-020-00765-5
42. Bose P, Vachhani P, Cortes JE. Treatment of Relapsed/Refractory Acute Myeloid Leukemia. *Curr Treat Options Oncol 2017 183*. 2017;18(3):1-30. doi:10.1007/S11864-017-0456-2
43. Schuurhuis G, Heuser M, Freeman S, et al. Minimal/measurable residual disease in AML: a consensus document from the European LeukemiaNet MRD Working Party. *Blood*. 2018;131(12):1275-1291. doi:10.1182/BLOOD-2017-09-801498
44. Araki D, Wood BL, Othus M, et al. Allogeneic Hematopoietic Cell Transplantation for Acute Myeloid Leukemia: Time to Move Toward a Minimal Residual Disease–Based Definition of Complete Remission? *J Clin Oncol*. 2016;34(4):329. doi:10.1200/JCO.2015.63.3826
45. Kazi J, Rönnstrand L. FMS-like Tyrosine Kinase 3/FLT3: From Basic Science to Clinical Implications. *Physiol Rev*. 2019;99(3):1433-1466. doi:10.1152/PHYSREV.00029.2018
46. Grafone T, Palmisano M, Nicci C, Storti S. An overview on the role of FLT3-tyrosine kinase receptor in acute myeloid leukemia: Biology and treatment. *Oncol Rev*. 2012;6(1):64-74. doi:10.4081/oncol.2012.e8
47. Gary Gilliland D, Griffin JD. The roles of FLT3 in hematopoiesis and leukemia. *Blood*. 2002;100(5):1532-1542. doi:10.1182/blood-2002-02-0492
48. Goh LK, Sorkin A. Endocytosis of Receptor Tyrosine Kinases. *Cold Spring Harb Perspect Biol*. 2013;5(5). doi:10.1101/CSHPERSPECT.A017459
49. Critchley W, Pellet-Many C, Ringham-Terry B, Harrison M, Zachary I, Ponnambalam S. Receptor Tyrosine Kinase Ubiquitination and De-Ubiquitination in Signal Transduction and Receptor Trafficking. *Cells*. 2018;7(3):22. doi:10.3390/CELLS7030022
50. Levis M, Perl AE. Gilteritinib: Potent targeting of FLT3 mutations in AML. *Blood Adv*. 2020;4(6):1178-1191. doi:10.1182/bloodadvances.2019000174
51. Kikushige Y, Yoshimoto G, Miyamoto T, et al. Human Flt3 Is Expressed at the Hematopoietic Stem Cell and the Granulocyte/Macrophage Progenitor Stages to Maintain Cell Survival. *J Immunol*. 2008;180(11):7358-7367. doi:10.4049/jimmunol.180.11.7358
52. Böiers C, Buza-Vidas N, Jensen CT, et al. Expression and role of FLT3 in regulation of the earliest stage of normal granulocyte-monocyte progenitor development. *Blood*. 2010;115(24):5061-5068. doi:10.1182/blood-2009-12-258756
53. Karsunky H, Merad M, Cozzio A, Weissman IL, Manz MG. Flt3 ligand regulates dendritic cell development from Flt3+ lymphoid and myeloid-committed progenitors to Flt3+ dendritic cells in vivo. *J Exp Med*. 2003;198(2):305-313. doi:10.1084/jem.20030323
54. Ambinder AJ, Levis M. Potential targeting of FLT3 acute myeloid leukemia. *Haematologica*. 2021;106(3):671-681. doi:10.3324/HAEMATOL.2019.240754
55. Kottaridis PD, Gale RE, Linch DC. FLT3 mutations and leukaemia. *Br J Haematol*. 2003;122(4):523-538. doi:10.1046/j.1365-2141.2003.04500.x
56. Brauchle B, Goldstein RL, Karbowski CM, et al. Characterization of a novel FLT3 BiTE molecule for the treatment of acute myeloid leukemia. *Mol Cancer Ther*. 2020;19(9):1875-1888. doi:10.1158/1535-7163.MCT-19-1093
57. Kuchenbauer F, Kern W, Schoch C, et al. Detailed analysis of FLT3 expression levels in acute myeloid leukemia. *Haematologica*. 2005;90(12):1617-1625. doi:https://doi.org/10.3324/%25x
58. Thiede C, Steudel C, Mohr B, et al. Analysis of FLT3-activating mutations in 979 patients with acute myelogenous leukemia: Association with FAB subtypes and identification of subgroups with poor prognosis. *Blood*. 2002;99(12):4326-4335. doi:10.1182/blood.V99.12.4326
59. Spiekermann K, Bagrintseva K, Schwab R, Schmieja K, Hiddemann W. Overexpression and constitutive activation of FLT3 induces STAT5 activation in primary acute myeloid leukemia blast cells. *Clin Cancer Res*. 2003;9(6):2140-2150.
60. Daver N, Schlenk RF, Russell NH, Levis MJ. Targeting FLT3 mutations in AML: review of current knowledge and evidence. *Leukemia*. 2019;33(2):299-312. doi:10.1038/s41375-

018-0357-9
61. Kiyoi H, Ohno R, Ueda R, Saito H, Naoe T. Mechanism of constitutive activation of FLT3 with internal tandem duplication in the juxtamembrane domain. *Oncogene*. 2002;21(16):2555-2563. doi:10.1038/sj.onc.1205332
62. Kiyoi H, Kawashima N, Ishikawa Y. FLT3 mutations in acute myeloid leukemia: Therapeutic paradigm beyond inhibitor development. *Cancer Sci*. 2020;111(2):312-322. doi:10.1111/cas.14274
63. Janke H, Pastore F, Schumacher D, et al. Activating FLT3 mutants show distinct gain-of-function phenotypes in vitro and a characteristic signaling pathway profile associated with prognosis in acute Myeloid Leukemia. *PLoS One*. 2014;9(3). doi:10.1371/journal.pone.0089560
64. Schranz K, Hubmann M, Harin E, et al. Clonal heterogeneity of FLT3-ITD detected by high-throughput amplicon sequencing correlates with adverse prognosis in acute myeloid leukemia. *Oncotarget*. 2018;9(53):30128-30145. doi:10.18632/oncotarget.25729
65. Cheng J, Qu L, Wang J, Cheng L, Wang Y. High expression of FLT3 is a risk factor in leukemia. *Mol Med Rep*. 2018;17(2):2885-2892. doi:10.3892/mmr.2017.8232
66. Stone RM, Mandrekar SJ, Sanford BL, et al. Midostaurin plus Chemotherapy for Acute Myeloid Leukemia with a *FLT3* Mutation. *N Engl J Med*. Published online 2017. doi:10.1056/NEJMoa1614359
67. Kennedy VE, Smith CC. FLT3 Mutations in Acute Myeloid Leukemia: Key Concepts and Emerging Controversies. *Front Oncol*. 2020;10. doi:10.3389/FONC.2020.612880
68. Reiter K, Polzer H, Krupka C, et al. Tyrosine kinase inhibition increases the cell surface localization of FLT3-ITD and enhances FLT3-directed immunotherapy of acute myeloid leukemia. *Leukemia*. Published online 2018. doi:10.1038/leu.2017.257
69. Hofmann M, Grobe-Hovest L, Nübling T, et al. Generation, selection and preclinical characterization of an Fc-optimized FLT3 antibody for the treatment of myeloid leukemia. *Leukemia*. 2012;26(6):1228-1237. doi:10.1038/leu.2011.372
70. Sanford D, Blum WG, Ravandi F, et al. Efficacy and safety of an anti-FLT3 antibody (LY3012218) in patients with relapsed acute myeloid leukemia. *J Clin Oncol*. 2015;33(15_suppl):7059-7059. doi:10.1200/jco.2015.33.15_suppl.7059
71. Kayser S, Heitmann JS, Dörfel D, et al. Interim Results of a First in Man Study with the Fc-Optimized FLT3 Antibody Flysyn for Treatment of Acute Myeloid Leukemia with Minimal Residual Disease. *Blood*. 2019;134(Supplement_1):3928. doi:10.1182/BLOOD-2019-125327
72. Stringaris K, Sekine T, Khoder A, et al. Leukemia-induced phenotypic and functional defects in natural killer cells predict failure to achieve remission in acute myeloid leukemia. *Haematologica*. 2014;99(5):836-847. doi:10.3324/HAEMATOL.2013.087536
73. Yeung YA, Krishnamoorthy V, Dettling D, et al. An Optimized Full-Length FLT3/CD3 Bispecific Antibody Demonstrates Potent Anti-leukemia Activity and Reversible Hematological Toxicity. *Mol Ther*. 2020;28(3):889-900. doi:10.1016/j.ymthe.2019.12.014
74. Lowe C, Rudra-Ganguly N, Malik FH, Sung Ju M. Patent Application Publication Pub. No.: US 2016/0272716 A1. Published online 2016:Appl. No.: 15/065,707.
75. Jetani H, Garcia-Cadenas I, Nerreter T, et al. CAR T-cells targeting FLT3 have potent activity against FLT3 - ITD + AML and act synergistically with the FLT3-inhibitor crenolanib. *Leukemia*. 2018;32(5):1168-1179. doi:10.1038/s41375-018-0009-0
76. Karbowski C, Goldstein R, B F, et al. Nonclinical Safety Assessment of AMG 553, an Investigational Chimeric Antigen Receptor T-Cell Therapy for the Treatment of Acute Myeloid Leukemia. *Toxicol Sci*. 2020;177(1):94-107. doi:10.1093/TOXSCI/KFAA098
77. Dean AQ, Luo S, Twomey JD, Zhang B. Targeting cancer with antibody-drug conjugates: Promises and challenges. *https://doi.org/101080/1942086220211951427*. 2021;13(1):1951427. doi:10.1080/19420862.2021.1951427
78. Beck A, Goetsch L, Dumontet C, Corvaïa N. Strategies and challenges for the next generation of antibody-drug conjugates. *Nat Rev Drug Discov*. 2017;16(5):315-337. doi:10.1038/nrd.2016.268
79. Goulet DR, Atkins WM. Considerations for the Design of Antibody-Based Therapeutics. *J*

Pharm Sci. 2020;109(1):74. doi:10.1016/J.XPHS.2019.05.031
80. Hafeez U, Parakh S, Gan HK, Scott AM. Antibody⇓drug conjugates for cancer therapy. *Molecules*. 2020;25(20). doi:10.3390/molecules25204764
81. Nejadmoghaddam M, Minai-tehrani A, Ghahremanzadeh R. Antibody-Drug Conjugates : Possibilities and Challenges. 2019;11(1).
82. Vidarsson G, Dekkers G, Rispens T. IgG subclasses and allotypes: From structure to effector functions. *Front Immunol*. 2014;5(OCT):1-17. doi:10.3389/fimmu.2014.00520
83. Tur MK, Huhn M, Jost E, Thepen T, Brümmendorf TH, Barth S. In vivo efficacy of the recombinant anti-CD64 immunotoxin H22(scFv)-ETA′ in a human acute myeloid leukemia xenograft tumor model. *Int J Cancer*. 2011;129(5):1277-1282. doi:10.1002/ijc.25766
84. Dunphy CH, Tang W. The value of CD64 expression in distinguishing acute myeloid leukemia with monocytic differentiation from other subtypes of acute myeloid leukemia: A flow cytometric analysis of 64 cases. *Arch Pathol Lab Med*. 2007;131(5):748-754. doi:10.5858/2007-131-748-tvocei
85. Kostova V, Désos P, Starck JB, Kotschy A. The chemistry behind adcs. *Pharmaceuticals*. 2021;14(5). doi:10.3390/ph14050442
86. Masters JC, Nickens DJ, Xuan D, Shazer RL, Amantea M. Clinical toxicity of antibody drug conjugates: a meta-analysis of payloads. *Invest New Drugs*. 2018;36(1):121-135. doi:10.1007/s10637-017-0520-6
87. Donaghy H. Effects of antibody, drug and linker on the preclinical and clinical toxicities of antibody-drug conjugates. *MAbs*. 2016;8(4):659-671. doi:10.1080/19420862.2016.1156829
88. Kovtun Y, Audette C, Mayo M, et al. Antibody-maytansinoid conjugates designed to bypass multidrug resistance. *Cancer Res*. 2010;70(6):2528-2537. doi:10.1158/0008-5472.CAN-09-3546
89. Dan N, Setua S, Kashyap VK, et al. Antibody-drug conjugates for cancer therapy: Chemistry to clinical implications. *Pharmaceuticals*. Published online 2018. doi:10.3390/ph11020032
90. Kasper MA, Stengl A, Ochtrop P, et al. Ethynylphosphonamidates for the Rapid and Cysteine-Selective Generation of Efficacious Antibody–Drug Conjugates. *Angew Chemie - Int Ed*. 2019;58(34):11631-11636. doi:10.1002/anie.201904193
91. Kasper MA, Glanz M, Stengl A, et al. Cysteine-Selective Phosphonamidate Electrophiles for Modular Protein Bioconjugations. *Angew Chemie - Int Ed*. 2019;58(34):11625-11630. doi:10.1002/anie.201814715
92. Schumacher D, Hackenberger CPR, Leonhardt H, Helma J. Current Status: Site-Specific Antibody Drug Conjugates. *J Clin Immunol*. 2016;36:100-107. doi:10.1007/s10875-016-0265-6
93. Drago JZ, Modi S, Chandarlapaty S. Unlocking the potential of antibody–drug conjugates for cancer therapy. *Nat Rev Clin Oncol*. 2021;18(6):327-344. doi:10.1038/s41571-021-00470-8
94. Junutula JR, Raab H, Clark S, et al. Site-specific conjugation of a cytotoxic drug to an antibody improves the therapeutic index. *Nat Biotechnol 2008 268*. 2008;26(8):925-932. doi:10.1038/nbt.1480
95. Gerlach M, Stoschek T, Leonhardt H, Hackenberger C, Schumacher D, Helma J. Tubulin Tyrosine Ligase-Mediated Modification of Proteins. *Methods Mol Biol*. 2019;2012:327-355. doi:10.1007/978-1-4939-9546-2_17
96. Helma J, Leonhardt H, Hackenberger C, Schumacher D. Tub-Tag Labeling; Chemoenzymatic Incorporation of Unnatural Amino Acids. *Methods Mol Biol*. 2018;1728:67-93. doi:10.1007/978-1-4939-7574-7_4
97. Junttila TT, Li G, Parsons K, Phillips GL, Sliwkowski MX. Trastuzumab-DM1 (T-DM1) retains all the mechanisms of action of trastuzumab and efficiently inhibits growth of lapatinib insensitive breast cancer. *Breast Cancer Res Treat*. 2011;128(2):347-356. doi:10.1007/s10549-010-1090-x
98. Weiskopf K, Weissman IL. Macrophages are critical effectors of antibody therapies for

cancer. *MAbs*. 2015;7(2):303-310. doi:10.1080/19420862.2015.1011450
99. Li F, Ulrich M, Jonas M, et al. Tumor-associated macrophages can contribute to antitumor activity through FcγR-mediated processing of antibody–drug conjugates. *Mol Cancer Ther*. 2017;16(7):1347-1354. doi:10.1158/1535-7163.MCT-17-0019
100. Uppal H, Doudement E, Mahapatra K, et al. Potential mechanisms for thrombocytopenia development with trastuzumab emtansine (T-DM1). *Clin Cancer Res*. 2015;21(1):123-133. doi:10.1158/1078-0432.CCR-14-2093
101. Zhao H, Gulesserian S, Ganesan SK, et al. Inhibition of megakaryocyte differentiation by Antibody–Drug Conjugates (ADCs) is mediated by macropinocytosis: Implications for ADC-induced thrombocytopenia. *Mol Cancer Ther*. 2017;16(9):1877-1886. doi:10.1158/1535-7163.MCT-16-0710
102. de Goeij BECG, Lambert JM. New developments for antibody-drug conjugate-based therapeutic approaches. *Curr Opin Immunol*. Published online 2016. doi:10.1016/j.coi.2016.02.008
103. Vick B, Rothenberg M, Sandhöfer N, et al. An advanced preclinical mouse model for acute myeloid leukemia using patients' cells of various genetic subgroups and in vivo bioluminescence imaging. *PLoS One*. 2015;10(3):1-20. doi:10.1371/journal.pone.0120925
104. Wenk C, Garz AK, Grath S, et al. Direct modulation of the bone marrow mesenchymal stromal cell compartment by azacitidine enhances healthy hematopoiesis. *Blood Adv*. 2018;2(23):3447-3461. doi:10.1182/bloodadvances.2018022053
105. Opatz S, Polzer H, Herold T, et al. Exome sequencing identifies recurring FLT3 N676K mutations in core-binding factor leukemia. *Blood*. 2013;122(10):1761-1769. doi:10.1182/blood-2013-01-476473
106. Chou T-C, Martin N. *CompuSyn for Drug Combinations and for General Dose-Effect Analysis User's Guide A Computer Program for Quantitation of Synergism and Antagonism in Drug Combinations, and the Determination of IC 50 , ED 50 , and LD 50 Values*.; 2005. www.combosyn.com
107. Ashton JC. Drug combination studies and their synergy quantification using the chou-talalay method-letter. *Cancer Res*. 2015;75(11):2400. doi:10.1158/0008-5472.CAN-14-3763
108. Ianevski A, Giri AK, Aittokallio T. SynergyFinder 2.0: Visual analytics of multi-drug combination synergies. *Nucleic Acids Res*. 2021;48(1):W488-W493. doi:10.1093/NAR/GKAA216
109. Yadav B, Wennerberg K, Aittokallio T, Tang J. Searching for Drug Synergy in Complex Dose-Response Landscapes Using an Interaction Potency Model. *Comput Struct Biotechnol J*. 2015;13:504-513. doi:10.1016/j.csbj.2015.09.001
110. Schaefer J V., Honegger A, Plückthun A. Construction of scFv Fragments from Hybridoma or Spleen Cells by PCR Assembly. In: *Antibody Engineering*. Springer Berlin Heidelberg; 2010:21-44. doi:10.1007/978-3-642-01144-3_3
111. Dodev TS, Karagiannis P, Gilbert AE, et al. A tool kit for rapid cloning and expression of recombinant antibodies. *Sci Rep*. 2014;4. doi:10.1038/srep05885
112. Bamopoulos S, Sauerland M, Görlich D, et al. Clinical presentation and differential splicing of SRSF2, U2AF1 and SF3B1 mutations in patients with Acute Myeloid Leukemia. GSE146173. https://www.ncbi.nlm.nih.gov/geo/query/acc.cgi?acc=GSE146173
113. Fenton C, Scott LI, Plosker GL. Palivizumab: A review of its use as prophylaxis for serious respiratory syncytial virus infection. *Pediatr Drugs*. 2004;6(3):177-197. doi:10.2165/00148581-200406030-00004
114. Product information Flebogamma DIF 50 mg/ml solution for infusion.
115. Hoffmann JHO, Enk AH. High-Dose Intravenous Immunoglobulin in Skin Autoimmune Disease. *Front Immunol*. 2019;10(JUN):1090. doi:10.3389/FIMMU.2019.01090
116. Herold T, Jurinovic V, Batcha AMN, et al. A 29-gene and cytogenetic score for the prediction of resistance to induction treatment in acute myeloid leukemia. *Haematologica*. 2018;103(3):456-465. doi:10.3324/haematol.2017.178442
117. Bagnoli JW, Ziegenhain C, Janjic A, et al. Sensitive and powerful single-cell RNA sequencing using mcSCRB-seq. 2018;9(1):1-8. doi:10.1038/s41467-018-05347-6

118. Paschka P, Schlenk RF, Weber D, et al. Adding dasatinib to intensive treatment in core-binding factor acute myeloid leukemia-results of the AMLSG 11-08 trial. *Leukemia*. 2018;32(7):1621-1630. doi:10.1038/s41375-018-0129-6
119. Kayser S, Levis MJ. Updates on targeted therapies for acute myeloid leukaemia. *Br J Haematol*. Published online 2021. doi:10.1111/BJH.17746
120. Müller J, Schmidt-Arras D. Novel Approaches to Target Mutant FLT3 Leukaemia. *Cancers (Basel)*. 2020;12(10):1-18. doi:10.3390/CANCERS12102806
121. Haubner S, Perna F, Köhnke T, et al. Coexpression profile of leukemic stem cell markers for combinatorial targeted therapy in AML. *Leukemia*. 2019;33(1):64-74. doi:10.1038/s41375-018-0180-3
122. Hospital MA, Green AS, Maciel TT, et al. FLT3 inhibitors: Clinical potential in acute myeloid leukemia. *Onco Targets Ther*. 2017;10:607-615. doi:10.2147/OTT.S103790
123. Hofmann S, Schubert M-L, Wang L, et al. Chimeric Antigen Receptor (CAR) T Cell Therapy in Acute Myeloid Leukemia (AML). *J Clin Med*. 2019;8(2):200. doi:10.3390/JCM8020200
124. Tang L, Wu J, Li C-G. Characterization of Immune Dysfunction and Identification of Prognostic Immune-Related Risk Factors in Acute Myeloid Leukemia. *Clin Cancer Res*. 2020;26(7):1763-1772. doi:10.1158/1078-0432.CCR-19-3003
125. Almagro JC, Daniels-Wells TR, Perez-Tapia SM, Penichet ML. Progress and challenges in the design and clinical development of antibodies for cancer therapy. *Front Immunol*. 2018;8(JAN). doi:10.3389/fimmu.2017.01751
126. Getts DR, Getts MT, McCarthy DP, Chastain EML, Miller SD. Have we overestimated the benefit of human(ized) antibodies? *MAbs*. 2010;2(6):682-694. doi:10.4161/mabs.2.6.13601
127. Hoffmann RM, Coumbe BGT, Josephs DH, et al. Antibody structure and engineering considerations for the design and function of Antibody Drug Conjugates (ADCs). *Oncoimmunology*. 2018;7(3):1-11. doi:10.1080/2162402X.2017.1395127
128. The Human Protein Atlas. transcriptomics datasets (HPA, GTEx and FANTOM5). http://www.proteinatlas.org
129. Mladenov R, Hristodorov D, Cremer C, et al. CD64-directed microtubule associated protein tau kills leukemic blasts ex vivo. *Oncotarget*. 2016;7(41):67166-67174. doi:10.18632/oncotarget.11568
130. Li Y, Li H, Wang MN, et al. Suppression of leukemia expressing wild-type or ITD-mutant FLT3 receptor by a fully human anti-FLT3 neutralizing antibody. *Blood*. 2004;104(4):1137-1144. doi:10.1182/blood-2003-07-2585
131. Walter RB, Raden BW, Kamikura DM, Cooper JA, Bernstein ID. Influence of CD33 expression levels and ITIM-dependent internalization on gemtuzumab ozogamicin–induced cytotoxicity. *Blood*. 2005;105(3):1295-1302. doi:10.1182/BLOOD-2004-07-2784
132. You M, Yang Y, Zhong C, et al. Efficient mAb production in CHO cells with optimized signal peptide, codon, and UTR. *Appl Microbiol Biotechnol 2018 10214*. 2018;102(14):5953-5964. doi:10.1007/S00253-018-8986-5
133. Brader ML, Estey T, Bai S, et al. Examination of Thermal Unfolding and Aggregation Profiles of a Series of Developable Therapeutic Monoclonal Antibodies. Published online 2015. doi:10.1021/mp400666b
134. Tiller KE, Tessier PM. Advances in Antibody Design. *Annu Rev Biomed Eng*. 2015;17:191. doi:10.1146/ANNUREV-BIOENG-071114-040733
135. Yaghoubi S, Karimi MH, Lotfinia M, et al. Potential drugs used in the antibody–drug conjugate (ADC) architecture for cancer therapy. *J Cell Physiol*. 2020;235(1):31-64. doi:10.1002/jcp.28967
136. Ponziani S, Di Vittorio G, Pitari G, et al. Antibody-drug conjugates: The new frontier of chemotherapy. *Int J Mol Sci*. 2020;21(15):1-28. doi:10.3390/ijms21155510
137. Joubert N, Beck A, Dumontet C, Denevault-Sabourin C. Antibody–drug conjugates: The last decade. *Pharmaceuticals*. 2020;13(9):1-30. doi:10.3390/ph13090245
138. Ali S, Dunmore H, Karres D, et al. The EMA Review of Mylotarg (Gemtuzumab Ozogamicin) for the Treatment of Acute Myeloid Leukemia. *Oncologist*. 2019;24(5). doi:10.1634/theoncologist.2019-0025

139. Cowan AJ, Laszlo GS, Estey EH, Walter RB. Antibody-based therapy of acute myeloid leukemia with gemtuzumab ozogamicin. *Front Biosci*. 2013;18(4):1311-1334. doi:10.2741/4181
140. Mori M, Kaneko N, Ueno Y, et al. Gilteritinib, a FLT3/AXL inhibitor, shows antileukemic activity in mouse models of FLT3 mutated acute myeloid leukemia. *Invest New Drugs*. 2017;35(5):556. doi:10.1007/S10637-017-0470-Z
141. Göllner S, Oellerich T, Agrawal-Singh S, Schenk T, Klein H, Rohde C. Loss of the histone methyltransferase EZH2 induces resistance to multiple drugs in acute myeloid leukemia. *Nat Med*. 2017;23(1):69-78. doi:10.1038/NM.4247
142. Kempf JM, Weser S, Bartoschek MD, et al. Loss-of-function mutations in the histone methyltransferase EZH2 promote chemotherapy resistance in AML. *Sci Rep*. 2021;11(1):1-13. doi:10.1038/s41598-021-84708-6
143. Derebe MG, Nanjunda RK, Gilliland GL, Lacy ER, Chiu ML. Human IgG subclass cross-species reactivity to mouse and cynomolgus monkey Fcγ receptors. *Immunol Lett*. 2018;197:1-8. doi:10.1016/j.imlet.2018.02.006
144. Bruhns P, Jönsson F. Mouse and human FcR effector functions. *Immunol Rev*. 2015;268(1):25-51. doi:10.1111/imr.12350
145. Cortes J, Perl AE, Döhner H, et al. Quizartinib, an FLT3 inhibitor, as monotherapy in patients with relapsed or refractory acute myeloid leukaemia: an open-label, multicentre, single-arm, phase 2 trial. *Lancet Oncol*. 2018;19(7):889-903. doi:10.1016/S1470-2045(18)30240-7
146. Roboz GJ, Strickland SA, Litzow MR, et al. Updated safety of midostaurin plus chemotherapy in newly diagnosed FLT3 mutation–positive acute myeloid leukemia: the RADIUS-X expanded access program. *Leuk Lymphoma*. 2020;61(13):3146-3153. doi:10.1080/10428194.2020.1805109/SUPPL_FILE/ILAL_A_1805109_SM2808.DOCX
147. Scott LJ. Brentuximab Vedotin: A Review in CD30-Positive Hodgkin Lymphoma. *Drugs*. 2017;77(4):435-445. doi:10.1007/s40265-017-0705-5
148. Gong Q, Ou Q, Ye S, et al. Importance of Cellular Microenvironment and Circulatory Dynamics in B Cell Immunotherapy. *J Immunol*. 2005;174(2):817-826. doi:10.4049/jimmunol.174.2.817
149. Niwa R, Satoh M. The current status and prospects of antibody engineering for therapeutic use: Focus on glycoengineering technology. *J Pharm Sci*. 2015;104(3):930-941. doi:10.1002/jps.24316
150. Weisberg E, Sattler M, Manley PW, Griffin JD. Spotlight on midostaurin in the treatment of FLT3-mutated acute myeloid leukemia and systemic mastocytosis: Design, development, and potential place in therapy. *Onco Targets Ther*. Published online 2018. doi:10.2147/OTT.S127679
151. Weisberg E, Ray A, Nelson E, et al. Reversible resistance induced by FLT3 inhibition: A novel resistance mechanism in mutant FLT3-Expressing cells. *PLoS One*. 2011;6(9):e25351. doi:10.1371/journal.pone.0025351
152. Knapper S, Burnett AK, Littlewood T, et al. A phase 2 trial of the FLT3 inhibitor lestaurtinib (CEP701) as first-line treatment for older patients with acute myeloid leukemia not considered fit for intensive chemotherapy. *Blood*. 2006;108(10):3262-3270. doi:10.1182/BLOOD-2006-04-015560
153. Walker R, Watkins K, Zweidler-McKay P. Combination treatment with antibody-drug-conjugates and FLT3 inhibitors PCT/US20 19/032090 Immunogen, Inc. 2019;2(51).
154. Watkins, Krystal. *Robust In Vivo Synergy Between the Anti-CD33 ADC IMGN779 and the FLT3 Inhibitor Quizartinib in Human FLT3-ITD AML Models*.
155. Staudt D, Murray HC, McLachlan T, et al. Targeting oncogenic signaling in mutant FLT3 acute myeloid leukemia: The path to least resistance. *Int J Mol Sci*. 2018;19(10):1-26. doi:10.3390/ijms19103198
156. Williams BA, Law A, Hunyadkurti J, Desilets S, Leyton J V., Keating A. Antibody Therapies for Acute Myeloid Leukemia: Unconjugated, Toxin-Conjugated, Radio-Conjugated and Multivalent Formats. *J Clin Med*. 2019;8(8):1261. doi:10.3390/jcm8081261

6 Annex

6.1 Supplementary figures and tables

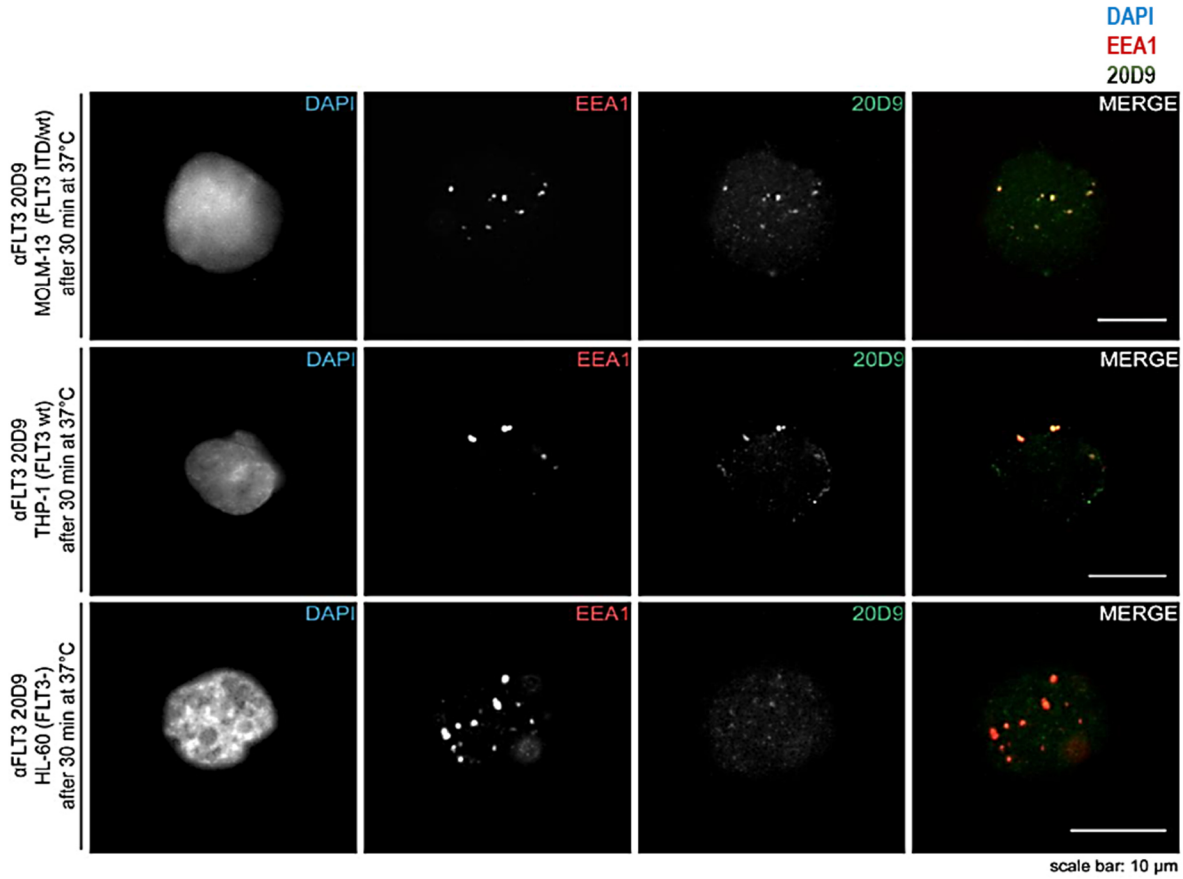

Supplementary Figure 1 Internalization of 20D9-mab and co-localization with endosomes. Temperature induced internalization of 20D9 antibody in MOLM-13 and THP-1 (FLT3 positive) and HL-60 (FLT3 negative) cell lines after 37 °C incubation for 30 min and colocalization with early -endosomal marker EEA1 assessed in immunofluorescence staining. Green = 20D9-mab. Red = EEA1. Blue = DAPI nuclear staining. Scale bar 10 µm. This experiment was done by Verena Waller.

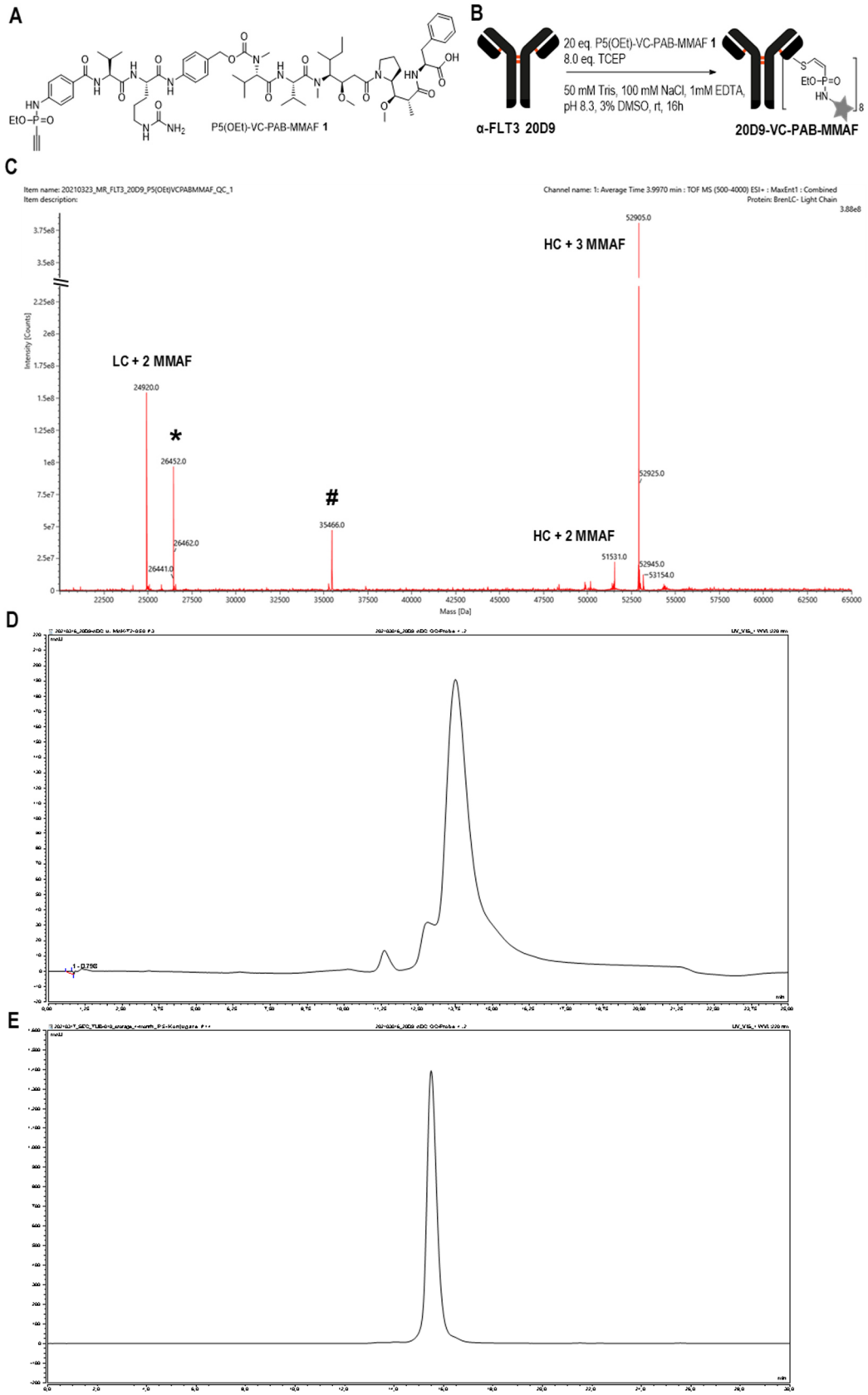

Supplementary Figure 2 Quality analysis of 20D9-ADC. (A) Chemical structure of P5(OEt)-VC-PAB-MMAF. P5(OEt)=phosphonamidite linker; VC-PAB=valine-citrulline-p-aminobenzoyloxycarbonyl; MMAF=monomethyl auristatin F. (B) Schematic reaction of P5 conjugation. (C) Spectrogram of LC/ESI-MS of 20D9-ADC with DAR 7.8; *=Deconvolution artefact from HC + 3MMAF; # = PNGase-F. (D) Chromatogram of A-HIC of 20D9-ADC, absorbance at 220 nm, DAR7.7. (E) Chromatogram of analytical size exclusion chromatography (A-SEC), absorbance at 220 nm – less than 1 % aggregates. Quality analysis was done by Marc-Andre Kasper.

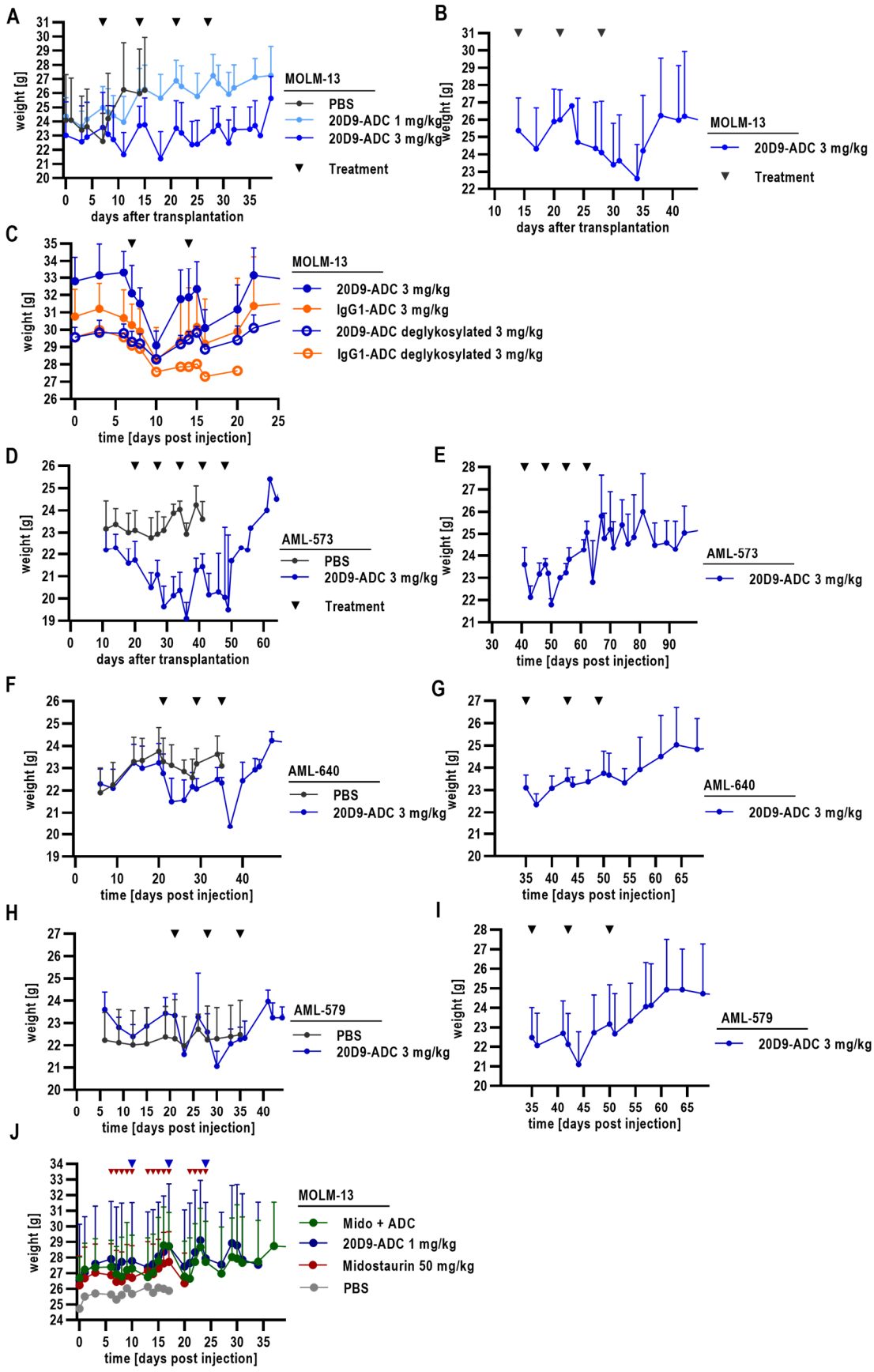

Supplementary Figure 3 Weight curves of NSG mice during *in vivo* experiments. Weight curves of all *in vivo* experiments using MOLM-13, AML-573, AML-579 and AML-640 samples. Treatment timepoints are indicated with black arrows, treatments are indicated in light blue (1 mg/kg 20D9-ADC), dark blue (3 mg/kg 20D9-ADC), orange (3 mg/kg IgG1-ADC), red (50 mg/kg midostaurin), green (combination of midostaurin and 20D9-ADC) and grey (PBS).

% Identity of the variable regions of the heavy chains

	2F12	4B12	20D9	27E7	29H1	30B12	19H5
2F12	100.00%	48.31%	63.33%	94.92%	94.07%	48.78%	47.22%
4B12	48.31%	100.00%	52.54%	48.31%	49.15%	75.83%	99.03%
20D9	63.33%	52.54%	100.00%	63.33%	62.50%	58.33%	51.85%
27E7	94.92%	48.31%	63.33%	100.00%	92.37%	47.97%	48.15%
29H1	94.07%	49.15%	62.50%	92.37%	100.00%	49.59%	48.15%
30B12	48.78%	75.83%	58.33%	47.97%	49.59%	100.00%	74.55%
19H5	47.22%	99.03%	51.85%	48.15%	48.15%	74.55%	100.00%

% Identity of the variable regions of the light chains

	2F12	4B12	20D9	27E7	29H1	30B12	19H5
2F12	100.00%	49.11%	60.75%	52.68%	50.00%	50.00%	63.55%
4B12	49.11%	100.00%	47.32%	82.14%	81.25%	81.25%	43.75%
20D9	60.75%	47.32%	100.00%	49.11%	48.21%	49.11%	58.88%
27E7	52.68%	82.14%	49.11%	100.00%	95.54%	97.32%	46.43%
29H1	50.00%	81.25%	48.21%	95.54%	100.00%	95.54%	42.86%
30B12	50.00%	81.25%	49.11%	97.32%	95.54%	100.00%	44.64%
19H5	63.55%	43.75%	58.88%	46.43%	42.86%	44.64%	100.00%

Supplementary Table 1 Sequence identities of variable light and variable heavy chains of anti-FLT3 antibodies. Analysis was performed using NCBI Protein Blast

sample	disease stage	age [years]	sex	cytogenetics	mutations (panel seq) *	FLT3-ITD (VAF)
AML-361	ID	40	f	normal	DNMT3A^{R882H}, NPM1^{L287fs}, FLT3-ITD, BCOR^{D551N}	K602delinsNFYVDFREYEYDLK (0.3)
AML-372	R1	42	m	complex karyotype, including -17	TP53^{R209Q}, NRAS^{Q61K}, KRAS^{G12V}	
AML-388	ID	57	m	KMT2A/AFDN	KRAS^{Q61H}	
AML-393	R1	47	f	ins(10;11)(p12;q23q23) KMT2A/MLLT10	KRAS^{G12A}, BCOR^{1012del}	
AML-407	R1	58	f	complex karyotype, including +12	DNMT3A^{R882C}, NRAS^{Q61H}, NRAS^{G12V}, NOTCH1^{S1690L}, SRSF2^{P95H}	
AML-415	R2	69	f	normal	DNMT3A^{V527I}, DNMT3A^{S714C}, NPM1^{L287fs}, FLT3-ITD, IDH1^{R132H}	E598delinsDDFREYE (1.0)
AML-491	R1	53	f	del(7) (q2?1)	DNMT3A^{R882S}, RUNX1^{N136K}, BCOR$^{c.2048fs}$, ETV6^{P214L}, PTPN11^{D61H}, KRAS^{G12A}, NRAS^{Q61K}	
AML-538	R	68	f	normal	DNMT3A^{A380fs}, IDH1^{R132C}	
AML-573	R1	64	f	t(5;11)(p1?;q?13)	DNMT3A^{S663L},DNMT3A^{A644S}, FLT3-ITD, WT1$^{c.1075fs}$, WT1$^{c.1054fs}$, IDH2^{R140Q}	E604delinsDPSDNEYFYVDFREYEYDLKWE (0.35)
AML-579	R	51	m	normal	DNMT3A^{R882C},DNMT3A^{F868L}, NPM1^{L287fs}, FLT3-ITD, IDH1^{R132H}	E598delinsDYVDFREYE (1.0)

AML-602	R1	40	f	complex karyotype	DNMT3A$^{c.1122fs}$,NPM1^{W288fs}, FLT3$^{c.1837fs}$, TET2 ^{S280fs}, JAK3^{V722I}, CEBPA^{D262fs}	
AML-640	ID	79	m	t(11;15)(p1?1;q?22)	DNMT3A$^{c.2173fs}$, NPM1^{L287fs}, FLT3-ITD, IDH1^{R132H}	F612delinsVDFREYEYDLKWEFPRENLEF (0.5);L610delinsFGSSDNEYFYVDFREYEYDLKWEFPRENL (0.2)
AML-661	R2	54	f	del(7) (q2?1)	DNMT3A^{R882S}, RUNX1^{N136K}, BCOR$^{c.2048fs}$, ETV6^{P214L}, PTPN11^{D61H}, KRAS^{G12A}, NRAS^{Q61K}, JAK1^{V658F}, EZH2^{A692G}	
AML-663	R	13	f	*ND*	WT1^{T382fs}, WT1^{C453Y}, FLT3-ITD	18 nt (0.5)
AML-664	R	6	f	*ND*	WT1^{D469V}	
AML-669	R2	49	f	KMT3A/MLLT3	KRAS^{G13D}	
AML-896	ID	52	f	normal	DNMT3A^{R882H}, NPM1^{W288fs}, FLT3-ITD,	GNSHLRSYSYSLKS (1.0)
AML-955	?	?	?	?	DNMT3A^{S714C}, NPM1^{W288fs}, WT1 .1142C>A	
AML-959	?	?	?	?	DNMT3A^{R882H}, NPM1^{W288fs}, FLT3-ITD, TET2^{Y1294C}, TET2^{R1261S}	63 nt (0.5)
AML-979	R	56	f	normal	DNMT3A^{R882H}, NPM1^{W288fs}, FLT3-ITD, IDH2^{R140Q}	25 nt, 36 nt
AML-981	R	76	m	normal	DNMT3A^{Y448*}, NPM1^{W288fs}, FLT3-ITD, FLT3^{D835H}, TET2^{R1404*}, ASXL1^{P783A}, WT1$^{c.491ins}$	SYSLKSTYKY (1.0)

Supplementary Table 2 Characteristics of AML-PDX samples. ID: initial diagnosis; R1: first relapse; R2: second relapse; f: female; m: male; fs: frameshift; ITD=internal tandem duplication; VAF: variant allele frequency; delins: deletion-insertion

6.2 Abbreviations

A	Ampere
ADC	Antibody-drug-conjugates
ADCC	Antibody dependent cell-mediated cytotoxicity
AML	Acute myeloid leukemia
APL	Acute promyelocytic leukemia
APS	Ammonium persulfate
AraC	Cytarabine
ARCH	Age-associated clonal hematopoiesis
BGG	Bovine gamma globulin
BLI	Bioluminescence imaging
BM	Bonemarrow
bp	Base pairs
BSA	Bovine serum albumin
CDC	Complement-dependent cytotoxicity
CDR	Complementarity-determining regions
CH	Constant heavy
CAR	Chimeric antigen receptor
CI	Combination index
CL	Constant light

CN	Cytogenetical normal
CR	Complete remission
Cri	Incomplete hematologic recovery
d	Day
DAPI	4,6-Diamidino-2-phenylindol
DAR	Drug to Antibody Ratio
del	Deletion
DM1	Maytansine derivatives 1
DMEM	Dulbecco´s Modified Eagle Medium
DMSO	Demethylsulfoxide
DNA	Deoxyribonucleic acid
dNTP	Desoxynucleotide triphospahate
DSMZ	German Collection of Microorganisms and cell culture
e.g.	For example
ECL	Enhanced chemoluminescence
EDTA	Ethylene diamine tetraacetic acid
ELISA	Enzyme-linked Immunosorbent Assay
Em	Emission
ev	Empty vector
Ex	Excitation
f	Female
FAB	American-French-British
Fab	Antigen-binding fragments
FACS	Fluorescence activated cell sorting
FBS	Fetal bovine serum
Fc	Fragment crystallizable
FcR	Fc receptor
FDA	Food and Drug Administration
FITC	Fluorescein isothiocyanate
FL	FLT3 ligand
FLT3	Fms-Like Tyrosine kinase 3
g	Gravity acceleration, gramm
GFP	Green fluorescent protein
h	Hour
HC	Heavy chains
HMWS	High molecular weight species
HRP	Horse redish peroxidase
HSC	Hematopoietic Stem Cell
HSPC	Hematopoietic Stem and Progenitor Cell
i.v.	Intravenous
IC_{50}	Half-inhibitory concentration
IF	Immunofluorescence staining
Ig	Immunglobuline
IL -3	Interleukin-3
inv	Inversion
IRES	Internal ribosomal entry site
ITD	Internal tandem duplications
k	Kilo
Kd	Dissociation constant
Da	Dalton
l	Litre
LC	Light chains
LSC	Leukemic stem cell
m	Male, meter, milli
M	Molar

mab	Monoclonal antibody
MDR1	Multidrug transporter 1
MDS	Myelodysplastic syndromes
MFI	Mean fluorescent intensity
min	Minute
MMAE	Monomethyl auristatin E
MMAF	Monomethyl auristatin F
MM -1	Mono-Mac 1
MM -6	Mono-Mac 6
MRD	Minimal residual disease
n	Nano
NK cells	Natural killer cell
NSG	NOD scid gamma
PTK	Protein tyrosine kinase
P5-(OEt)	Phosphonamidate linker
OS	5-year overall survival
PBD	Pyrrolobenzodiazepine
PBS	Phosphate buffered saline
PCR	Polymerase chain reaction
pdx	Patient derived xenograft
pH	Potentia hydrogenii
PR	Partial remission
qPCR	Quantitative PCR
rh	Recombinant human
RNA	Ribonucleic acid
rpm	Rounds per minute
RPMI	Roswell Park Memorial Institute
RT	Room temperature
RTK	Receptor tyrosine kinases
s.d.	Standard deviation
SCT	Stem cell transplantation
SDS	Sodium dodecyl sulfate
sec	Second
t	Translocation
TDCC	T-cell dependent cellular cytotoxicity
T-DM1	Trastuzumab-emantisine
TEMED	Tetramethylethylenediamine
TKD	Tyrosine kinase domains
TKI	Tyrosine kinase inhibitor
U	Units
US	United states
UV	Ultraviolet
V	Volt
VAF	Variant allele frequency
VC-PAB	Valine-citrulline-p-aminobenzoyloxycarbonyl
VH	Variable heavy
VL	Variable light
WB	Western blot
WHO	World health organisation
wt	Wildtype
YFP	Yellow fluorescent protein
%	Percentage
°C	Grad celsius
µ	Micro

Nonpolar/hydrophobic amino acids	
A	Alanine (Ala)
V	Valine (Val)
L	Leucine (Leu)
I	Isoleucine (Ile)
M	Methionine (Met)
P	Proline (Pro
W	Tryptophan (Trp)
F	Phenylalanine (Phe)
Polar/neutral amino acids	
G	Glycine (Gly)
S	Serine (Ser)
T	Threonine (Thr)
Y	Tyrosine (Tyr)
C	Cysteine (Cys)
N	Asparagine (Asn)
Q	Glutamine (Gln)
Polar/acidic amino acids	
E	Glutamic acid (Glu)
D	Aspartic acid (Asp)
Polar/basic amino acids	
K	Lysine (Lys)
R	Arginine (Arg)
H	Histidine (His)

6.3 Lists of figures and tables

List of figures

List of tables

6.4 Publications of this project

- Most of the results described in this work are part of the study "Targeting FLT3 by new-generation antibody-drug-conjugate in combination with kinase inhibitors for treatment of AML", Roas et al., unpublished.

Maike Roas, Binje Vick, Marc-Andre Kasper, Marina Able, Harald Polzer, Marcus Gerlach, Elisabeth Kremmer, Judith S. Hecker, Saskia Schmitt, Andreas Stengl, Verena Waller, Natascha Hohmann, Moreno Festini, Alexander Ludwig, Lisa Rohrbacher, Tobias Herold, Marion Subklewe, Katharina S. Götze, Christian P. R. Hackenberger, Dominik Schumacher, Jonas Helma-Smets, Irmela Jeremias, Heinrich Leonhardt and Karsten Spiekermann: Targeting FLT3 by new-generation antibody-drug-conjugate in combination with kinase inhibitors for treatment of AML; Blood, 2022, unpublished.

- The presented work is part of a pending patent application.

Acknowledgements

I would like to thank everyone who supported me and made this cooperative venture possible.
My deepest thanks go to Karsten Spiekermann and Heinrich Leonhardt for the opportunity to work on this exciting cooperative project, for support, fruitful discussions and reviewing my doctoral thesis. Special thanks go to Karsten Spiekermann for continuous guidance and great mentoring. My thank also goes to Binje Vick, Jonas Helma-Smets and Dominik Schumacher for their great input and discussion in the TAC meetings, which guided my doctoral project essentially.

My sincere thanks go to all colleagues and former colleagues in the ELLF department and particularly to the Spiekermann lab group for scientific advice, motivation and a fantastic working atmosphere. Anna Vetter, Belay Tizazu, Julia Kempf, Natascha Hohmann, Matthias Oettle, Moreno Festini, Alexander Ludwig and Marina Able, thank you for your help and cordiality. It was great fun to work with you! Also, I want to thank Harald Polzer, who helped initiating the project. Thanks go to Bianka Ksienzyk and Belay Tizazu for their professional technical support.

I would like to thank all cooperation partners for their valuable contribution to the success of the project in terms of laboratory work, a pleasant working atmosphere and great discussion. I am thankful to the colleagues from Tubulis GmbH, which provided the P5 technology and were always ready and willing to help: Dominik Schumacher, Jonas Helma-Smets, Markus Gerlach, Marc-Andre Kasper, Saskia Schmitt and Annette Vogl. Especially, I want to thank Marc for ADC generation, Marcus for analytics and Saskia for FLT3 induction experiments. Further, my thanks go to the group of Professor Leonhardt, to Heinrich Flaswinkel and Jonathan Schwach for their antibody expertise and to Elisabeth Kremmer, Andreas Stengl, Verena Waller which helped starting the project. I want to thank Tobias Herold from the LMU Klinikum for providing RNA Seq data. I also want to thank Katharina Götze and Judith Hecker from TU Munich for scientific advice and *in vitro* toxicity analysis. Many thanks go to Binje Vick and Irmela Jeremias from the Helmholtz Zentrum for the ADC *in vivo* analysis and fruitful discussions. I am thankful to Annette Frank and Maike Fritschle for laboratory *in vivo* work. I also want to thank Lesca Holdt from the Laboratoriumsmedizin from the LMU Klinikum for mouse blood analysis.

To finish, lovely thanks go to my friends and family for their never-ending support. I am deeply grateful to my husband Korbinian for his unremitting support, patience and encouragement.